



Icelandic Hyaloclastite Tuffs

Petrophysical Properties, Alteration and Geochemical Mobility

Hjalte Franzson
Gudmundur H. Gudfinnsson
Julia Frolova
Helga M. Helgadóttir
Bruce Pauly
Anette K. Mortensen
Sveinn P. Jakobsson

Prepared for National Energy Authority
and Reykjavík Energy

ÍSOR-2011/064

ICELAND GEOSURVEY

Reykjavík: Orkugardur, Grensásvegur 9, 108 Reykjavík, Iceland - Tel.: 528 1500 - Fax: 528 1699

Akureyri: Rangárvellir, P.O. Box 30, 602 Akureyri, Iceland - Tel.: 528 1500 - Fax: 528 1599

isor@isor.is - www.isor.is

Icelandic Hyaloclastite Tuffs

Petrophysical Properties, Alteration and Geochemical Mobility

Hjalti Franzson
Gudmundur H. Gudfinnsson
Julia Frolova
Helga M. Helgadóttir
Bruce Pauly
Anette K. Mortensen
Sveinn P. Jakobsson

Prepared for National Energy Authority
and Reykjavík Energy


Report no. ÍSOR-2011/064	Date December 2011	Distribution <input checked="" type="checkbox"/> Open <input type="checkbox"/> Closed
Report name / Main and subheadings Icelandic Hyaloclastite Tuffs. Petrophysical Properties, Alteration and Geochemical Mobility	Number of copies 7	Number of pages 103
	Authors Hjalti Franzson, Gudmundur H. Gudfinnsson, Julia Frolova, Helga M. Helgadóttir, Bruce Pauly, Anette K. Mortensen and Sveinn P. Jakobsson	
Project manager Hjalti Franzson		Classification of report Project no. 540105
Prepared for National Energy Authority and Reykjavík Energy		
Cooperators Moscow University, University of California in Davis, Natural History Museum in Iceland		
Abstract <p>This study attempts to define the properties of hyaloclastite formations which control their petrophysical characteristics during their progressive alteration. It is based on 140 tuffaceous cores from last glaciation to 2–3 m y. The water content shows a progressive increase with alteration to about 12%, which mainly is bound in the smectite and zeolite alteration minerals. It diminishes when altered to chlorite and disappearance of zeolites indicating the dehydration of the alteration minerals. CO₂ content appears to increase stepwise, firstly at about 30%, secondly at 65% and thirdly near 100% alteration. The rock oxidation increases concomitantly with the water content in the rock. This is reflected in the grain density which also diminishes with increasing alteration but increases again when entering into the chlorite-epidote alteration. Changes in porosity show that larger pores (macro porosity) are filled as alteration proceeds, while secondary micro porosity increases, mainly at palagonite/glass margins and not the least within the smectite clays. Micro porosity in fully altered tuffs ranges from about 7–35%. This type of porosity may explain the “aquiclude character” of hyaloclastites. Permeability ranges from 0.1 to about 12000 mD and a close correlation is shown between porosity and permeability. This correlation, however, is stronger between macro porosity and permeability than the micro porosity. Chemical analysis of fresh glass and palagonite shows the notable leaching of Na₂O in the latter and to some extent the CaO, while FeO and TiO₂ are slightly enriched. Other oxides do not show obvious tendencies for mobility. The assessment of chemical mobility during alteration, taking into account the filling of macro pores, was unsuccessful, and may be due to the formation of secondary micro porosity which is not the case in alteration of crystallized rocks. A geochemical comparison of the variably altered tuffs with the compositional field of equivalent fresh rocks indicate the limited mobility of the chemical components, except for CaO, Na₂O and Rb which show clear indication of being removed.</p>		
Key words Hyaloclastite tuffs, petrophysics, alteration, palagonite, grain density, geochemistry, mobility,	ISBN-number	
	Project manager's signature 	
	Reviewed by HMH	

Table of contents

1	Introduction	13
2	Sample collection, measurements and chemical analyzes	14
3	Sample description	15
4	Alteration.....	16
5	Volatile content	17
6	Grain density	19
7	Porosity	20
	7.1 Changes in porosity	20
	7.2 The sources of micro porosity	21
	7.3 Permeability and porosity	22
8	Chemical transfer	22
	8.1 Chemical mobility in basaltic glass caused by palagonitization	23
	8.2 Changes in whole-rock chemical composition by palagonitization	23
	8.3 Composition of hyaloclastite tuff samples compared to crystallized whole-rock samples	24
	8.4 Chemical changes with increasing secondary mineralization	25
	8.5 Evidence for element mobility from geochemical trends.....	27
	8.6 Evidence for element mobility from the relationship between Zr and some major and trace elements	28
9	Conclusions	29
10	Recommendations for further work.....	30
11	References.....	31
12	Figures.....	33

List of figures

Figure 1.	<i>SiO₂ content versus MgO content of the hyaloclastite tuff samples. The samples are classified according to petrological series.....</i>	33
Figure 2.	<i>Histogram showing sample frequency depending on the original amount of glass as a proportion of solid rock.</i>	33
Figure 3.	<i>Histogram showing sample frequency depending on the abundance of unaltered glass as a proportion of solid rock.</i>	34
Figure 4.	<i>Histogram showing sample frequency depending on the abundance of altered glass as a proportion of solid rock.</i>	34
Figure 5.	<i>Histogram showing sample frequency depending on the extent to which the primary glass has been altered.</i>	35

Figure 6. Histogram showing sample frequency depending on the abundance of primary minerals as a proportion of solid rock.	35
Figure 7. Histogram showing sample frequency depending on the abundance of altered primary minerals as a proportion of solid rock.	36
Figure 8. Histogram showing the sample frequency depending on the proportion of pores in the samples as determined by point counting in thin sections.	36
Figure 9. Histogram showing sample frequency depending on the original proportion of pores in the samples as determined by point counting in thin sections.	37
Figure 10. Histogram showing sample frequency depending on the amount of porosity in the samples as measured in air.	37
Figure 11. Histogram showing sample frequency depending on the abundance of secondary minerals as a proportion of solid rock.	38
Figure 12. Histogram showing sample frequency depending on the abundance of clay as a proportion of solid rock.	38
Figure 13. Histogram showing sample frequency depending on the abundance of zeolites as a proportion of solid rock.	39
Figure 14. BEI photograph of a slightly palagonitized hyaloclastite tuff sample from Vigdísarvellir on Reykjanes Peninsula.	40
Figure 16. BEI photograph of a moderately palagonitized hyaloclastite tuff sample from near Landmannahellir.	41
Figure 18. BEI photograph of a moderately palagonitized hyaloclastite tuff sample from Skefilsfjöll eldri.	42
Figure 20. BEI photograph of an extensively palagonitized hyaloclastite tuff sample from Meðalfell in West Iceland.	43
Figure 22. The amount of altered glass versus the extent of alteration of the hyaloclastite tuff samples.	44
Figure 23. The extent of glass alteration versus the total alteration of the hyaloclastite tuff samples.	44
Figure 24. The extent of primary mineral alteration versus the total alteration of the hyaloclastite tuff samples.	45
Figure 25. Molar ferric-ferrous ratio versus the amount of alteration of the hyaloclastite tuff samples.	45
Figure 26. Molar ferric-ferrous ratio versus the amount of glass alteration of the hyaloclastite tuff samples.	46
Figure 27. The amount of deposition versus the alteration of the hyaloclastite tuff samples.	46
Figure 28. The extent of filling of primary porosity with secondary minerals versus the extent of alteration of the hyaloclastite tuff samples.	47
Figure 29. The amount of clay versus alteration of the hyaloclastite tuff samples.	47
Figure 30. The amount of zeolites versus alteration of the hyaloclastite tuff samples.	48
Figure 31. The amount of calcite versus the degree of alteration of the hyaloclastite tuff samples.	48

Figure 32. <i>The amount of deposition versus the ratio between ferric iron and total iron content of the hyaloclastite tuff samples.</i>	49
Figure 33. <i>Loss on ignition versus the alteration of the hyaloclastite tuff samples.</i>	49
Figure 34. <i>The CO₂ content versus the alteration of the hyaloclastite tuff samples.</i>	50
Figure 35. <i>Measured H₂O content versus H₂O content calculated as LOI minus measured CO₂ content of the hyaloclastite tuff samples.</i>	50
Figure 36. <i>H₂O content versus alteration of the hyaloclastite tuff samples.</i>	51
Figure 37. <i>H₂O content versus the amount of altered glass in the hyaloclastite tuff samples.</i> .	51
Figure 38. <i>H₂O content versus the amount of altered glass as a proportion of total glass in the hyaloclastite tuff samples.</i>	52
Figure 39. <i>Loss on ignition versus the amount of deposition of secondary minerals.</i>	52
Figure 40. <i>CO₂ content versus the amount of calcite deposition in the hyaloclastite tuff samples.</i>	53
Figure 41. <i>Loss on ignition versus the molar ratio between ferric iron and total iron content of the hyaloclastite formations.</i>	53
Figure 42. <i>H₂O content versus the molar ratio between ferric iron and total iron content of the hyaloclastite formations.</i>	54
Figure 43. <i>H₂O content versus Na₂O content of the hyaloclastite formations.</i>	54
Figure 44. <i>Molar ratio of ferric iron content and total iron content versus Na₂O content of the hyaloclastite tuff samples.</i>	55
Figure 45. <i>Molar ratio of ferric iron content and total iron content versus the CaO content of the hyaloclastite tuff samples.</i>	55
Figure 46. <i>Grain density vs. the extent of glass alteration of the hyaloclastite tuff samples.</i> ...	56
Figure 47. <i>Grain density versus the alteration of the hyaloclastite tuff samples.</i>	56
Figure 48. <i>Grain density versus loss on ignition of the hyaloclastite tuff samples.</i>	57
Figure 49. <i>Grain density versus H₂O content of the hyaloclastite tuff samples.</i>	57
Figure 50. <i>Grain density versus the molar ratio of ferric iron content and total iron content of the hyaloclastite formations.</i>	58
Figure 51. <i>Porosity determined by point counting in thin sections versus porosity measured in air in drill cores of the hyaloclastite tuff samples.</i>	58
Figure 52. <i>Infilling of primary porosity determined by point counting versus measured porosity of the hyaloclastite tuff samples.</i>	59
Figure 53. <i>Porosity measured in drill cores versus the extent of alteration of the hyaloclastite tuff samples.</i>	59
Figure 54. <i>Micro porosity versus alteration of the hyaloclastite tuff samples.</i>	60
Figure 55. <i>Micro porosity versus the amount of deposition of secondary minerals in the hyaloclastite tuff samples.</i>	60
Figure 56. <i>Micro porosity versus the amount of clay in the hyaloclastite tuff samples.</i>	61
Figure 57. <i>BEI photograph of palagonitized hyaloclastite tuff.</i>	62
Figure 58. <i>Close-up view of a sideromelane glass particle rimmed with layered palagonite.</i> ...	62
Figure 60. <i>BEI photograph of a palagonitized sideromelane glass particle.</i>	63

Figure 62. BEI photograph of palagonitized hyaloclastite tuff.....	64
Figure 64. BEI photograph of hyaloclastite tuff.	65
Figure 66. BEI photograph of a highly altered hyaloclastite tuff sample.	66
Figure 67. Close-up view of a particle in a hyaloclastite tuff sample where the original sideromelane glass has been replaced by smectite	67
Figure 68. Air permeability versus porosity determined by point counting in thin sections in the hyaloclastite tuff samples.	68
Figure 69. Air permeability and measured porosity of the hyaloclastite tuff samples.	68
Figure 70. Klinkenberg air permeability versus porosity determined by point counting in thin sections in the hyaloclastite tuff samples.	69
Figure 71. Klinkenberg air permeability and measured porosity in the hyaloclastite tuff samples.	69
Figure 72. Comparison of the concentrations of 9 different oxides in fresh glass and palagonite rinds in a hyaloclastite tuff formation at Fjallabaksleið.....	70
Figure 73. Comparison of the concentrations of 9 different oxides in fresh glass and palagonite rinds in a hyaloclastite tuff formation at Hveradalaskáli	70
Figure 74. Comparison of the concentrations of 9 different oxides in fresh glass and palagonite rinds in a hyaloclastite tuff formation at Reyðarbarmur	71
Figure 75. Comparison of the concentrations of 9 different oxides in fresh glass and palagonite rinds in a hyaloclastite tuff formation at Silfurberg.....	71
Figure 76. Comparison of the concentrations of 9 different oxides in fresh glass and in palagonite rind in a hyaloclastite tuff formation at Votuklettur.	72
Figure 77. Comparison of a whole-rock analysis of a hyaloclastite sample from Fjallabaksleið with an EMP analysis of fresh glass from the same formation	72
Figure 78. Comparison of a whole-rock analysis of a hyaloclastite sample from Hveradalaskáli with an EMP analysis of fresh glass from the same formation.....	73
Figure 79. Comparison of a whole-rock analysis of a hyaloclastite sample from Ingólfsfjall with an EMP analysis of fresh glass from the same formation	73
Figure 80. Comparison of a whole-rock analysis of a hyaloclastite sample from Mosfell with an EMP analysis of fresh glass from the same formation	74
Figure 81. Comparison of a whole-rock analysis of a hyaloclastite sample from Reyðarbarmur with an EMP analysis of fresh glass from the same formation.....	74
Figure 82. Comparison of a whole-rock analysis of a hyaloclastite sample from Silfurberg with an EMP analysis of fresh glass from the same formation	75
Figure 83. Comparison of a whole-rock analysis of a hyaloclastite sample from Votuklettur with an EMP analysis of fresh glass from the same formation	75
Figure 84. Comparison of the WR composition of a hyaloclastite sample and a related crystallized sample from Mosfell.....	76
Figure 85. Comparison of the WR composition of a hyaloclastite sample and a related crystallized sample from Skefilsfjöll eldri.....	76
Figure 86. Comparison of the WR composition of a hyaloclastite sample and a related crystallized sample from Skefilsfjöll yngri	77

Figure 87. Comparison of the WR composition of a hyaloclastite sample and a related crystallized sample from Stóri-Dímon.....	77
Figure 88. Deposition of secondary minerals versus SiO ₂ content of the hyaloclastite tuff samples.....	78
Figure 89. Deposition of secondary minerals versus TiO ₂ content of the hyaloclastite tuff samples.....	78
Figure 90. Deposition of secondary minerals versus Al ₂ O ₃ content of the hyaloclastite tuff samples.....	79
Figure 91. Deposition of secondary minerals versus Fe ₂ O ₃ content of the hyaloclastite tuff samples.....	79
Figure 92. Deposition of secondary minerals versus MnO content of the hyaloclastite tuff samples.....	80
Figure 93. Deposition of secondary minerals versus MgO content of the hyaloclastite tuff samples.....	80
Figure 94. Deposition of secondary minerals versus CaO content of the hyaloclastite tuff samples.....	81
Figure 95. Deposition of secondary minerals versus Na ₂ O content of the hyaloclastite tuff samples.....	81
Figure 97. Deposition of secondary minerals versus P ₂ O ₅ content of the hyaloclastite tuff samples.....	82
Figure 98. Deposition of secondary minerals versus the V content of the hyaloclastite tuff samples.....	83
Figure 99. Deposition of secondary minerals versus Cr content of the hyaloclastite tuff samples.....	83
Figure 100. Deposition of secondary minerals vs. Ni content of hyaloclastite tuff samples.	84
Figure 101. Deposition of secondary minerals vs. Cu content of hyaloclastite tuff samples. ...	84
Figure 102. Deposition of secondary minerals vs. Zn content of hyaloclastite tuff samples. ...	85
Figure 103. Deposition of secondary minerals vs. Rb content of hyaloclastite tuff samples.....	85
Figure 104. Deposition of secondary minerals vs. Sr content of hyaloclastite tuff samples.	86
Figure 105. Deposition of secondary minerals vs. Y content of the hyaloclastite tuff samples.....	86
Figure 106. Deposition of secondary minerals vs. Zr content of the hyaloclastite tuff samples.....	87
Figure 107. Deposition of secondary minerals vs. Nb content of the hyaloclastite tuff samples.....	87
Figure 108. Deposition of secondary minerals vs. Ba content of the hyaloclastite tuff samples.....	88
Figure 109. Deposition of secondary minerals versus La content of the hyaloclastite tuff samples.....	88
Figure 110. The relationship between the Ni and Cr contents of the hyaloclastite tuff samples.....	89

Figure 111. <i>The relationship between the Zr and Nb contents of the hyaloclastite tuff samples.....</i>	89
Figure 112. <i>The relationship between the Rb and K₂O contents of the hyaloclastite tuff samples.....</i>	90
Figure 113. <i>The relationship between the Ni and MgO contents of the hyaloclastite tuff samples.....</i>	90
Figure 114. <i>The relationship between the Cr and MgO contents of the hyaloclastite tuff samples.....</i>	91
Figure 115. <i>The relationship between the Zr and TiO₂ contents of the hyaloclastite tuff samples.....</i>	91
Figure 116. <i>The relationship between the Nb and TiO₂ contents of the hyaloclastite tuff samples.....</i>	92
Figure 117. <i>The relationship between the Zr and Zn contents of the hyaloclastite tuff samples.....</i>	92
Figure 118. <i>The relationship between the Zr and P₂O₅ contents of the hyaloclastite tuff samples.....</i>	93
Figure 119. <i>Zr content versus SiO₂ content of the tholeiitic hyaloclastite tuff samples from the WRZ in comparison with samples of fresh Holocene lavas</i>	93
Figure 120. <i>Zr content versus TiO₂ content of tholeiitic hyaloclastite tuff samples from the WRZ in comparison with samples of fresh Holocene lavas</i>	94
Figure 121. <i>Zr content versus Al₂O₃ content of tholeiitic hyaloclastite tuff samples from the WRZ in comparison with samples of fresh Holocene lavas</i>	94
Figure 122. <i>Zr content versus FeO content of tholeiitic hyaloclastite tuff samples from the WRZ in comparison with samples of fresh Holocene lavas</i>	95
Figure 123. <i>Zr content versus MnO content of tholeiitic hyaloclastite tuff samples from the WRZ in comparison with samples of fresh Holocene lavas</i>	95
Figure 124. <i>Zr content versus MgO content of tholeiitic hyaloclastite tuff samples from the WRZ in comparison with samples of fresh Holocene lavas</i>	96
Figure 125. <i>Zr content versus CaO content of tholeiitic hyaloclastite tuff samples from the WRZ in comparison with samples of fresh Holocene lavas</i>	96
Figure 126. <i>Zr content versus Na₂O content of tholeiitic hyaloclastite tuff samples from the WRZ in comparison with samples of fresh Holocene lavas</i>	97
Figure 127. <i>Zr content versus K₂O content of tholeiitic hyaloclastite tuff samples from the WRZ in comparison with samples of fresh Holocene lavas</i>	97
Figure 128. <i>Zr content versus P₂O₅ content of tholeiitic hyaloclastite tuff samples from the WRZ in comparison with samples of fresh Holocene lavas</i>	98
Figure 129. <i>Zr content versus V content of tholeiitic hyaloclastite tuff samples from the WRZ in comparison with samples of fresh Holocene lavas</i>	98
Figure 130. <i>Zr content versus Cr content of tholeiitic hyaloclastite tuff samples from the WRZ in comparison with samples of fresh Holocene lavas</i>	99
Figure 131. <i>Zr content versus Ni content of tholeiitic hyaloclastite tuff samples from the WRZ in comparison with samples of fresh Holocene lavas</i>	99

Figure 132. <i>Zr content versus Cu content of tholeiitic hyaloclastite tuff samples from the WRZ in comparison with samples of fresh Holocene lavas</i>	100
Figure 133. <i>Zr content versus Zn content of tholeiitic hyaloclastite tuff samples from the WRZ in comparison with samples of fresh Holocene lavas</i>	100
Figure 134. <i>Zr content versus Rb content of tholeiitic hyaloclastite tuff samples from the WRZ in comparison with samples of fresh Holocene lavas</i>	101
Figure 135. <i>Zr content versus Sr content of tholeiitic hyaloclastite tuff samples from the WRZ in comparison with samples of fresh Holocene lavas</i>	101
Figure 136. <i>Zr content versus Y content of tholeiitic hyaloclastite tuff samples from the WRZ in comparison with samples of fresh Holocene lavas</i>	102
Figure 137. <i>Zr content versus Nb content of tholeiitic hyaloclastite tuff samples from the WRZ in comparison with samples of fresh Holocene lavas</i>	102
Figure 138. <i>Zr content versus Ba content of tholeiitic hyaloclastite tuff samples from the WRZ in comparison with samples of fresh Holocene lavas</i>	103
Figure 139. <i>Zr content versus La content of tholeiitic hyaloclastite tuff samples from the WRZ in comparison with samples of fresh Holocene lavas</i>	103

Abstract

Iceland has vast groundwater and geothermal resources in the presently active volcanic zones. Hyaloclastites, which constitute a major part of the strata in these systems, act in a curious way both as a source rock and an aquiclude. This study aims at defining the properties of hyaloclastite formations which control these petrophysical characteristics. It is based on surface coring of 140 tuffaceous formations ranging in age from the latest glaciations to glaciations of 2–3 m.y. ago and of variable alteration. They have been analyzed in several ways, including petrography, geochemistry, petrophysics and SEM. The main emphasis here was to study changes that occur during progressive alteration. The volatile content, which mainly is water, shows a progressive increase with alteration to about 12%, which mainly is bound in the smectite and zeolite alteration minerals. The water content is drastically diminished when these have been altered to chlorite and disappearance of zeolites indicating the dehydration of the alteration minerals. CO₂ content appears to increase stepwise, firstly at about 30%, secondly at 65% and thirdly near 100% alteration. The rock oxidation increases concomitantly with the water content in the rock. This is reflected in the grain density which also diminishes with increasing alteration but increases again when entering into the chlorite-epidote alteration zone. Changes in porosity show that larger pores (macro porosity) are filled as alteration proceeds, while secondary micro porosity increases, mainly at palagonite/glass margins and not the least within the smectite clays. Micro porosity in fully altered tuffs ranges from about 7–35%. This type of porosity may explain the “aquiclude character” of hyaloclastites. Permeability ranges from 0.1 to about 12000 mD and a close correlation is shown between porosity and permeability. This correlation, however, is stronger between macro porosity and permeability than the micro porosity. Chemical analysis of fresh glass and palagonite shows the notable leaching of Na₂O in the latter and to some extent the CaO, while FeO and TiO₂ are slightly enriched. Other oxides do not show obvious tendencies for mobility. The assessment of chemical mobility during alteration, taking into account the filling of macro pores, was unsuccessful, and may be due to the formation of secondary micro porosity which is not the case in alteration of crystallized rocks. A geochemical comparison of the variably altered tuffs with the compositional field of equivalent fresh rocks indicate the limited mobility of the chemical components, except for CaO, Na₂O and Rb which show clear indication of being removed.

1 Introduction

This project is sponsored by Reykjavik Energy, National Energy Authority of Iceland and Iceland GeoSurvey and in co-operation with Moscow University, University of California, Davis and the Natural History Museum of Iceland. Its purpose is to study the role of hyaloclastites in the groundwater and geothermal systems in Iceland. This included the study of progressive palagonitization and succeeding alteration (Helgadóttir, 2005), petrophysical properties (Frolova et al., 2005; Franzson et al., 2010) and then this study of petrophysics and geochemistry which aims at finding relations between petrophysical properties, alteration and geochemical mobility.

The onset of major glaciations about 3 million years ago had profound influence on volcanism in Iceland, both in terms of the landforms produced and the physical properties of the erupted material. Extensive hyaloclastites, mainly comprising pillow basalts, breccias and tuffs, formed in subglacial eruptions during glaciations. In contrast, basalt lava successions dominate Miocene and Pliocene formations in Iceland. This also led to important changes in the physical and chemical properties of the basement when the hyaloclastite formations, intercalated with lava sequences and lesser amounts of sedimentary rocks, became buried in the volcanic pile.

Hyaloclastite tuff particles mostly comprise volcanic glass, i.e., sideromelane and tachylite, and smaller amounts of minerals. The glass, sideromelane in particular, is chemically highly unstable and undergoes alteration at low temperatures, even with minor amounts of water present. In addition to volcanic glass, hyaloclastite formations contain variable amounts of crystalline and partly crystalline rock fragments. Hyaloclastite formations tend to be highly porous, which promotes circulation both of cold groundwater and geothermal fluids. However, with increasing alteration, the permeability tends to decrease markedly.

The difference between hyaloclastites and basalt layers in terms of chemical stability, porosity and other petrophysical properties means that geothermal systems will have different properties, including vigor and duration, depending on whether the main reservoir rock type is hyaloclastite or crystalline basalt. A systematic study of hyaloclastite formations with respect to their chemical and physical properties as reservoir rocks and the changes that occur with time due to the flow of groundwater and geothermal fluids is therefore of great interest. It is also of interest to compare these properties between reservoirs dominated by basalt layers, on the one hand, and hyaloclastites, on the other.

Earlier studies of the petrophysical properties of Icelandic rock formations include the report of Gudmundsson et al. (1995), who collected a wide range of core samples in Iceland for the study of reservoir parameters. Subsequently, the samples went through chemical analysis and a number of tests and point counting in thin sections that were made from the samples. The samples used in the study of Gudmundsson et al. were mostly derived from systems dominated by basalt lava flows. The study of Frolova et al. (2005), however, concentrated on the petrophysical properties of fresh to mildly altered hyaloclastite tuffs. The samples used in this report also include the samples used by Frolova et al. (2005). Franzson et al. (2008) studied chemical transport in fossil geothermal systems dominated by lava flows, and in this report, we adopt some of

their methodology in trying to understand chemical transport in Icelandic hyaloclastites. Recently, a co-author of this report, Pauly (2011) submitted a PhD Dissertation on palagonitization where samples included a few of those dealt with in this report and has furthermore submitted part of his research as an article into G-Cubed.

The emphasis of this report is on the petrophysical properties and chemistry of hyaloclastite tuffs at a relatively low grade of alteration, although some samples are more altered and data on higher grade rocks are also included. In this report, we attempt to unravel changes in petrophysical properties with increasing alteration and to understand element transfer in Icelandic hyaloclastite tuffs. Many studies have shown that palagonitization involves extensive element transfer, probably as a result of dissolution and precipitation, but the length scale or distance of this element transfer has not been studied to the same degree. Here, we try to shed light on the length scales and extent of element transport during the alteration process.

2 Sample collection, measurements and chemical analyzes

For this study, 100 near-surface core samples, about 2 cm in diameter and up to 15 cm long, were collected from hyaloclastite tuff formations in and just outside the neo-volcanic zones in southwest and south Iceland. The formations chosen are subglacial volcanic products, mostly from the last two glaciations but some are as old as 2 Ma. The samples are in general relatively fresh to moderately altered. The cores were split and pieces of each one of them sent to commercial laboratories for bulk-rock chemical and petrophysical analyses. This includes chemical analyses of 10 major oxides, 15 trace elements and loss on ignition (LOI). Additionally, the amount of CO₂ has been determined in most of the samples, and H₂O in 10 of them.

Petrophysical properties, including air permeability, porosity fraction and grain density, were also measured in all core samples, except four, which were unsuitable for the measurements. Earlier, Frolova et al. (2005) measured and reported on the petrophysical properties of about 80 of the samples.

Thin sections were also made of all samples, and subsequently point counting was conducted. In most cases, 1000 points were counted and grouped as one of the following: porosity, unaltered glass, altered glass, unaltered primary mineral, altered primary mineral, zeolite, clay, calcite or other.

In addition to the aforementioned 100 samples, we used chemical and petrophysical data from hyaloclastite formations published by Sigurdsson and Stefánsson (1997), Gudmundsson et al. (1995), Franzson et al. (1997) and Stefánsson et al. (1997). Some of these samples have experienced relatively high grade geothermal alteration or up to the chlorite-epidote zone.

3 Sample description

Most of the new hyaloclastite tuff samples that are presented in this study have a basaltic chemical composition with $\text{SiO}_2 < 51\%$ (Figure 1). As discussed in later sections, the composition is affected by alteration to a variable degree but the evidence, e.g. the phenocryst assemblages, is nevertheless clear that most of the formations that were sampled are basaltic. Some of the samples are ultramafic with $\text{MgO} > 12\%$ and up to $> 25\%$, most likely because of olivine accumulation, whereas a few samples have a composition which suggests an intermediate rock type.

As the histogram in Figure 2 shows, prior to the onset of alteration the hyaloclastite tuff samples generally contain over 80% glass as a portion of solid rock. Since then, the glass has been partly or completely altered and secondary minerals have precipitated to a different extent into the voids. A comparison of the histograms in Figures 3 and 4 reveals that, in most specimens, unaltered glass constitutes less than half of the solid rock by volume, and that altered glass generally comprises about half of the rock. This means that the amount of altered glass as a proportion of the original glass content is in most cases more than 50% (Figure 5). The least amount of alteration of the original glass seen in the samples was 30%. This seems to be the minimum amount of glass alteration required for enough consolidation of the hyaloclastite formations to allow coring.

Primary minerals can constitute a significant part of the tuff samples or up to almost half of the solid rock. In the histogram in Figure 6, the samples have been classified according to the abundance of primary minerals and it can be seen that although most samples have primary mineral content in the range 1–5 vol. %, many samples contain significantly more. In many cases, the primary minerals have been affected by alteration, but they are nevertheless much more resistant to alteration than the glass, and in general the alteration of primary minerals is minor, as a comparison of Figure 6 and Figure 7 shows.

The porosity of the hyaloclastite tuffs was determined by two methods in this study. Firstly, by point counting in thin sections with the aid of a petrographic microscope, and, secondly, the total porosity of the drill cores was measured in air. Hyaloclastites tend to be highly porous, especially the tuffs, where the primary porosity is between grains and also as vesicles in individual grains. In a later section, we discuss evidence for secondary porosity that forms when the tuffs get compacted and altered. From the histogram in Figure 8, which shows the frequency of samples according to porosity determined by point counting in thin sections, one can see that the distribution is bimodal. Most samples have 20–30% porosity but almost as many have 0–10% porosity, and the most porosity determined in the samples is 47%. When original porosity is estimated as the counted porosity plus the amount of secondary minerals filling pores, there is only one peak close to 30% porosity and close to a normal distribution (Figure 9), and the maximum porosity is about 54%. There is also only one peak in a histogram for measured porosity with the largest number of samples with 30–40% porosity (Figure 10). The maximum measured porosity is about 53%.

In addition to fresh and altered glass and primary minerals, the samples contain secondary minerals that have precipitated into voids in the rocks, mostly smectite,

zeolites and calcite. A histogram for the amount of secondary minerals reveals a slightly bimodal distribution, i.e. most samples contain ≤ 1 vol. % secondary minerals but there is a smaller second peak at 20–40 vol. % (Figure 11). It should be noted, however, that the bins are of different size. A similar kind of distribution can be seen in the amount of clay, albeit not as marked (Figure 12). The amount of zeolites is generally smaller and bimodality is not as clear (Figure 13).

The hyaloclastite tuff samples in this study have been inspected by means of secondary electron microscopy (SEM). A selection of BEI (Backscattered Electron Image) photographs of the tuff samples can be seen in Figures 14–21. The samples are at a variable stage of alteration, from slightly altered, where the surface of sideromelane glass particles are only replaced with a thin layer of palagonite (Figure 14), to heavily altered, where all glass has been replaced by a well crystallized mass of smectite and where most porosity has been filled with secondary minerals (Figure 21).

4 Alteration

All the hyaloclastite tuff samples in the study have suffered alteration, with 25–100% of the rocks comprising alteration products. Less altered hyaloclastite formations were not sampled as they were not consolidated enough for coring. The sideromelane glass, which is always by far the most abundant primary constituent of the tuffs, has been either partially or completely transformed into palagonite. Palagonite is the product of hydration, oxidation, and the partial loss of many elements compared to sideromelane. It is generally believed that palagonite is composed of smectite, and that the difference between early-stage gel-palagonite and later-stage fibro-palagonite lies in the crystallinity of the smectite, with gel-palagonite containing embryonic smectite and fibro-palagonite comprising well developed crystals and less H₂O content (see Stroncik and Schmincke, 2002).

Figure 22 shows the relationship between the amount of altered glass and the total alteration of the hyaloclastite tuff samples. Alteration is defined as the abundance of altered primary phases plus secondary minerals filling primary pore space as a proportion of solid rock. Because altered glass is part of the alteration, no points can be found above a diagonal line on the diagram. It can be seen that alteration of glass is dominant in samples with alteration less than 50–60%, but in samples with more extensive alteration, other sources of alteration have become important. Figure 23 shows that the rate of alteration of glass in the samples is fairly well correlated with the total alteration of the rocks. In contrast, alteration of primary minerals generally starts at about 70% total rock alteration (Figure 24), consistent with minerals being more resistant to alteration than glass. Oxidation of Fe in the rocks increases with the amount of alteration as Figure 25 shows, but it appears that the rate of oxidation as a function of alteration increases when the alteration has reached 50–60%. A correlation can also be seen between the ferric-ferrous ratio and the extent of glass alteration in the hyaloclastites with the proportion of ferric iron increasing with increasing glass alteration (Figure 26).

Deposition of secondary minerals, which are generally the most important manifestation of alteration in addition to palagonitization of the glass, also increases at more

than about 50% alteration (Figure 27). This is in agreement with Figure 22, which indicates increasing amount of alteration products other than palagonite from about 50% total alteration. Figure 28, which shows how large part of the primary porosity has been filled as a function of total alteration, suggests a fairly sudden increase in deposition into the pores of the hyaloclastites at about 60% alteration. When the types of deposition minerals are inspected, one can see that the amount of clay (Figure 29), which is probably mostly smectite, and zeolites (Figure 30), tends to increase significantly at about 50% alteration, especially the former. However, the amount of calcite (Figure 31) tends to increase at a higher degree of alteration, or when it is about 60–70%. There is only a weak correlation between the extent of oxidation of Fe and the precipitation of secondary minerals (Figure 32).

5 Volatile content

From Figure 33, which shows the relationship between the LOI (volatile content) and the degree of alteration of the tuff samples, it can be seen that below 50% alteration, LOI does not vary much and is in the range 2–4 wt%. Above 50% alteration, however, LOI tends to increase with increasing alteration, although there could be two jumps in the LOI at about 50% and 70% alteration. Nevertheless, there is clearly a positive correlation between LOI and alteration in the range 50–100%. In Figure 33, we have also plotted previously published data (Franzson et al., 1997; Gudmundsson et al., 1995) that represent samples some of which have experienced mixed-layered-clay grade or chlorite-epidote grade metamorphism. These data show that LOI tends to decrease again as hyaloclastites experience metamorphism of a higher grade than the smectite-zeolite zone.

The H₂O content has only been measured directly in ten of the samples. Since the CO₂ content of the hyaloclastites is in most cases low (Figure 34) compared to the H₂O content, most of the LOI can be explained by H₂O loss. In Figure 35, which shows the relationship between the measured H₂O content and H₂O content calculated as the difference between LOI and CO₂, it can be seen that there is good correlation between the two. However, the calculated H₂O content becomes systematically lower with increasing measured H₂O content, although not by a large amount. Hence, in Figure 36, the amount of H₂O calculated as the difference between LOI and the CO₂ content, shows very much the same trends as LOI (Figure 33), i.e. in the 25–50% alteration range, the H₂O content does not change much and remains at 2–4 wt%. The H₂O content of unaltered hyaloclastite tuffs is likely to be ≤1 wt% and <0.5 wt% in most cases (Nichols et al., 2002). This means that with increasing alteration, the H₂O content increases from this level and reaches 2–4 wt% at about 50% alteration. Like LOI, the H₂O content then increases steadily in the 50–100% alteration range and reaches in some cases concentration over 10 wt%. This change seems to be related to an increase in the amount of hydrous secondary minerals (Figure 27), in particular zeolites (Figure 30) and clay (Figure 29), but smectite and zeolites are generally the most abundant secondary minerals produced by low-grade alteration of hyaloclastites. The chlorite-epidote zone samples in Figure 36 have as little as about 2 wt% H₂O. The H₂O content is not correlated with the total amount of altered glass (Figure 37), presumably because zeolites and clay are also important sources of H₂O in the rocks, but when altered glass

is plotted as a proportion of total glass, it can be seen that the H₂O content starts to increase at about 50% glass alteration (Figure 38). It should be noted, though, that there is some spread, and even at relatively high degree of alteration some of the samples do not have particularly high H₂O content. Still, Figure 39 shows that even when there is no noticeable deposition of secondary minerals, LOI is from 2–8%, but this is probably to a large extent caused by the hydration associated with palagonite formation.

Hence, it appears that at up to about 50% alteration there is a gradual increase in H₂O content, mainly related to palagonite formation, but at that point precipitation of zeolites and smectite increases significantly, and with this the H₂O content of the hyaloclastites. Frolova et al. (2005) noted similar behavior of the Icelandic hyaloclastite samples in their study, and explain this as a consequence of the formation of H₂O-rich minerals, such as zeolites and smectite, at relatively low temperatures. The H₂O-rich mineral assemblage is then replaced by a mineral assemblage poorer in H₂O at higher temperatures and higher degree of alteration. Pauly (2011) has showed that H₂O in palagonite can reach values up to 38%, which may contribute to the relatively high water content measured in the rocks. It must, however, be taken into account that the palagonite has been transformed into lower H₂O content smectite in most of the high water samples.

The CO₂ content of the hyaloclastite samples is generally much lower than the H₂O content, but higher values are seen in some samples at above 60–70% alteration (Figure 34). There is a fairly large range in the CO₂ content at the highest level of alteration but the highest measured abundance is over 8%. The CO₂ content is related to the amount of calcite in the rock (Figure 40), which can be highly variable in rocks at a comparable stage of alteration. The correlation is poor, however, possibly because calcite precipitations are sporadic due to the very slight oversaturation of CO₂. Subsequently, there can be considerable variations in the amount of calcite in different splits of a single sample. The amount of calcite starts to increase at about 70% alteration, i.e. at a higher amount of alteration than smectite and zeolites, and is highly variable at the highest degree of alteration (Figure 31). It should be noted, though, that most of the samples are calcite-free.

As previously noted, oxidation is a ubiquitous feature of the alteration of hyaloclastite formations. Figure 41 shows that there is strong positive correlation between LOI and the ratio between ferric iron and the total iron content. The strong positive correlation is also seen when the H₂O content is plotted instead of LOI (Figure 42), suggesting that oxidation is intimately related to the hydration of the rocks. This also explains why the ferric-ferrous ratio starts to increase at about 50–60% alteration (Figure 25) because the H₂O content shows the same trend when plotted against alteration (Figure 36). Interestingly, there is also correlation between the H₂O (and LOI) and Na₂O contents of the hyaloclastites (Figure 43) with Na₂O concentration decreasing with increasing hydration. This seems to be related to increasing Na₂O losses with increasing alteration as discussed in later sections. Correspondingly, Na₂O losses are also correlated to oxidation of the rocks (Figure 44). There also appears to be a weaker correlation for CaO (Figure 45).

It is not clear why there is an apparent threshold at about 50% alteration, above which hydration and precipitation into the primary pore space tends to increase markedly,

but it could be related to temperature. Obviously, groundwater level also needs to be high enough in the hyaloclastite formation to allow migration of water causing dissolution of the rocks and precipitation of secondary minerals.

6 Grain density

Because of the incorporation of H₂O and CO₂ and the precipitation of hydrous minerals and carbonates, the alteration of hyaloclastites often involves considerable changes in rock density. The grain density (density of rock without voids) of unaltered sideromelane glass is commonly about 2.75 g/cm³ (Stroncik and Schmincke, 2002), whereas palagonite typically has density in the range 1.9–2.1 g/cm³ (Hay and Iijima 1968, Staudigel and Hart, 1983). In agreement with this, a weak negative correlation can be seen between grain density and the extent of glass alteration (Figure 46). The alteration of hyaloclastite also includes precipitation of secondary minerals, at a low grade mainly smectite and zeolites. As these are relatively H₂O-rich minerals, they tend to have low density. At a higher degree of alteration, minerals that are poorer in volatiles replace zeolites and smectite, often leading to higher density of the rock (Frolova et al., 2005).

A diagram showing the average grain density as a function of alteration (Figure 47) bears a resemblance to a diagram showing the relationship between LOI and alteration (Figure 33), however as an upside down image. The grain density is relatively constant up to 50% alteration, at which point it tends to decrease. Then, at over 70% alteration, the grain density tends to level off, and in the samples which have experienced the highest degree of alteration, the density increases again and can be higher than of fresh samples. The most likely explanation for these trends is that the average grain density decreases as low-density zeolites and clay minerals start to form. In the most altered samples, these minerals have then been replaced by less hydrous and denser minerals that tend to be denser than the original basaltic glass comprising the bulk of the original rock. Figures 48 and 49 demonstrate the tendency for a negative correlation between grain density, on the one hand, and LOI and the H₂O content of the rock samples, on the other. This can be explained by the relatively low density of hydrous and CO₂-rich minerals. Considering the strong correlation between the H₂O content and the ratio of ferric iron to total iron content, it comes as no surprise that a weak negative correlation can be seen between grain density and oxidation represented by the ferric iron-total iron ratio (Figure 50).

7 Porosity

Fresh, unconsolidated hyaloclastites are generally highly porous but the visible porosity tends to decrease with increasing amount of alteration as secondary minerals precipitate into the voids. The filling of the voids is promoted by the addition of H₂O, CO₂ and other volatiles through precipitation of hydrous minerals, carbonates, sulfides etc., helped by the element transport associated with palagonitization and the migration of groundwater and geothermal fluids. As discussed above, this affects the density of the rocks, but another important effect is that it influences porosity and hence fluid flow, which in turn affects alteration and precipitation of secondary phases.

As discussed earlier, the porosity of the hyaloclastite tuffs was determined by point counting in thin sections (macro porosity) and measurements in air (measured porosity). A comparison of the porosity determined by the two methods, shown in Figure 51, indicates that as a general rule, measured porosity is higher, and usually much higher, than thin-section porosity. Even where thin-section inspection suggests that all pores have been filled with secondary minerals, measured porosity is up to a third of the bulk rock (Figure 52). This means that hyaloclastite tuffs must contain a significant amount of voids that cannot be detected with the naked eye or even with the aid of a microscope. Franzson et al. (2001) observed this and termed this type of porosity as micro porosity which is the difference between measured porosity and the porosity determined by point counting. The size of micro pores is therefore likely to be smaller than the standard thickness of a thin section, or < 30 μm. The term primary porosity may also be added which is the original porosity of the rock, deduced from the petrographic analysis being the sum of empty pores and mineral deposition into the pores. The point counts in thin sections give % volumes, but in retrospect should be termed area% or % counted.

7.1 Changes in porosity

With increasing alteration, the amount of precipitation of secondary minerals generally increases. However, as discussed earlier, even when no infilling of primary porosity is observed under the microscope, considerable alteration of the samples (Figure 28) can already have occurred. In this case, palagonitization of the primary glass usually accounts for most of the alteration. Figure 53 shows that there is only a relatively weak negative correlation between alteration and measured porosity. This reinforces the conclusion that as the primary pores are being filled with secondary minerals, new porosity, micro porosity, is forming. Thorseth et al. (1991) note large amount of porosity in palagonite in Icelandic hyaloclastite formations.

As a first approximation, micro porosity can be calculated as the difference between the porosity measured in air and the point-counting porosity because it is likely that there is a strong correlation between micro porosity thus calculated and the amount of pores too small to be observed in thin sections by a petrographic microscope. Figure 54 depicts the relationship between micro porosity so defined and the amount of alteration in the hyaloclastite tuffs. A few data points with negative micro porosity indicate that this is not a perfect way of estimating micro porosity. But this could also be due to heterogeneity in porosity of individual samples. Nevertheless, although there

is considerable scatter of data points, a weak positive correlation between micro porosity and alteration can be seen. In Figure 54, the previously published data points of Gudmundsson et al. (1995) have been color coded according to the alteration zone to which they belong. The evidence is inconclusive, but there is a hint that the amount of micro porosity may actually be decreasing at the highest level of alteration.

Figure 55 indicates that there is not an obvious connection between micro porosity and the extent of deposition of secondary minerals, and therefore it does not seem that the formation of the new porosity is closely related to infilling of the rock with alteration minerals. However, there could be a weak positive correlation between micro porosity and the amount of clay deposition in the hyaloclastite samples (Figure 56), suggesting that either the clay precipitations are relatively porous or the process that causes micro porosity also results in clay formation. The lowering of micro porosity in the chlorite-epidote zone could be caused by the compaction of the clay mineral structure as smectite transforms to chlorite.

7.2 The sources of micro porosity

It therefore appears that as primary porosity is being filled during the alteration process; a new type of porosity is being formed, which partly compensates for the loss of the primary porosity. SEM photography yields further clues as to the hidden porosity of the hyaloclastite tuffs.

Fine fractures or micro fractures are an obvious source of porosity in the samples (Figures 57 and 58). In Figure 57, the fractures are commonly partly or wholly lined with palagonite. In some cases, micro fractures penetrate both fresh sideromelane glass and palagonite rinds (Figure 58). In some other cases, the fractures are only seen in the palagonite, often between different layers of palagonite (Figure 59). In the latter case, it is possible that the fractures actually developed because of dehydration after the sample collection, and therefore do not represent micro porosity in the hyaloclastite formation. In fact, it was observed during the SEM work that micro fractures became wider while the samples were inside the instrument. In some samples, sealed micro fractures are also seen alongside open fractures (Figures 60 and 61).

It is generally thought that the formation of palagonite from sideromelane glass occurs by a dissolution-precipitation process (Stroncik and Schmincke, 2002). Microbial activity may also be a contributing factor. Many workers have described microscopic tubules at the rims of glass grains undergoing palagonitization (e.g. Melson and Thompson, 1973; Staudigel and Hart, 1983; Thorseth et al., 1992; Walton and Schiffman, 2003). Similar tubules are seen in some samples in this study (Figures 62 and 63). Additionally, in other samples, rather than tubules, there are microscopic pits between the palagonite rind and the sideromelane glass (Figures 64 and 65). Thorseth et al. (1992) describe similar textures in their study, and propose that different kinds of microbes are active in producing tubules and pits. Drief and Schiffman (2004) report a "leached layer" formed as a result of glass dissolution and may be part of micro porosity. Because of the large surface area of the glass particles and the pervasiveness of the tubules and pits, they could be the source of considerable amount of micro porosity, albeit quite variable between samples.

The sample in Figures 66 and 67 is a hyaloclastite tuff that has suffered relatively high degree of alteration, as seen by the considerable deposition of secondary minerals and the fact that the primary basaltic glass has been replaced by a smectite. It can also be seen that the smectite is highly porous, which in this particular sample could be a source of significant amount of micro porosity. This is in agreement with the observation that there is a hint of a correlation between micro porosity and the clay content of the hyaloclastite tuff samples (Figure 56). The amount of porosity is also likely to be affected by the grain size and the development of the smectite.

The evidence presented above indicates that micro porosity could arise from at least three different classes of phenomena within the hyaloclastite tuffs; micro fractures, tubules and pits at glass rims, and smectite intergrowth. Moreover, the importance of different types of micro porosity could be highly variable between hyaloclastite formations or even from one place to another within a single formation. With increasing alteration, palagonite disappears when it is replaced by secondary minerals, initially, a volatile-rich phase assemblage and then at a high degree of alteration, a relatively volatile-poor, more dense phase assemblage where smectite has transformed to chlorite. A possible consequence of these changes is the gradual decrease in micro porosity.

7.3 Permeability and porosity

Air permeability was among the petrophysical properties that were measured in most of the samples. The permeability is obviously closely related to the porosity as Figures 68–71 show. In Figure 68, where air permeability versus the porosity determined by point counting in thin sections is shown, it can be seen that there is a positive correlation between these two features, and that even when no porosity is seen under the microscope there is some permeability. The likely reason for this is the presence of micro porosity. Figure 69 shows that the lowest measured porosity is about 10% and that the permeability in the least porous samples is low, suggesting that fluid flow through micro pores is likely to be ineffective. Recalculation of air permeability by the Klinkenberg correction leads to only minor changes in permeability (Figures 70 and 71).

8 Chemical transfer

The chemical instability of hyaloclastite tuffs is evident from the alteration that occurs even at low temperatures soon after an eruption, and the abundant secondary mineralization seen in such formations. It is well established that different elements behave differently during the alteration of hyaloclastites, and that there are many different chemical, physical and even biological variables that affect the alteration process and lead to a range of outcomes (e.g. see Stroncik and Schmincke, 2002). In the following section, we attempt, step-by-step, to unravel the relative mobility of different major and trace elements in the Icelandic hyaloclastite tuffs. The emphasis is on resolving the relative mobility of the elements and the length scale (the distance), on which the chemical transfer occurs.

8.1 Chemical mobility in basaltic glass caused by palagonitization

Studies of the composition of palagonitized glass have shown that compared to unaltered sideromelane glass, the coexisting palagonite tends to have lower concentrations of all major cations except Fe and Ti (e.g. Jakobsson, 1996; Stroncik and Schmincke, 2002). In detail, Stroncik and Schmincke (2001) propose that the formation of gel-palagonite involves loss of Si, Al, Mg, Ca, Na and K, whereas Ti and Fe are immobile. However, they maintain that while Ca and Na losses continue with growing maturity of the palagonite, the concentrations of Si, Al, Mg and K in the palagonite start to increase and those of H₂O, Ti and Fe decrease. The evidence regarding trace elements is more contradictory. Pauly (2011) concluded that REE were immobile during palagonitization. Palagonitization also involves considerable hydration (10–40 wt %, Stroncik and Schmincke 2002) and oxidation of Fe. The palagonitization process seems to be nearly isovolumetric, however (e.g. Jakobsson and Moore, 1986).

Sideromelane glass and the palagonite product have not been systematically analyzed in the hyaloclastite tuffs of this study to compare their compositions, but a few samples have been analyzed with the electron microprobe. Figures 72–76 show the concentrations of nine major oxides in palagonite rinds in comparison with fresh glass in five different hyaloclastite formations. These are spot analyses acquired with an energy-dispersive spectrometer. Each symbol in the diagrams represents a comparison of an analysis of unaltered glass with one analysis of a palagonite rind in the same sample. The diagonal line indicates equal concentrations in the fresh glass and the palagonite rinds. As the glass becomes hydrated during palagonitization, which leads to low totals for electron-microprobe analyses, the palagonite analyses have been normalized so that the totals are 100%. These figures indicate that some oxides are highly mobile during palagonitization. This is especially true for Na₂O, which seems to be leached out of the palagonite rinds to a large extent. CaO also appears to be preferentially lost from the rinds. Other oxides do not show as obvious tendencies or, as in the case of FeO and TiO₂, increase in concentration, suggesting resistance to mobilization. This is in excellent agreement with the results of earlier studies on the palagonitization of Icelandic hyaloclastites (Jakobsson, 1996). Hence, the evidence points to considerable mobility of most major cations, except Fe and Ti, during palagonitization. Na seems to be the most mobile cation.

8.2 Changes in whole-rock chemical composition by palagonitization

Although palagonitization is pervasive in hyaloclastite formations, it is a microscopic process. Thus, our next step is to try to unravel how far the mobile elements are transported during this process and whether changes comparable to those occurring in palagonite rinds also occur on greater length scales, such as those of hand specimens and drill cores.

As a part of this study, the whole-rock compositions of the hyaloclastite tuff samples were determined. In Figures 77–83, these chemical analyses are compared to spot analyses of fresh glass from the same formations by means of the electron microprobe.

Here, the glass analyses are meant to represent the initial composition of the hyaloclastite tuff before palagonite alteration and related element transfer starts. It should be noted, however, that in phenocryst-rich tuffs, the whole-rock compositions could be considerably different from the melt compositions represented by the glasses. For instance, in a sample rich in the common phenocryst phases olivine and plagioclase, the whole-rock composition should be richer in MgO and Al₂O₃ than unaltered glass in the same sample.

All of the hyaloclastite samples, of which we have glass analyses, are indeed enriched in MgO compared to the glasses, and we interpret this as the effect of the accumulation of olivine phenocrysts. In all the samples, the Na₂O concentration is also lower in the bulk rock than the glass. However, Na₂O enrichment of the melt, represented by the glass, could be caused by the crystallization of phenocrysts. So the evidence is ambiguous as to whether the low Na₂O content of the bulk rock compared to the glass is caused by the loss of Na₂O from the rock as consequence of alteration or the enrichment of the glass by magmatic processes. The evidence for other oxides is also inconclusive.

In spite of this ambiguity, it is clear that the differences in composition between unaltered glass and whole-rock compositions are generally considerably smaller than between unaltered glass and palagonite rinds (Figures 72–76), which suggests that element transport is, at the very least, much less on the scale of a hand sample compared to the micro scale of palagonite rinds, with the possible exception of Na.

8.3 Composition of hyaloclastite tuff samples compared to crystallized whole-rock samples

In Figures 84–87, the whole-rock compositions of four of the hyaloclastite samples are compared to the compositions of crystallized rock fragments from the same formations. Both major and trace elements are used in the comparison. This is to test whether the hyaloclastites are systematically modified relative to crystallized rock samples, which at the time of eruption probably had a composition similar to the hyaloclastites but should be more resistant to alteration and chemical transfer (Franzson et al., 2008).

The points on the figures have considerable scatter, probably to some extent as a consequence of the combination of analytical uncertainty and heterogeneity of the respective formations. As a general rule, however, no element shows unequivocal evidence for being lost or gained during palagonite formation, except perhaps Na₂O, which is in all cases in lower concentration in the hyaloclastite than in the respective crystallized rock sample. So even if many elements become mobile when basaltic glass goes through palagonitization, the evidence so far suggests that they do not migrate far, and on the scale of a hand sample, the chemical compositions of the hyaloclastites is largely intact. The only oxide that appears to be an exception to this rule is Na₂O. However, there is too much scatter to draw any firm conclusions.

8.4 Chemical changes with increasing secondary mineralization

In their study of geothermally altered Icelandic rocks, Franzson et al. (2008) came to the conclusion that certain elements, notably Zr, are nearly immobile during geothermal alteration. However, their analysis is primarily based on the study of largely crystalline basalt samples. It is not given that these results are also valid for hyaloclastite tuffs that are largely composed of highly porous and chemically reactive volcanic glass particles, which release all elements on alteration. In contrast, basalts are less porous and largely crystalline and release elements into solution mostly according to the stability of the primary minerals in the rock.

In Figures 88–109, the concentrations of individual major oxides and trace elements in the hyaloclastite samples are plotted against the amount of deposition of secondary minerals into the pore space of the hyaloclastite tuffs. The concentrations have been recalculated to yield totals of 100% with H₂O and CO₂ excluded. Also drawn on each diagram are two lines that form the sides of a triangle with an apex at 100% deposition and 0% element concentration. In figures of this kind, as Franzson et al. (2008) demonstrate, one would expect different distribution patterns for elements depending on their mobility and whether the element concentration tends to increase or decrease with increasing precipitation of secondary minerals. For an immobile element, which is neither removed by a permeating fluid nor in the precipitates, the infilling of secondary minerals into the pore space should simply cause dilution. If this were the case, the concentrations in Figures 88–109 should tend to fall within the areas enclosed by the lines drawn on the diagrams, provided that the range of concentrations along the x-axes, where there is minimum amount of deposition, is representative of unaltered samples. By the same token, if mobile elements tend to decrease or increase in the formations with increasing deposition, they should trend toward the left or right side of the enclosed area, respectively.

None of the oxides shown in Figures 88–97 behave strictly in accordance with the criterion for being immobile. Most of them have a similar or a slightly larger range in samples with considerable deposition of secondary minerals as in samples free of deposition. However, some of the oxides, for instance Na₂O and K₂O, become significantly more scattered with increasing deposition. Using the rationale discussed earlier, this would suggest increasing concentrations of all the main oxides. This can obviously not be true. A more logical explanation is that the oxides are roughly in the same proportion in the altered rocks as in the unaltered rocks, unaffected by the secondary mineralization. This would also mean that the concentrations of the oxides are roughly the same in the secondary minerals as in the unaltered rock. One possible explanation is that although the major oxides are mobile on a microscopic scale during palagonitization, they are generally relatively immobile on the scale of a hand sample and are simply being transported from the glass during palagonitization to the secondary minerals precipitating nearby. The decreasing porosity of the samples with increasing alteration suggests addition of mass, but this can be explained by the addition of H₂O and CO₂ and by the replacement of the primary rock constituent, basaltic glass, by lower density secondary minerals. Also, as discussed in an earlier section, the loss of primary porosity is partially offset by the formation of micro

porosity, which means that the addition of mass is less than the decreasing primary porosity indicates.

Similar to major oxides, trace elements (Figures 98–109) do not show unequivocal signs of being immobile and they tend to be even more scattered than the oxides. This could be in part because of the larger primary concentration range of many of the trace elements and the effect of crystal accumulation. However, the same explanation is likely to be applicable to most of the trace elements as to the major oxides, that most of them are mobile on micro scale but relatively immobile on macro scale. Judging from Figures 98–109, Ni (Figure 100) and Sr (Figure 104) are the trace elements that seem to come closest to being immobile. This could be related to their strong affinity for olivine and plagioclase, respectively, and therefore Ni and Sr are likely to become mobile only when olivine and plagioclase start to be affected by alteration to a significant extent.

In calculating the amount of deposition in Figures 88–109, we have used the amount of porosity by point counting in thin sections. When measured porosity is used instead, the results are essentially the same, namely that deposition of secondary minerals has in most cases small effect on the distribution of major oxides and trace elements in the hyaloclastite tuff samples. Certainly, no coherent trends can be seen.

The effect of micro porosity has not been considered either. Because of micro porosity, the volume of secondary mineralization could be less than point counting in thin sections indicates. It was noted earlier that there could be a correlation between micro porosity and the amount of clay infilling (Figure 56), which could be caused by high porosity of clay. However, if one subtracts the amount of micro pores from deposition on the assumption that all of the micro porosity occurs in the secondary minerals, in many cases the amount of deposition becomes negative, i.e. the volume of micro pores often exceeds the volume of precipitates. This suggests that micro porosity not only forms in the secondary minerals that have precipitated in the voids in the rocks but is also in the primary rock, which is agreement with the conclusions in the earlier section on micro pores. As we are unable to quantify the proportion of micro pores in the precipitates, the effect of micro porosity on deposition cannot be adequately evaluated. Nevertheless, examination of the data where micro pores are considered does not suggest that it will change the trends, or the lack thereof, seen in Figures 88–109.

In essence, a comparison with the results of the study of Franzson et al. (2008), where the samples were basalts, in some cases of considerably higher metamorphic grade than the hyaloclastite tuffs, suggests that there is an important difference in chemical mobility during the alteration of basalts and hyaloclastites. Whereas Franzson et al. (2008) found that certain elements were largely immobile during the alteration process and were diluted by the deposition of secondary minerals, we find that no element in the hyaloclastite tuffs can be considered completely immobile during palagonitization. The elements that come closest to being immobile are a few trace elements, which are probably to a large degree incorporated into the crystal structures of phenocryst phases.

8.5 Evidence for element mobility from geochemical trends

One method of evaluating element mobility is to inspect the correlation of elements, i.e. chemical trends, produced by magmatic processes. If elements are mobile, alteration most likely will lead to the deterioration of such trends, especially if the elements that produce the trends behave differently during geothermal alteration. Here, we examine whether chemical trends, which are present in unaltered Holocene basaltic lavas from the Western Rift Zone (WRZ) of similar petrogenetic provenance as the hyaloclastite tuff samples, are still present in the tuff samples. It should be noted that only the tholeiitic tuff samples of the WRZ are directly comparable to the Holocene lava samples, whereas the transitional alkalic tuff samples of South Iceland tend to have different geochemical systematics. Since information on the compositions of fresh transitional alkalic lavas from South Iceland is scarce, a meaningful comparison cannot be made with the hyaloclastite samples from this area.

The trends of unaltered Holocene lavas from the WRZ shown in Figures 110–118 are based on unpublished analyses from Björn S. Harðarson and Sveinn P. Jakobsson, and published analyses from various sources retrieved from the GEOROC data base. An inspection of diagrams, which show the relationship between elements that correlate well in unaltered Holocene basalts from the WRZ, reveals that some trends are still present and apparently little affected by alteration of the hyaloclastite tuffs. This includes the relationship between Ni and Cr (Figure 110) and Zr and Nb (Figure 111). In other cases, such as Rb *vs.* K₂O (Figure 112), strong correlation present in the fresh lavas has become indistinct in the hyaloclastites. The concentration of Ni is likely to be largely controlled by its strong preference for entering olivine, and Cr is likely to be present mostly in chromian spinel phenocrysts, which tend to be trapped by growing olivine phenocrysts. This can be seen from the strong correlation between the MgO content, on the one hand, and Ni (Figure 113) and Cr (Figure 114) contents, on the other. Although olivine is highly sensitive to geothermal alteration and already altered in many of the samples, this does not seem to mobilize Ni and Cr. Plagioclase, which is the common phenocryst phase in addition to olivine, is highly resistant to geothermal alteration and only becomes markedly altered at over 200°C, considerably higher temperature than most of the samples in this study have experienced.

As basaltic glass is by far the most abundant phase comprising the tuff samples and is also highly susceptible to alteration, it is of interest to determine element mobility caused by the alteration of the glass. For this purpose, it is instructive to look at elements that are highly incompatible, and thus greatly prefer melt to crystals. In their study of chemical transport in geothermal systems in Iceland dominated by basaltic lavas, Franzson et al. (2008) came to the conclusion that the concentration of Zr is largely unaffected by the geothermal alteration, even at high-temperature conditions. This also seems to be the case in the hyaloclastite tuff samples. Plots of Zr and a few other elements (Figures 111, 115, 117 and 118), some with very different geochemical behavior than Zr, show a good correlation, similar to that seen in fresh basalts from the WRZ. This indicates that Zr is relatively immobile on a length scale comparable to the hand samples during the palagonitization process, and, by the same token, so seems to be the case for Nb, Zn, TiO₂, and P₂O₅. Moreover, because Zr is a highly incompatible element in basaltic systems, it has a relatively large range in concentration but

generally high enough abundance so that precise quantitative analyses are feasible. As a corollary, Zr is a good element to evaluate the mobility of other elements by plotting them together and ascertain the extent of scatter from the original magmatic trends, provided all samples have a similar petrogenetic provenance.

8.6 Evidence for element mobility from the relationship between Zr and some major and trace elements

In Figures 119–139, the concentration of Zr has been plotted against the concentrations of various major and minor oxides and trace elements in the hyaloclastite samples. These figures only include tholeiitic samples from the WRZ. Filled blue, yellow and red circles represent samples with 25–50%, 50–75% and 75–100% alteration, respectively, where, again, the alteration is defined as the sum of altered glass, altered primary minerals, and secondary minerals as a proportion of solid rock. For comparison and as an aid in evaluating deviations of the hyaloclastite data from the normal range of unaltered basalts, the outline of the trend of unaltered Holocene lavas from the WRZ has also been drawn on each diagram. Like before, this range is based on the unpublished data sets of Björn S. Harðarson and Sveinn P. Jakobsson, and published data from various sources retrieved from the GEOROC data base. The fact that Zr and some of the other elements form relatively tight and coherent trends that agree well with the Holocene lava trends indicates, firstly, that the concentration of Zr is indeed little affected by the alteration of the hyaloclastites, and, secondly, that there is probably no discernible geochemical difference between the Pleistocene and Holocene volcanic products.

The concentration of TiO_2 (Figure 120) seems to be largely intact by the palagonitization process. FeO , MnO and Al_2O_3 (Figures 122, 123 and 121, respectively) have a wider range of compositions, but the hyaloclastite tuffs fall mostly within the fields of unaltered lavas. A single point of unusually low Al_2O_3 content represents a highly olivine-phyric sample from Hellisskarð. MgO , Cr and Ni (Figures 124, 130 and 131, respectively) fall largely within the Holocene field but some of the samples appear to be affected by olivine accumulation, which causes them to extend to higher concentrations at about 100–150 ppm Zr concentration. SiO_2 also has a very wide range, and partly outside the Holocene field, but the most altered samples both have high and low SiO_2 contents (Figure 119). Na_2O is the oxide that is most obviously affected by alteration and its deviation from the field of fresh lavas shows strong correlation with the amount of alteration (Figure 126). Interestingly, Na_2O seems to be lost from most samples and to an increasing extent with increasing alteration, although there are two exceptions where the Na_2O concentration seems to be elevated. CaO does not exhibit as clear trends but the tendency seems to be the same (Figure 125). In the most altered samples, P_2O_5 (Figure 128) and especially K_2O (Figure 127) have become mobile and the hyaloclastites can either show gain or loss of these elements. Among trace elements, Zn , Cu and Sr (Figures 133, 132 and 135, respectively) appear to be relatively stable, but the Sr trend is probably affected by plagioclase accumulation. On the other hand, V seems to be quite mobile (Figure 129), and like Na_2O and CaO , its concentration tends to decrease with increasing alteration, whereas the concentration of Rb (Figure 134) appears to increase with increasing alteration. Ba (Figure 138) also

appears to become mobile with increasing alteration and tends to be lost from the hyaloclastite tuffs.

The conclusion is that despite the mobility caused by palagonitization most elemental trends seem to be little affected by the alteration of the hyaloclastite tuffs, with a few notable exceptions. The elements most affected are generally alkali or alkali earth elements. However, there are indications that in the most altered samples more elements are becoming mobile.

9 Conclusions

The hyaloclastite tuff samples in this study are about 25–100% altered. In the least altered samples, palagonitization is the dominant source of alteration. At about 50% alteration, the amount of secondary mineralization proliferates, especially by precipitation of smectite and zeolites. Calcite precipitation seems to start to grow at a higher degree of alteration or about 60–70%.

Changes in the volatile content of the hyaloclastites reflect the changes in the amount of secondary minerals. The H₂O content of fresh sideromelane is likely to be on the order of ≤ 1 wt% and the CO₂ content is negligible. At about 50% alteration, the H₂O content has reached about 2–4 wt%, at which point it starts to rise significantly, concurrently with the growth of H₂O-bearing smectite and zeolites. CO₂ concentration starts to increase at about 60–70% alteration, parallel with growth of calcite.

The average grain density of the samples appears to be relatively constant at about 2.65–2.8 g/cm³ at up to about 50% alteration, when it starts to decrease and falls down to about 2.3–2.6 g/cm³ at 100% alteration. However, previously published data show that hyaloclastite tuff samples that have reached chlorite-epidote zone metamorphism have become considerably denser and are even denser than fresh sideromelane glass. Apparently, palagonitization does not have much influence on the density of the tuff samples, even if palagonite is considerably less dense than sideromelane, probably because palagonite only forms thin rinds (usually ≤ 10 μ m) on glass particles. The grain density starts to decrease with the precipitation of smectite and zeolites, which have relatively low density.

As primary pores are being filled because of the precipitation of secondary minerals, a new type of porosity, micro porosity, forms, and partly compensates for the loss of the primary porosity. The diameter of the micro pores is likely to be smaller, in general, than the thickness of a standard thin-section (30 μ m). The possible sources of micro porosity include micro fractures, porous smectite and tubules and pits at the interface between sideromelane glass and palagonite rinds. The tubules and pits could be produced by biological activity.

During palagonitization, all elements in the sideromelane glass seem to become mobile. Trace elements that are to a large extent incorporated into common phenocryst phases appear to be the exception. However, the transport distance of most elements seems to be short. The whole-rock analyzes of the drill cores indicate little change in composition of the hyaloclastite tuff samples compared to unaltered Holocene lavas from the same region. The elements that do appear to be mobile are mostly alkali and alkali earth elements. This is most noticeable with Na and, to a lesser extent, Ca. Zr and

TiO₂ are shown to be immobile which is in line with other studies (e.g. Franzson et al., 2008). The latter may however be more mobile on the micro scale as the studies of Pauly (2011) have shown.

The samples in this study have experienced relatively low temperature alteration. It is possible that elements such as Na and Ca are transported toward hotter parts of geothermal systems and accumulate disproportionately there in high-temperature secondary minerals.

Hyaloclastites differ from largely crystalline basalts in element-deposition figures in that most elements are more mobile on microscopic scale. This means that element-deposition figures are generally not useful for hyaloclastites.

10 Recommendations for further work

This report describes the changes that take place within hyaloclastite tuffs from a relatively fresh state to total alteration. Most of the formations, however, would be synonymous to those expected to reside in the colder groundwater systems. The alteration, and especially where deposition sets in, appears at 50–70% alteration state of the tuffs. This state can be observed in some other parameters. A closer study should be made to find at what hydrological condition this occurs in the groundwater systems.

As these kinds of rocks are found in groundwater and geothermal systems worldwide, the data would be of interest outside Iceland. This report is written in English in order to comply with our collaborators abroad and also set up as a prelude to a paper in an international peer reviewed journal. We would propose two papers, where the first one would be mainly derived from the study of Helga Margrét Helgadóttir (2005) who made a close systematic study of the various types of palagonitization in the tuff, with additional data from the SEM study. The second paper would mainly contain data and interpretations from this study (which is organized in such a way) along with a closer connection to the groundwater systems. Contributions from our collaborators would be expected in these papers.

The data gathered has only partly been published and are archived in personal folders. The project is an extension of a larger petrophysical data bank which contains Icelandic samples of most rock types and alteration states. We consider this data collection to be of wide interest e.g. in evaluation of reservoir characteristics in groundwater and geothermal systems. For that to happen it is imperative that this data should be categorized into a computer data bank in such a way that interested parties could easily access the data of interest. We would think it appropriate to name that databank in honour of the late Valgardur Stefánsson, who was the instigator of the project.

11 References

- Drief, A. S. and Schiffman, P. (2004). Very low temperature alteration of sideromelane in hyaloclastites and hyalotuffs from Kilauea and Mauna Loa Volcanoes: implications for the mechanism of palagonite formation. *Clays and Clay Minerals*, 53, 5, 623–635.
- Franzson, H., Fridleifsson, G., Ó., Gudmundsson, Á. and Vilmundardóttir, E. G. (1997). *Reservoir parameters. Status of petrological studies by the end of 1997*. Report Orkustofnun OS-97077 (in Icelandic). 57 pp.
- Franzson, H., Gudfinnsson, G. H., Helgadóttir, H. M. and Frolova J. (2010). Porosity, density and chemical composition relationships in altered Icelandic hyaloclastites. In Birkle & Torres-Alvarado (ed.), *Water-Rock Interaction*. 199–202.
- Franzson, H., Gudlaugsson, S. Th. and Friðleifsson, G. Ó. (2001). Petrophysical properties of Icelandic rocks. *Proceedings of the 6th Nordic Symposium on Petrophysics, 15–16 May 2001, NTNU, Trondheim, Norway*, 14 pp.
- Franzson, H., Zierenberg, R. and Schiffmann, P. (2008). Chemical transport in geothermal systems in Iceland. Evidence from hydrothermal alteration. *Journal of Volcanology and Geothermal Research* 173, 217–229.
- Frolova, J., Ladygin, V., Franzson, H., Sigurdsson, Ó., Stefánsson, V. and Shustrov, V., (2005). Petrophysical properties of fresh to mildly altered hyaloclastite tuffs. *Proceedings World Geothermal Congress 2005, Antalya, Turkey, 24–29 April 2005*, 15 pp.
- Gudmundsson, Á., Franzson, H. and Fridleifsson, G. Ó. (1995). *Forðafræðistuðlar. Söfnun sýna*. Report Orkustofnun OS-95017/JHD-11 B, 72 pp.
- Hay, R. L. and Iijima, A. (1968). Nature and origin of palagonite tuffs of the Honolulu Group on Oahu, Hawaii. In: *Studies in volcanology – a memoir in honor of Howel Williams*. Geol. Soc. Am., Boulder, p. 331–376.
- Helgadóttir, H. M. (2005). *Formation of palagonite. Petrographical analysis of tuffs from the Western Volcanic Zone in Iceland*. Unpublished B.Sc. thesis, University of Iceland, 40 pp.
- Jakobsson, S. P. (1996). Eiga gerlar þátt í ummyndun basaltgjóskunnar í Surtsey? *Búvísindi* 10, 273–289.
- Jakobsson, S. P. and Moore, J. G. (1986). Hydrothermal minerals and alteration rates at Surtsey volcano, Iceland. *Geol. Soc. Am. Bull.* 97, 648–659.
- Melson, W. G. and Thompson, G. (1973). Glassy abyssal basalts, Atlantic sea floor near St. Paul's Rocks: petrography and composition of secondary clay minerals. *Geol. Soc. Am. Bull.* 84, 703–716.
- Nichols, A. R. L., Carroll, M. R. and Höskuldsson, Á. (2002). Is the Iceland hot spot also wet? Evidence from the water contents of undegassed submarine and subglacial pillow basalts. *Earth Planet. Sci. Lett.* 202, 77–87.

- Pauly B. P. (2011). *In Situ Micro-analytical Investigations of Palagonitization*. PhD dissertation from University of California in Davis. 180 pp.
- Sigurdsson, Ó. and Stefánsson, V. (1994). *Reservoir parameters. Measurements of rock samples*. Report Orkustofnun OS-94049/JHD-28 B (in Icelandic). 35 pp.
- Staudigel, H. and Hart, S. R. (1983). Alteration of basaltic glass: mechanisms and significance for the oceanic crust-sea water budget. *Geochim. Cosmochim. Acta* 47, 337–350.
- Stefánsson, V., Sigurdsson, Ó., Gudmundsson, Á., Franzson, H., Fridleifsson, G., Ó. and Tulinius, H. (1997). Core Measurements and Geothermal Modelling. Second Nordic Symposium on Petrophysics. Fractured reservoir. *Nordic Petroleum Series: One*, pp. 198–220.
- Stroncik, N. A. and Schmincke, H.-U. (2001). The evolution of palagonite: Crystallization, chemical changes, and element budget. *Geochem. Geophys. Geosyst.* 2, Paper number 2000GC000102.
- Stroncik, N. A. and Schmincke, H.-U. (2002). Palagonite – a review. *Int. J. Earth Sci. (Geol. Rundsch.)* 91, 680–697.
- Thorseth, I. H., Furnes, H. and Tumyr, O. (1991). A textural and chemical study of Icelandic palagonite of varied composition and its bearing on the mechanism of the glass-palagonite transformation. *Geochim. Cosmochim. Acta* 55, 731–749.
- Thorseth, I. H., Furnes, H. and Heldal, M. (1992). The importance of microbiological activity in the alteration of natural basaltic glass. *Geochim. Cosmochim. Acta* 56, 845–850.
- Walton, A. W. and Schiffman, P. (2003). Alteration of hyaloclastites in the HSDP 2 Phase 1 Drill Core: 1. Description and paragenesis. *Geochem. Geophys. Geosyst.* 4(5), 8707.

12 Figures

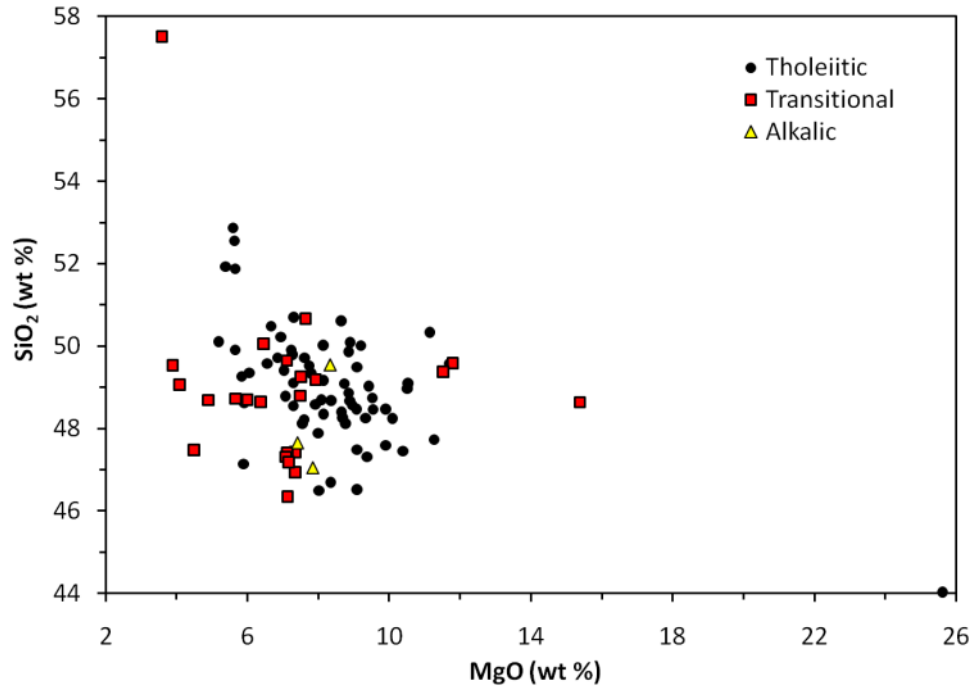


Figure 1. *SiO₂ content versus MgO content of the hyaloclastite tuff samples. The samples are classified according to petrological series.*

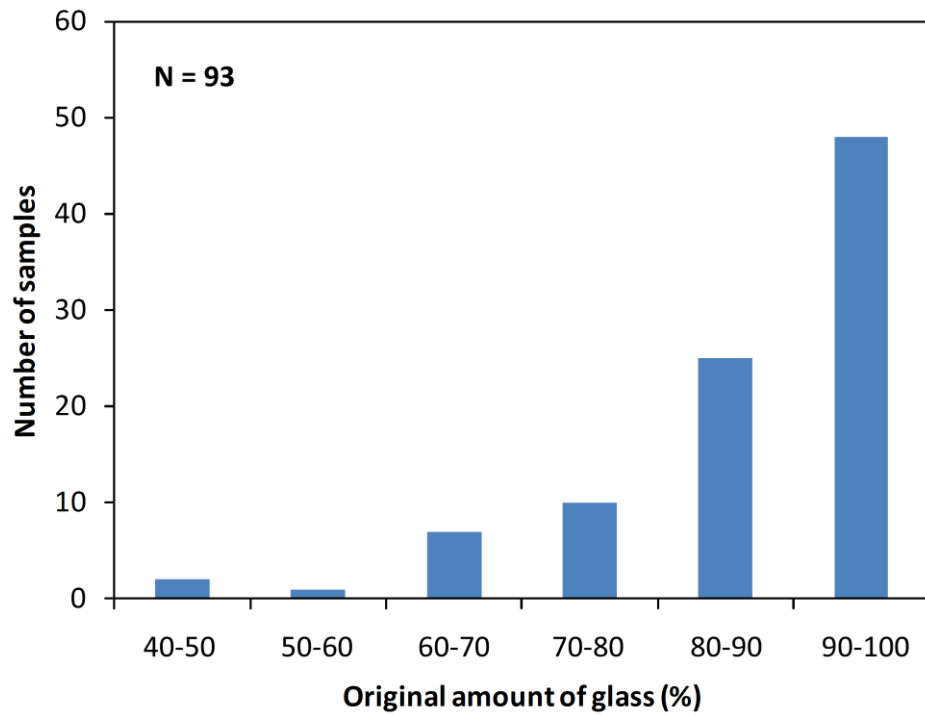


Figure 2. *Histogram showing sample frequency depending on the original amount of glass as a proportion of solid rock.*

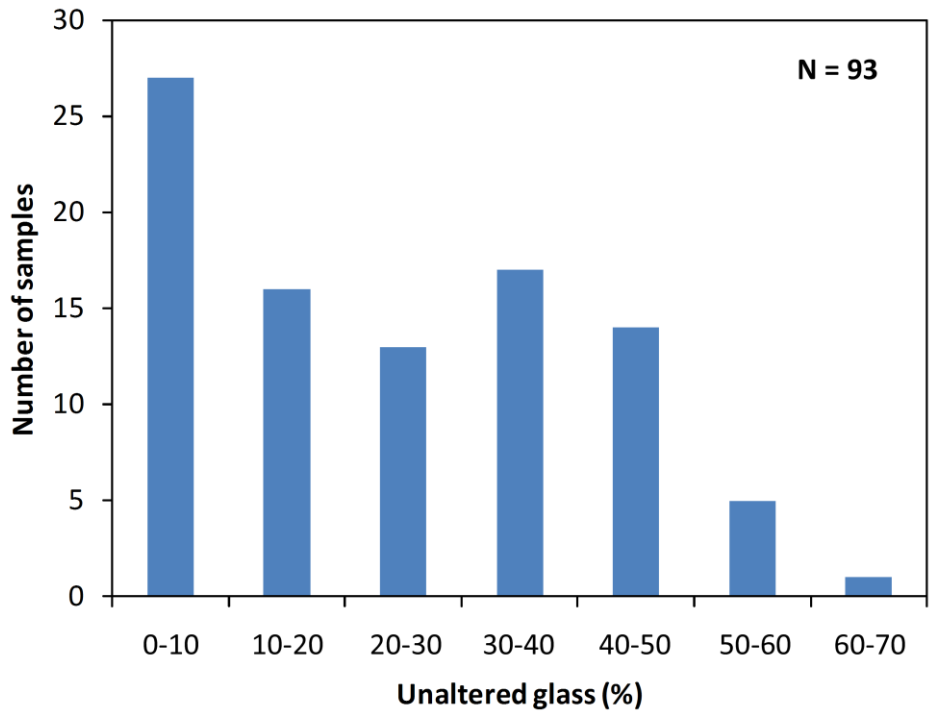


Figure 3. Histogram showing sample frequency depending on the abundance of unaltered glass as a proportion of solid rock.

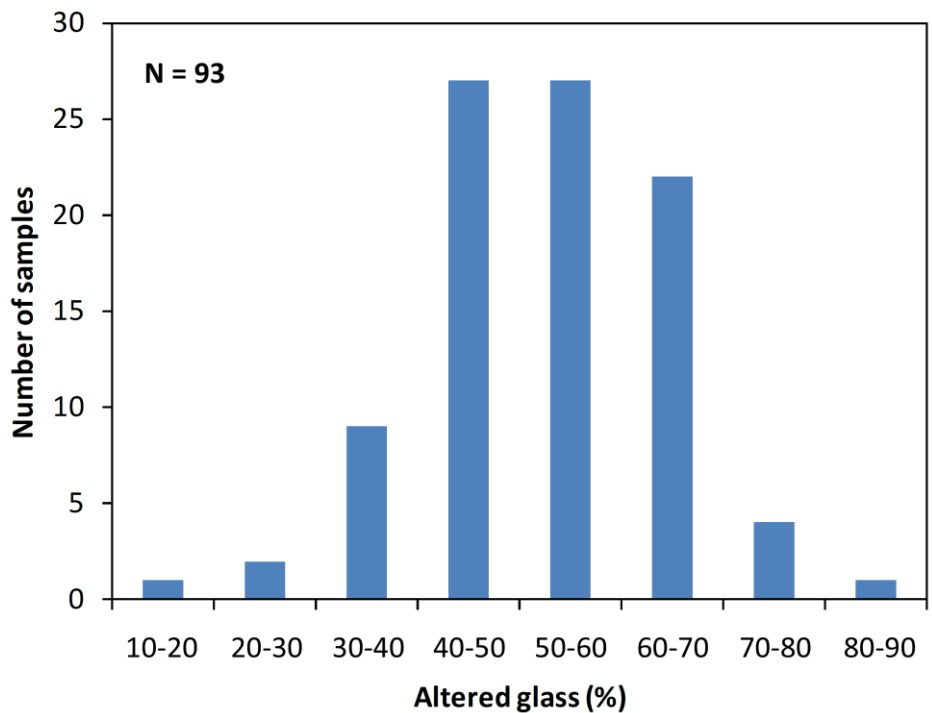


Figure 4. Histogram showing sample frequency depending on the abundance of altered glass as a proportion of solid rock.

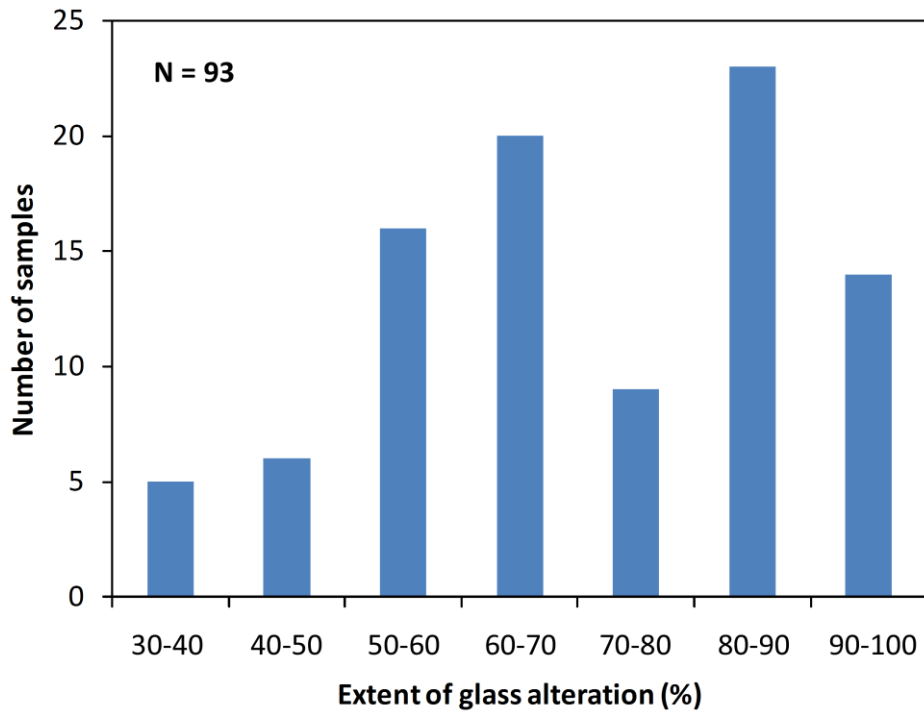


Figure 5. Histogram showing sample frequency depending on the extent to which the primary glass has been altered.

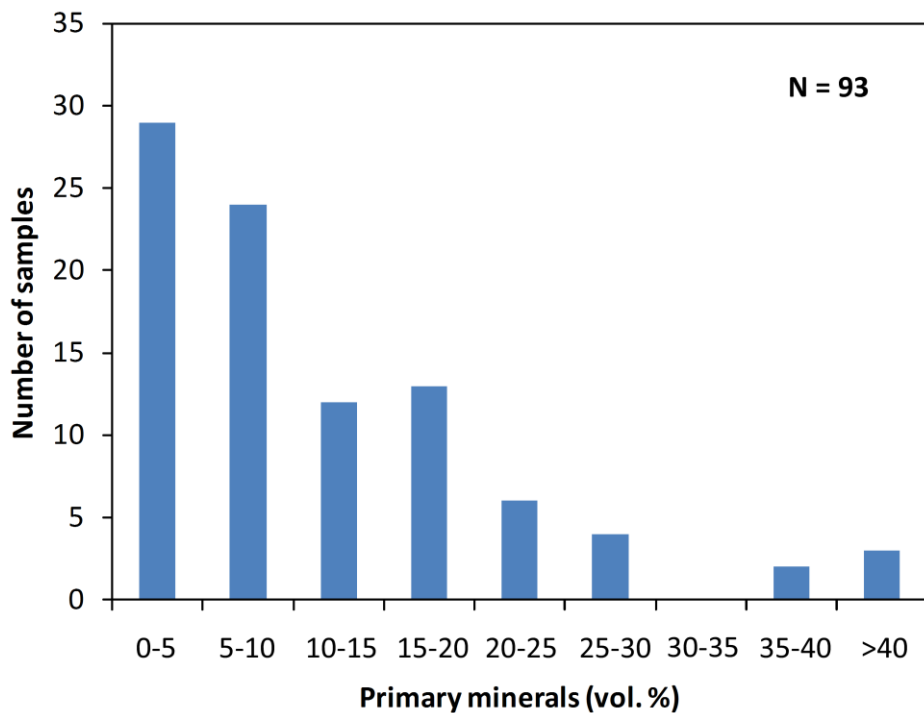


Figure 6. Histogram showing sample frequency depending on the abundance of primary minerals as a proportion of solid rock.

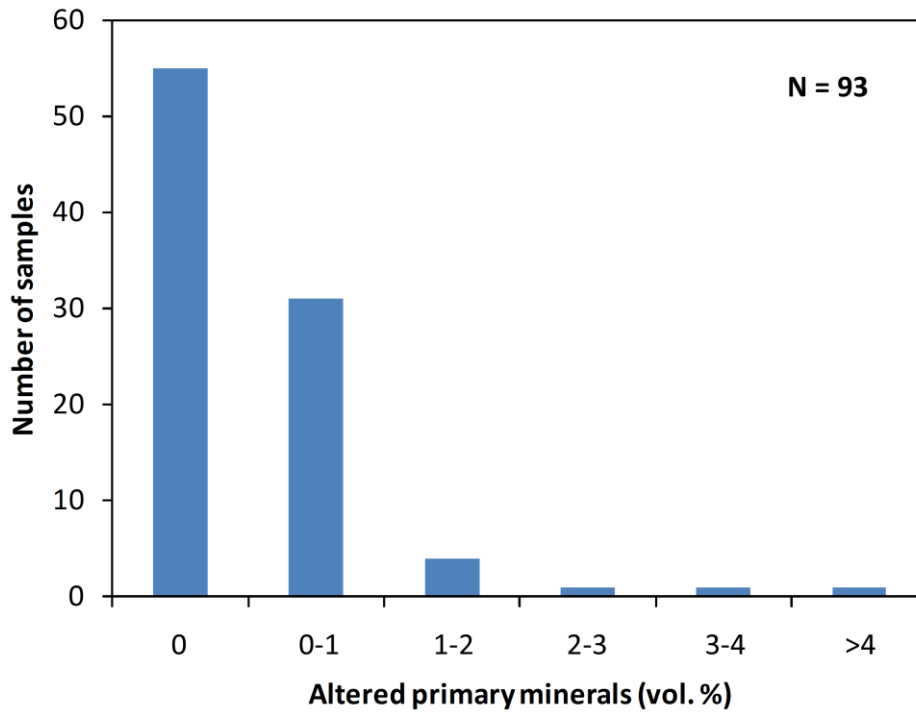


Figure 7. Histogram showing sample frequency depending on the abundance of altered primary minerals as a proportion of solid rock.

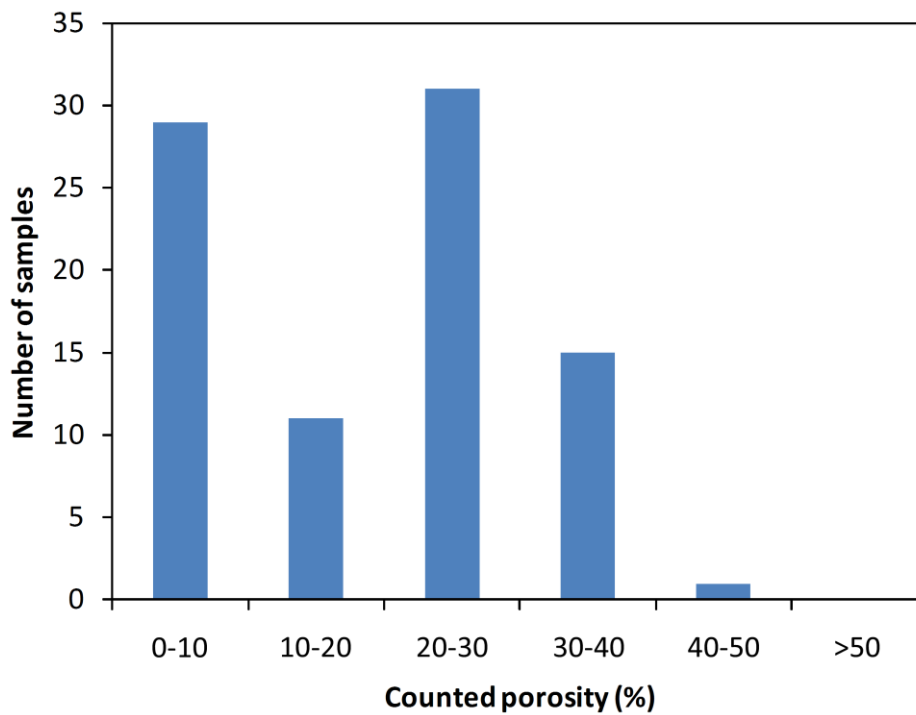


Figure 8. Histogram showing the sample frequency depending on the proportion of pores in the samples as determined by point counting in thin sections.

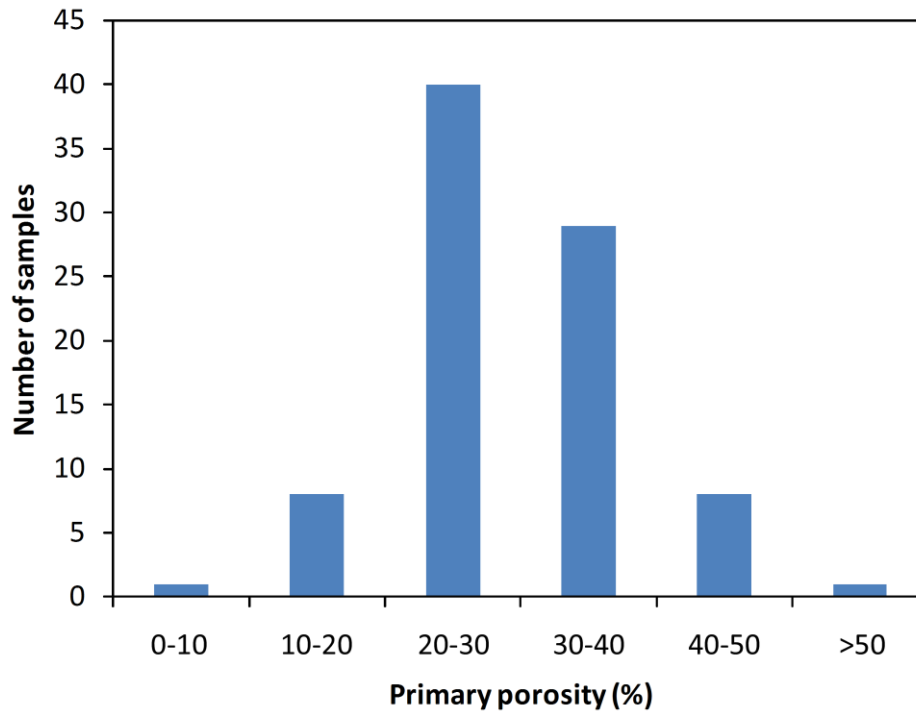


Figure 9. Histogram showing sample frequency depending on the original proportion of pores in the samples as determined by point counting in thin sections.

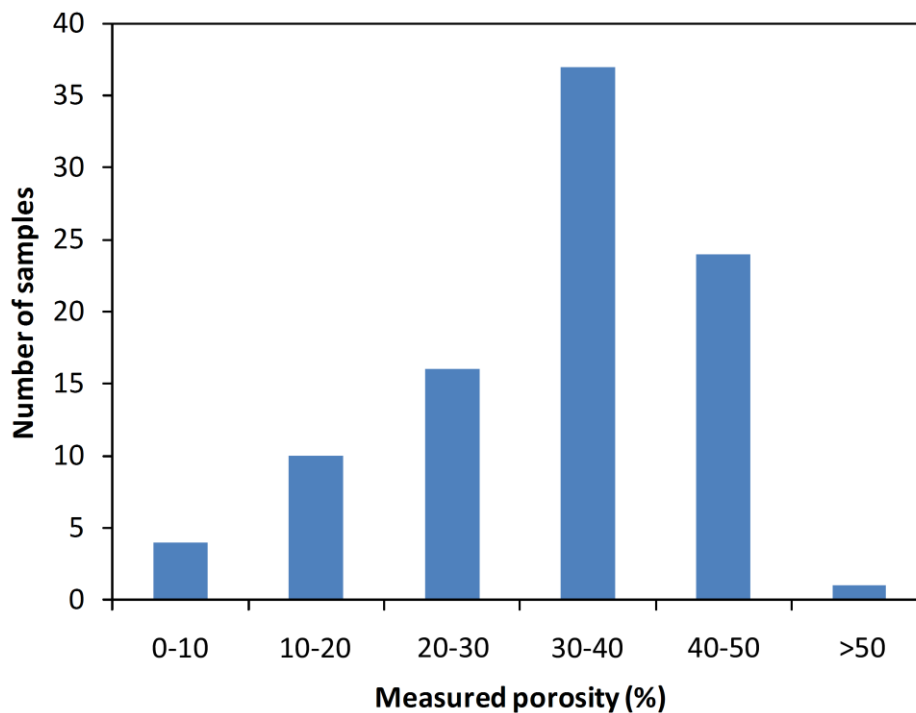


Figure 10. Histogram showing sample frequency depending on the amount of porosity in the samples as measured in air.

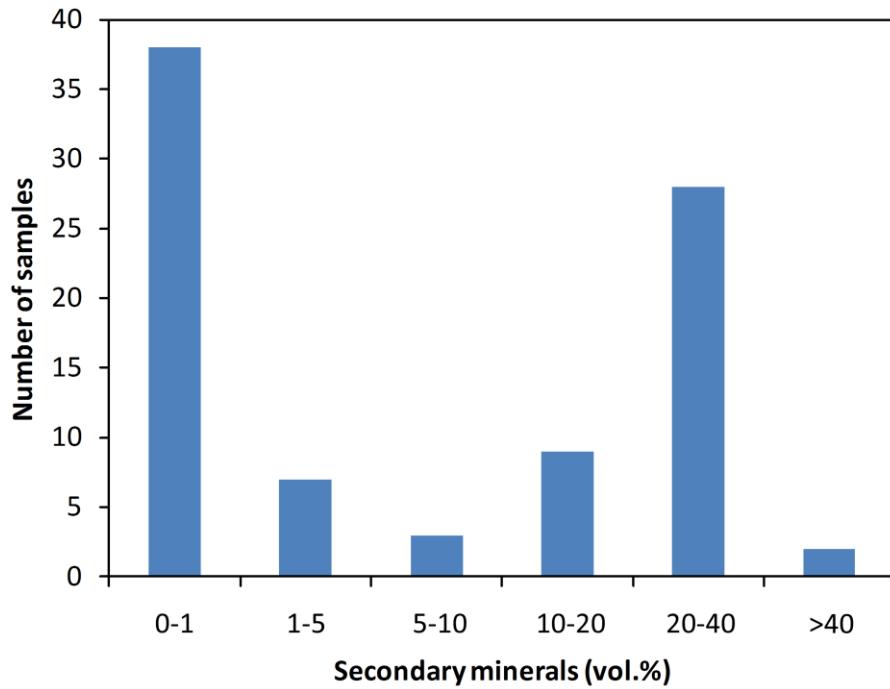


Figure 11. Histogram showing sample frequency depending on the abundance of secondary minerals as a proportion of solid rock.

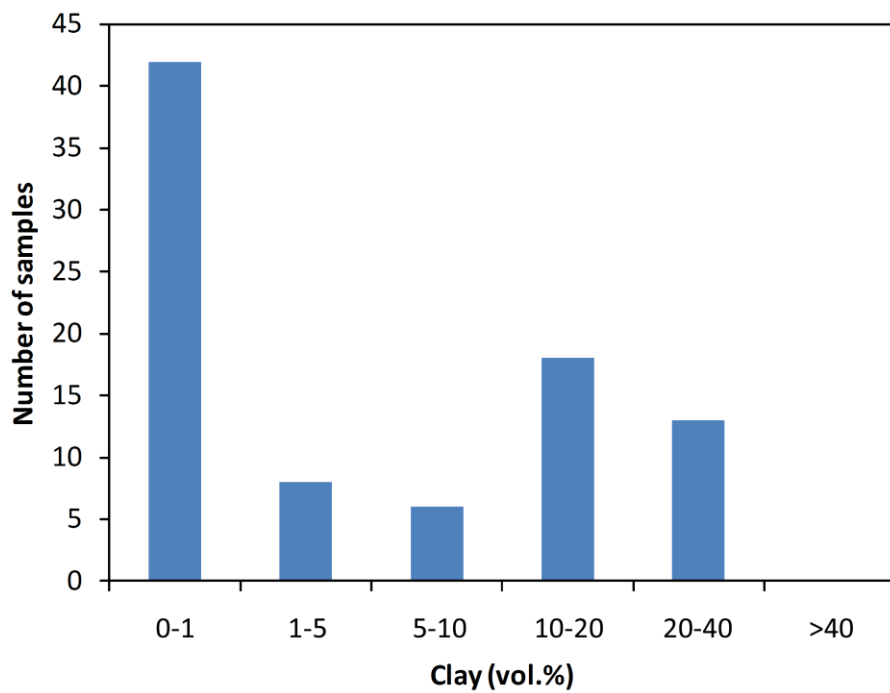


Figure 12. Histogram showing sample frequency depending on the abundance of clay as a proportion of solid rock.

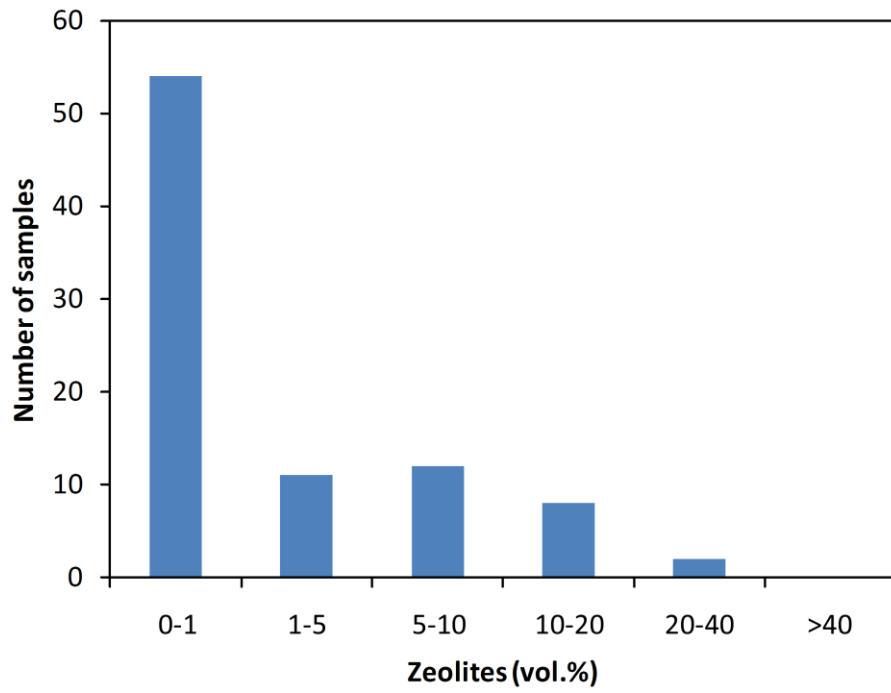


Figure 13. Histogram showing sample frequency depending on the abundance of zeolites as a proportion of solid rock.

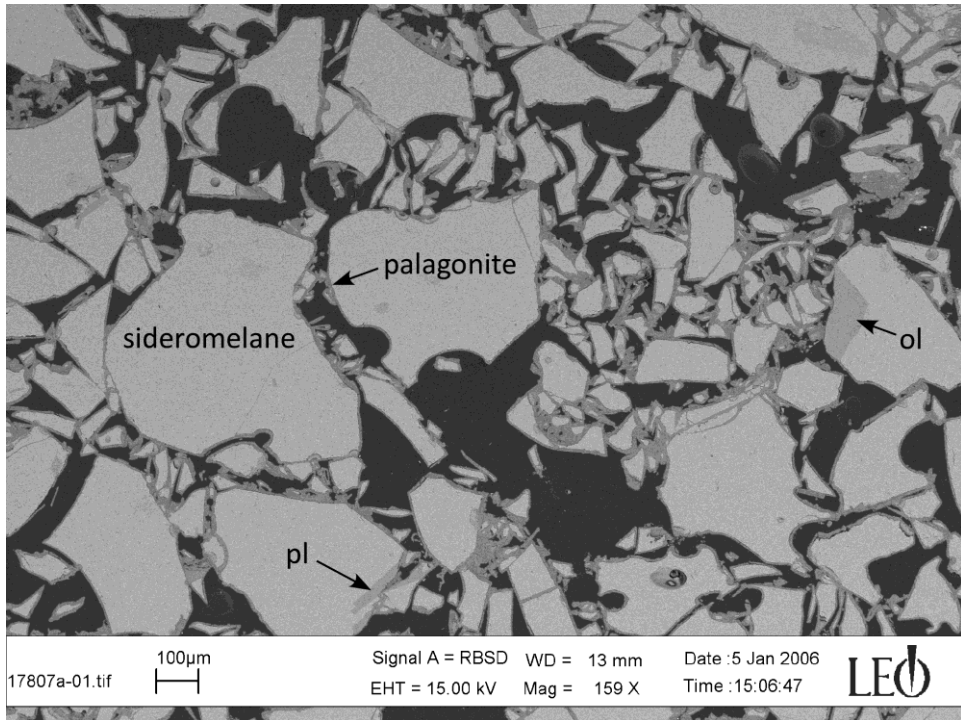


Figure 14. BEI photograph of a slightly palagonitized hyaloclastite tuff sample from Vigdísarvellir on Reykjanes Peninsula. Generally, the sideromelane glass particles have only a very thin palagonite rim. Plagioclase (pl) and olivine (ol) phenocrysts are unaffected by alteration.

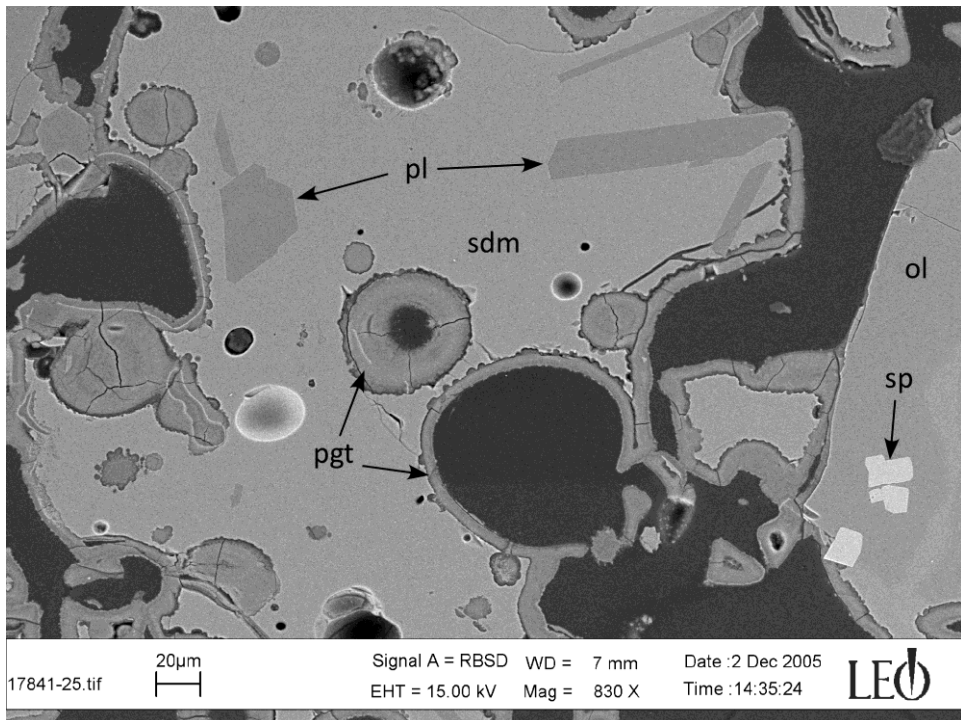


Figure 15. BEI photograph of a mildly palagonitized hyaloclastite tuff sample from Skeifilsfjöll eldri. Large amount of unaltered sideromelane glass (sdm) is still present. The palagonite rims (pgt) are generally 10-20 μm wide but some of the smaller vesicles are free of palagonitization. Plagioclase (pl), olivine (ol), and chromian spinel (sp) phenocrysts are unaltered.

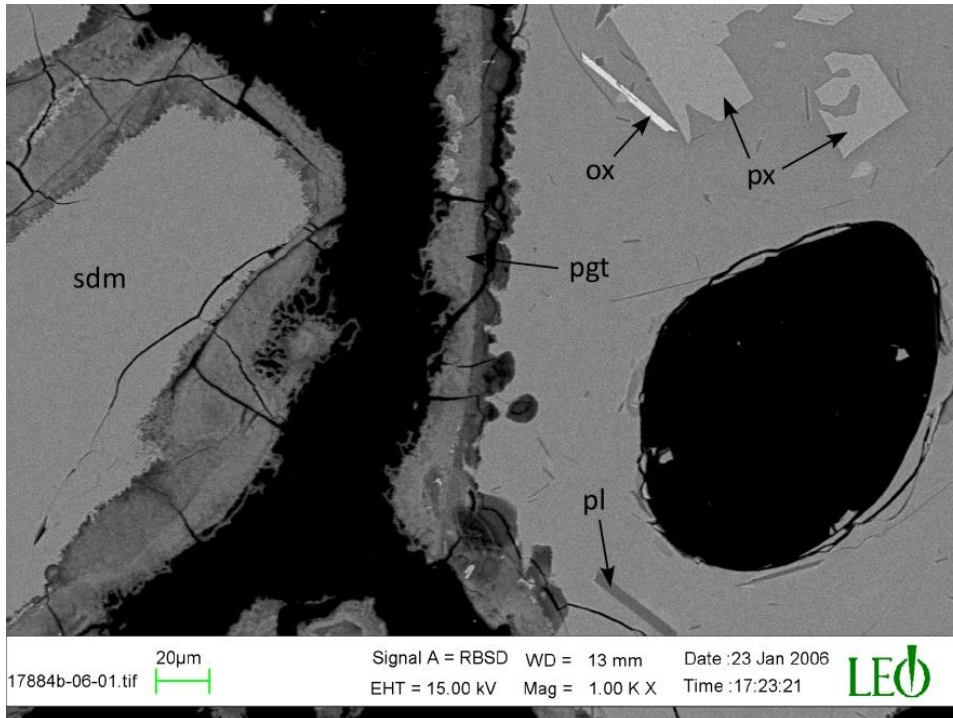


Figure 16. BEI photograph of a moderately palagonitized hyaloclastite tuff sample from near Landmannahellir. The thickness of the palagonite rim (pgt) is roughly 20 μm but large amount of unaltered sideromelane glass (sdm) persists. Phenocrysts of plagioclase (pl), pyroxene (px) and an oxide (ox) are unaffected by alteration. Notice that palagonitization has not reached the large vesicle on the right.

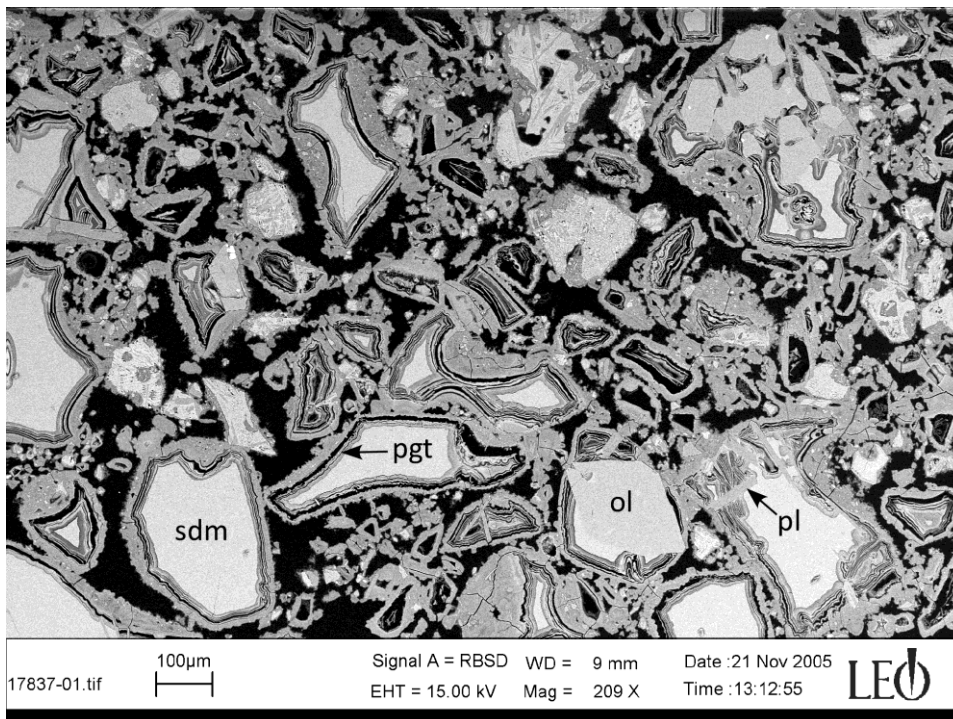


Figure 17. BEI photograph of a moderately palagonitized hyaloclastite tuff sample from Stóri-Dímon in South Iceland. Fair amount of sideromelane glass (sdm) remains but a thick rim of palagonite (pgt) has formed on the surface of the glass particles. The palagonite is strongly layered. Phenocrysts of plagioclase (pl) and olivine (ol) are unaltered.

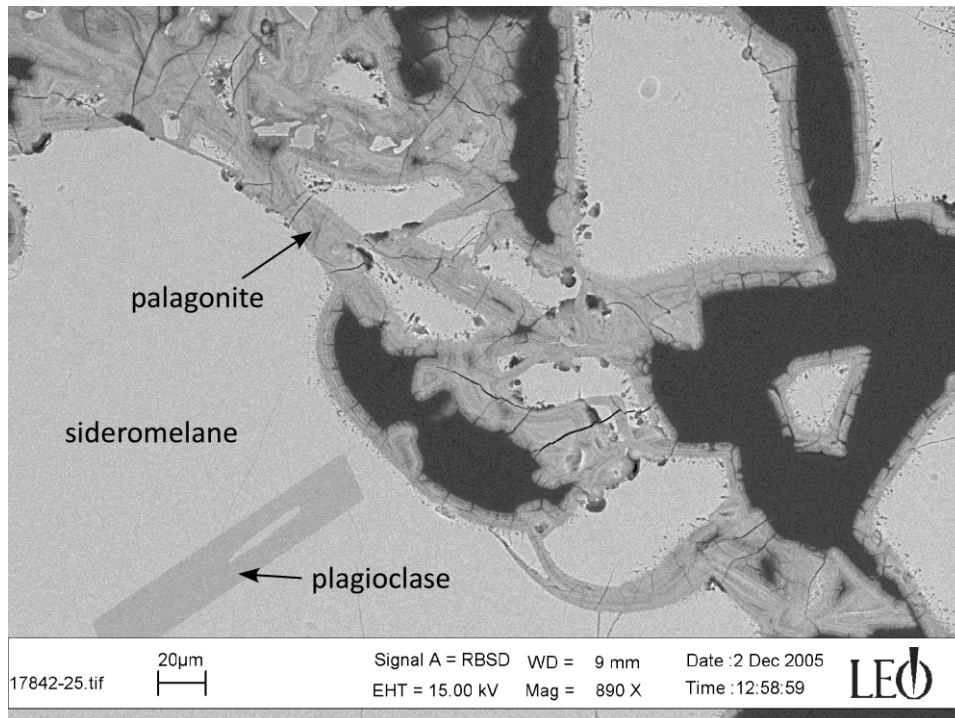


Figure 18. BEI photograph of a moderately palagonitized hyaloclastite tuff sample from Skefilsfjöll eldri. The thickness of the palagonite rims has generally reached 10-20 μm . Notice pores in the sideromelane glass at the interface with the palagonite rims. The plagioclase phenocryst is unaltered.

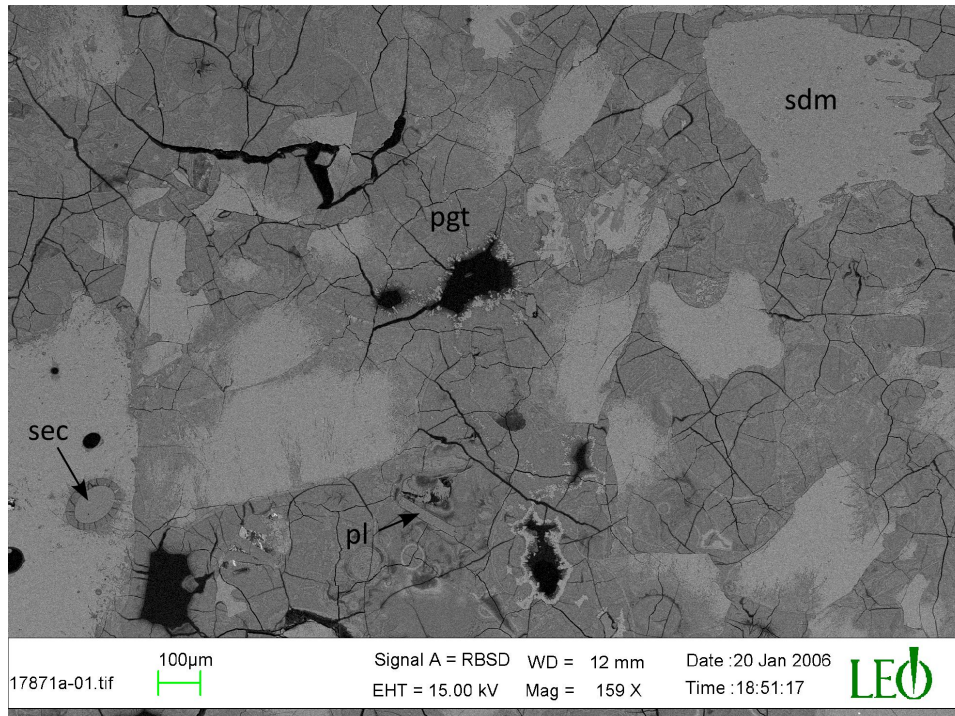


Figure 19. BEI photograph of an extensively palagonitized hyaloclastite tuff sample from Vörðufell in South Iceland. Some sideromelane glass remains but most of the sample is composed of palagonite (pgt). Plagioclase phenocryst (pl) appears unaltered. Secondary mineral (sec) is seen filling a vesicle.

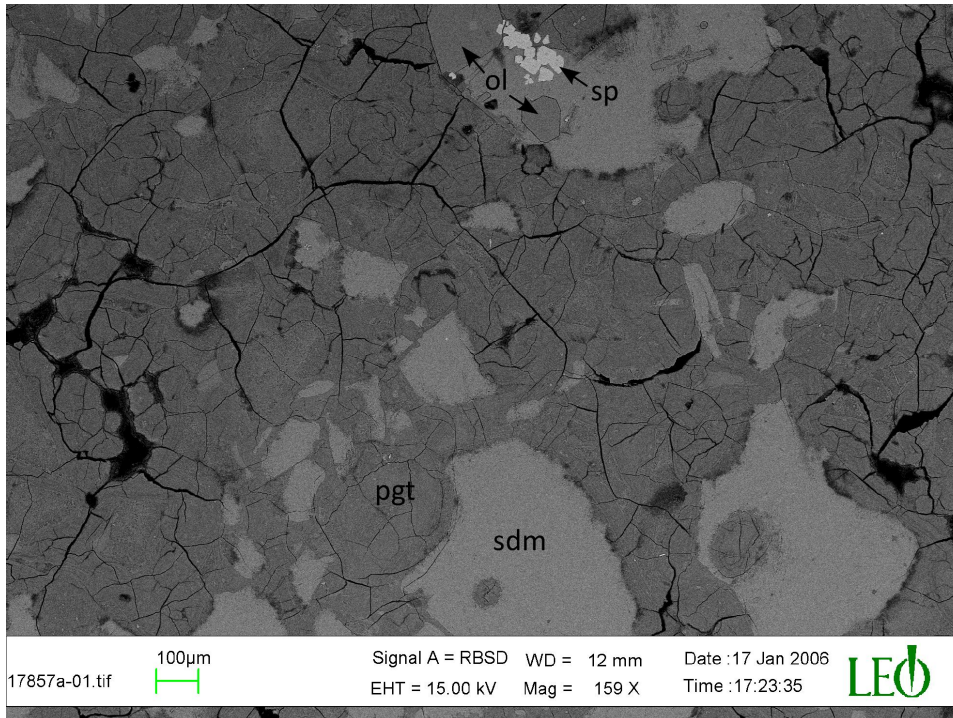


Figure 20. BEI photograph of an extensively palagonitized hyaloclastite tuff sample from Meðalfell in West Iceland. Some sideromelane (sdm) remains but palagonite (pgt) comprises most of the sample. Phenocrysts of olivine (ol) and chromian spinel (sp) appear unaffected by alteration.

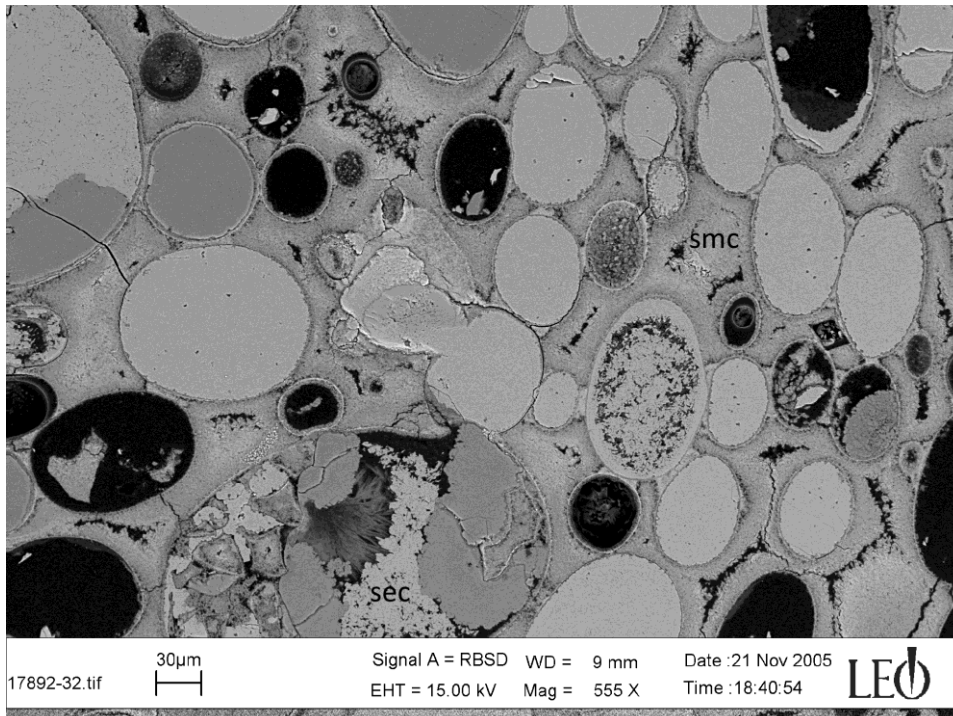


Figure 21. BEI photograph of a heavily altered hyaloclastite tuff sample from Hellisskarð. No unaltered volcanic glass remains. The original sideromelane glass has been replaced by a smectite (smc). Most vesicles are partly or completely filled with secondary minerals (sec). At least three different types of secondary minerals can be distinguished.

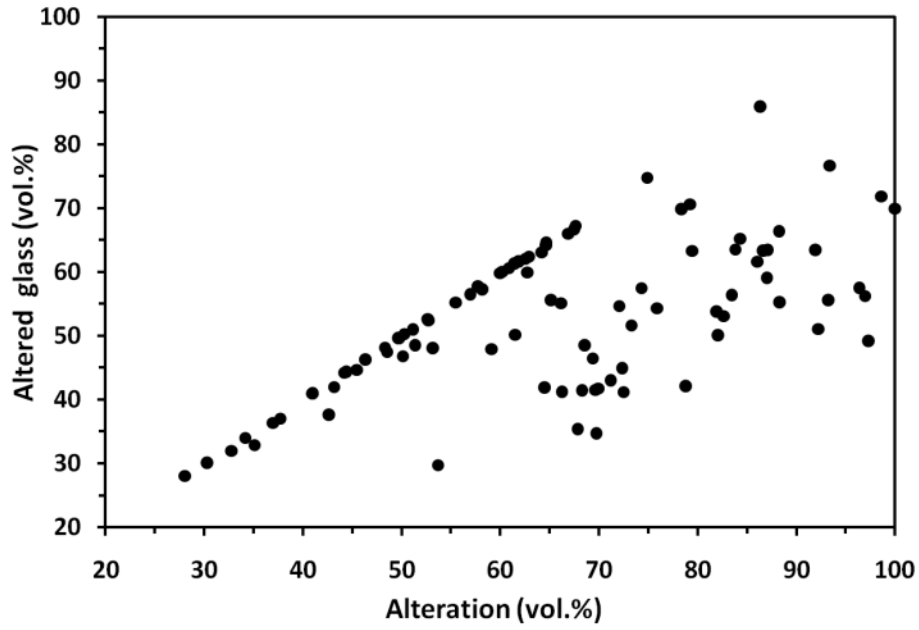


Figure 22. *The amount of altered glass versus the extent of alteration of the hyaloclastite tuff samples.*

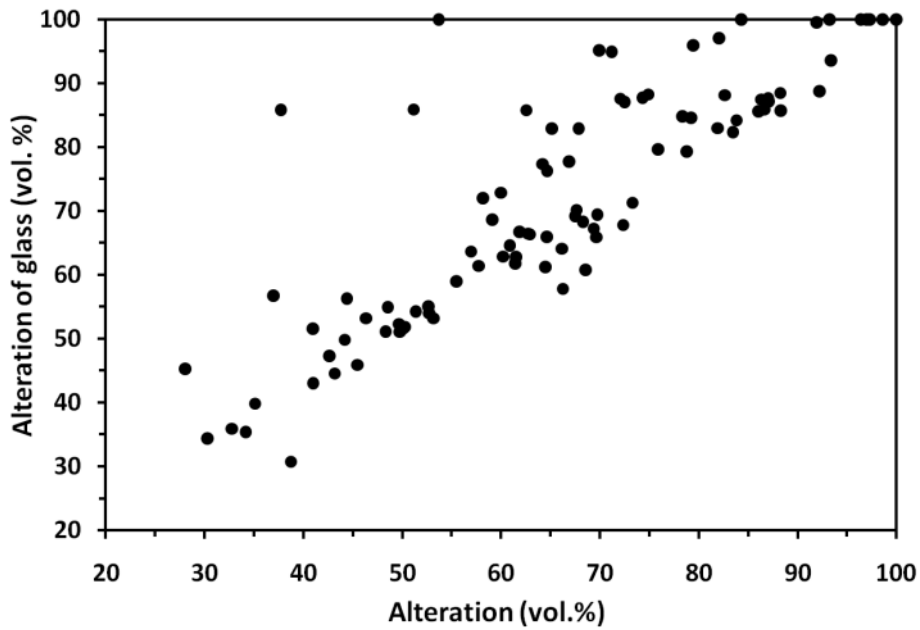


Figure 23. *The extent of glass alteration versus the total alteration of the hyaloclastite tuff samples.*

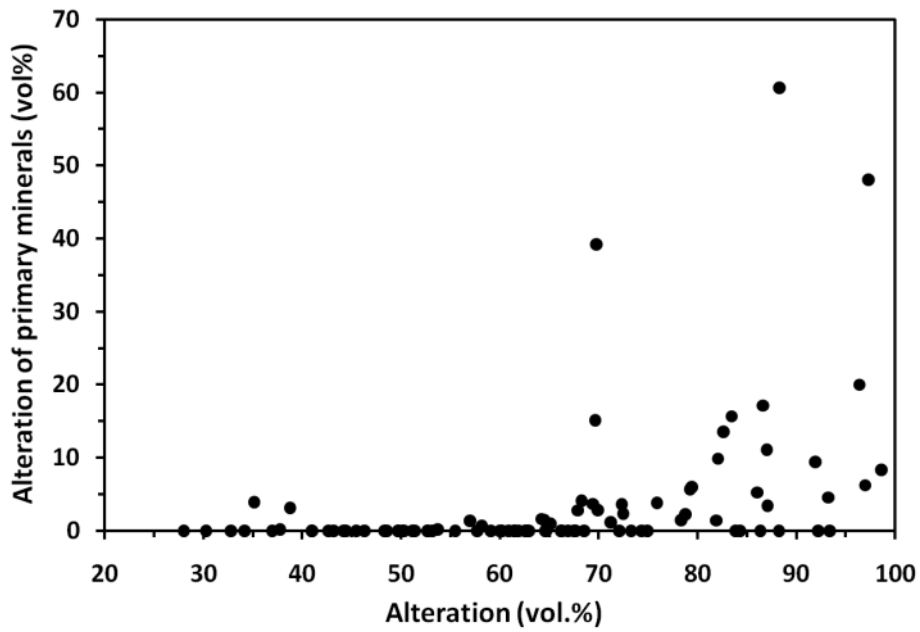


Figure 24. *The extent of primary mineral alteration versus the total alteration of the hyaloclastite tuff samples.*

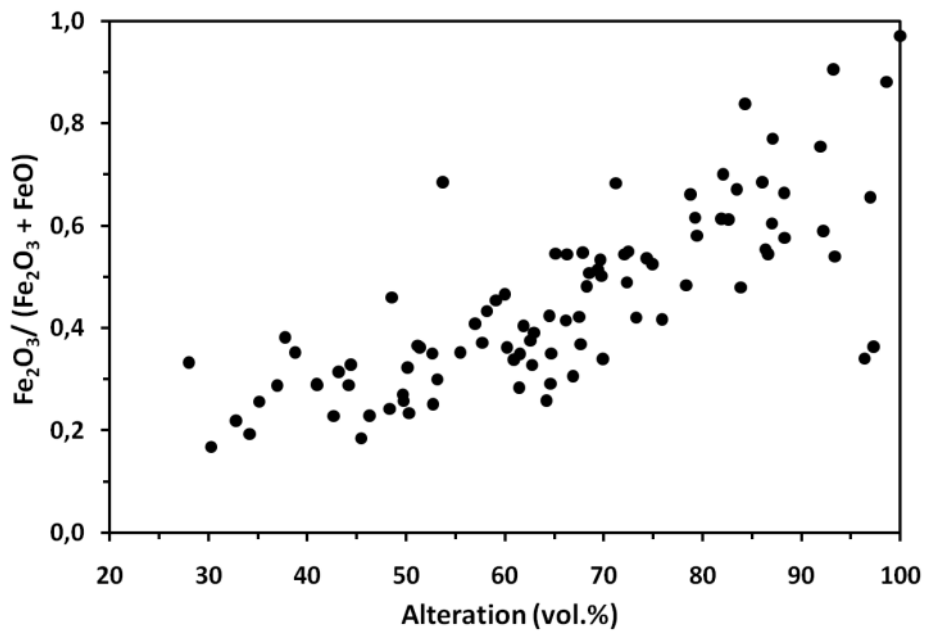


Figure 25. *Molar ferric-ferrous ratio versus the amount of alteration of the hyaloclastite tuff samples.*

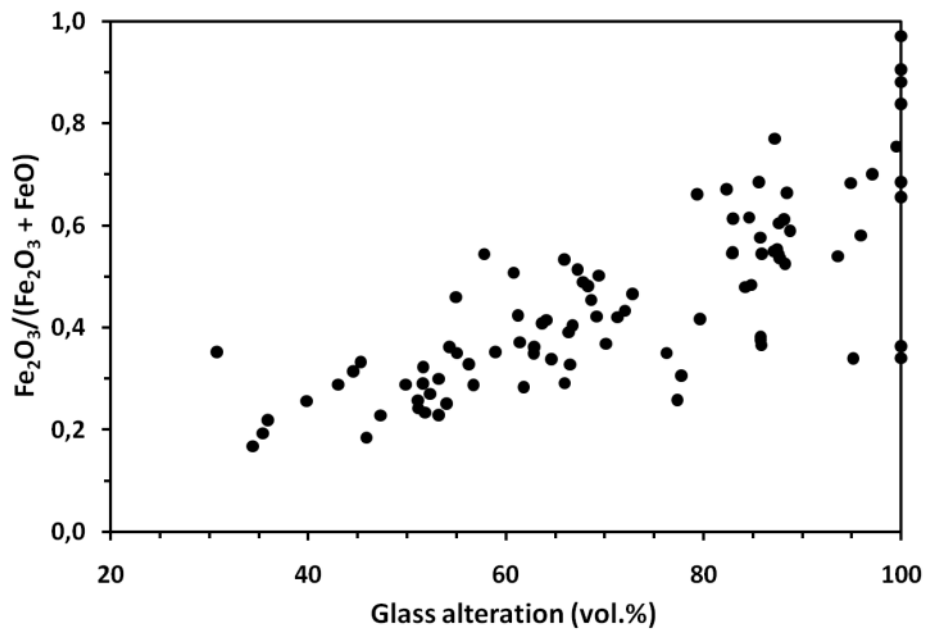


Figure 26. Molar ferric-ferrous ratio versus the amount of glass alteration of the hyaloclastite tuff samples.

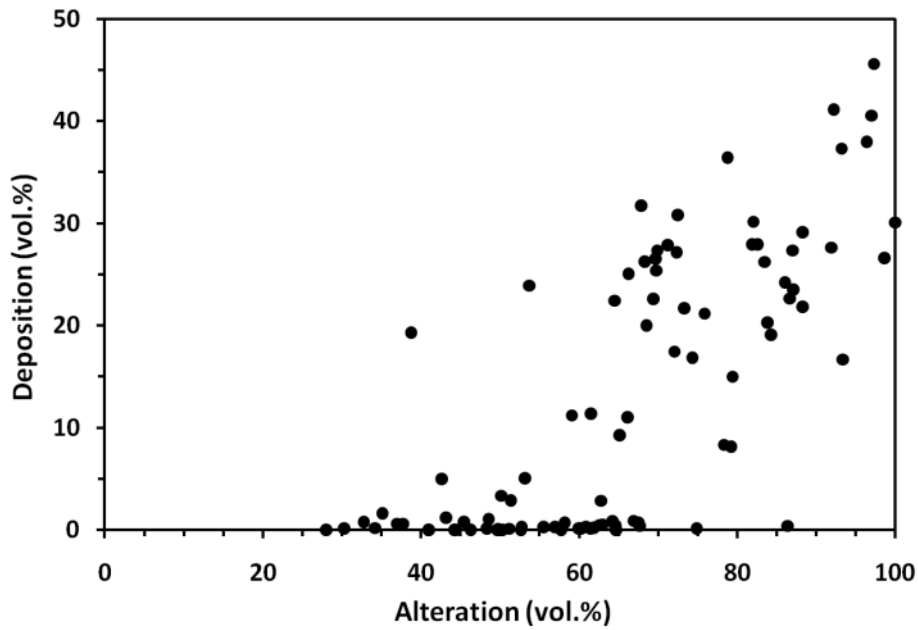


Figure 27. The amount of deposition versus the alteration of the hyaloclastite tuff samples.

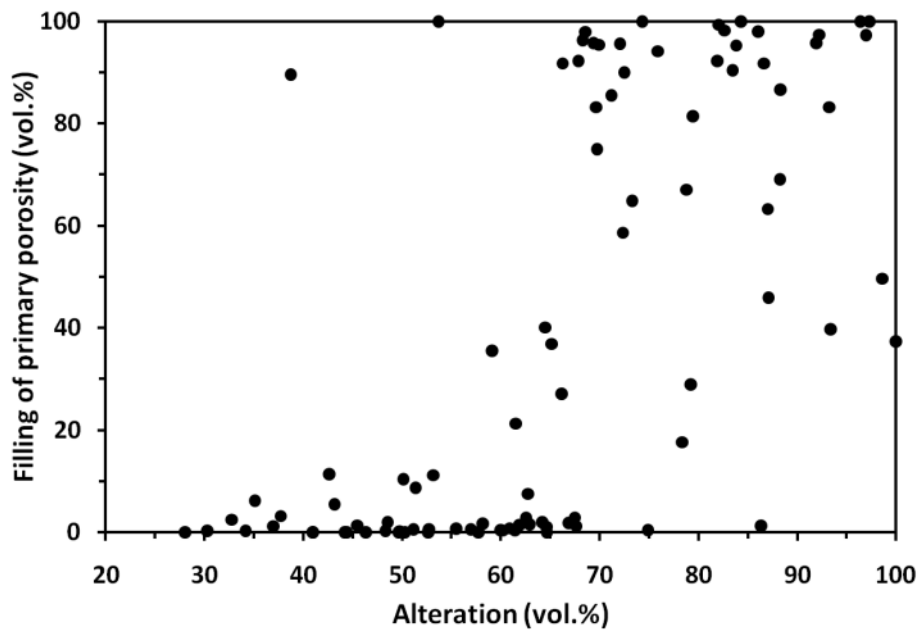


Figure 28. *The extent of filling of primary porosity with secondary minerals versus the extent of alteration of the hyaloclastite tuff samples.*

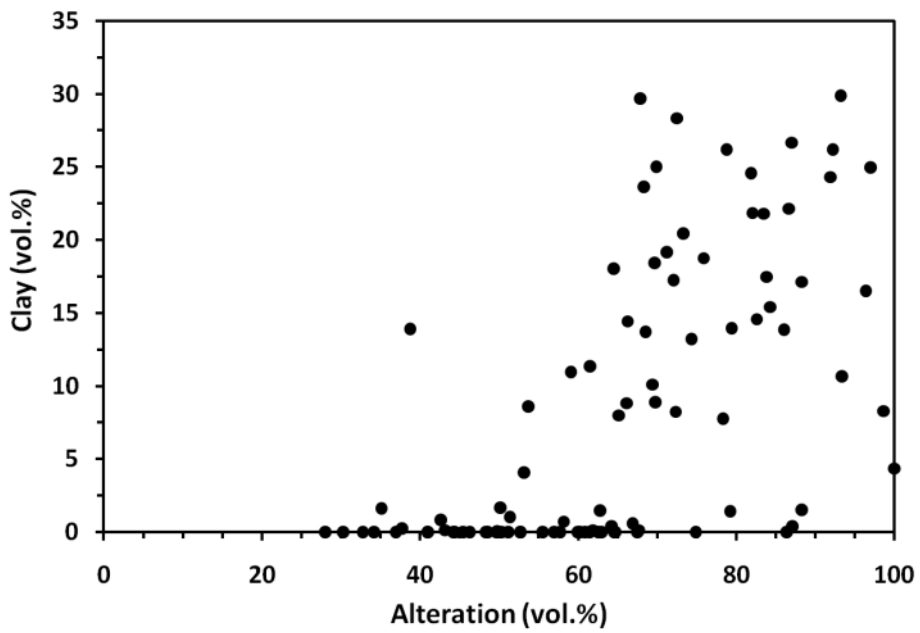


Figure 29. *The amount of clay versus alteration of the hyaloclastite tuff samples.*

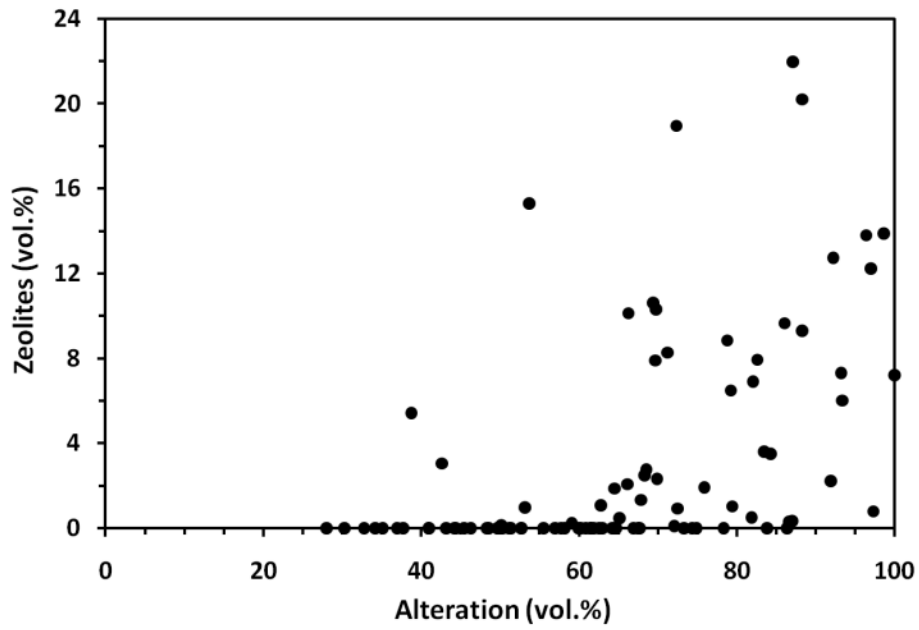


Figure 30. *The amount of zeolites versus alteration of the hyaloclastite tuff samples.*

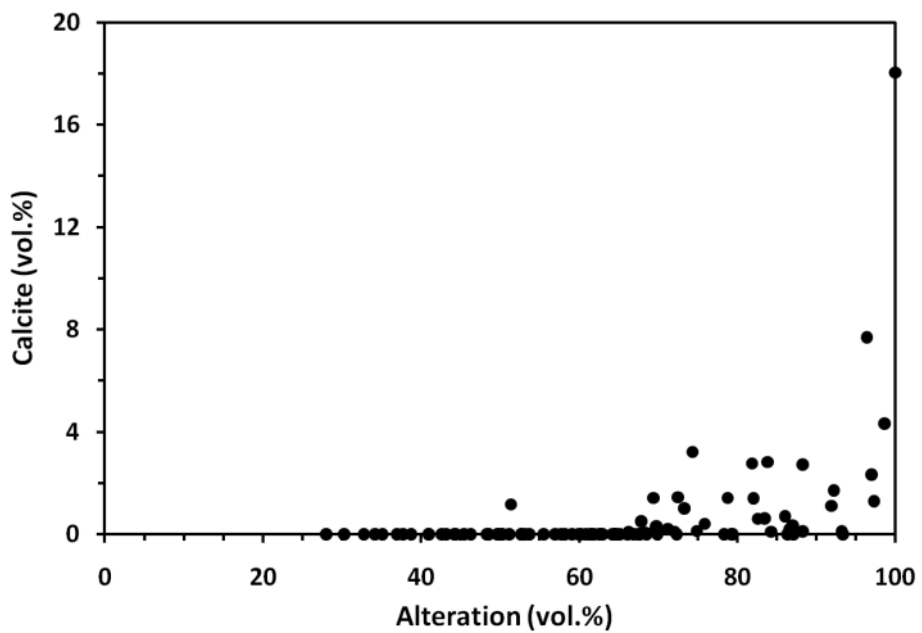


Figure 31. *The amount of calcite versus the degree of alteration of the hyaloclastite tuff samples.*

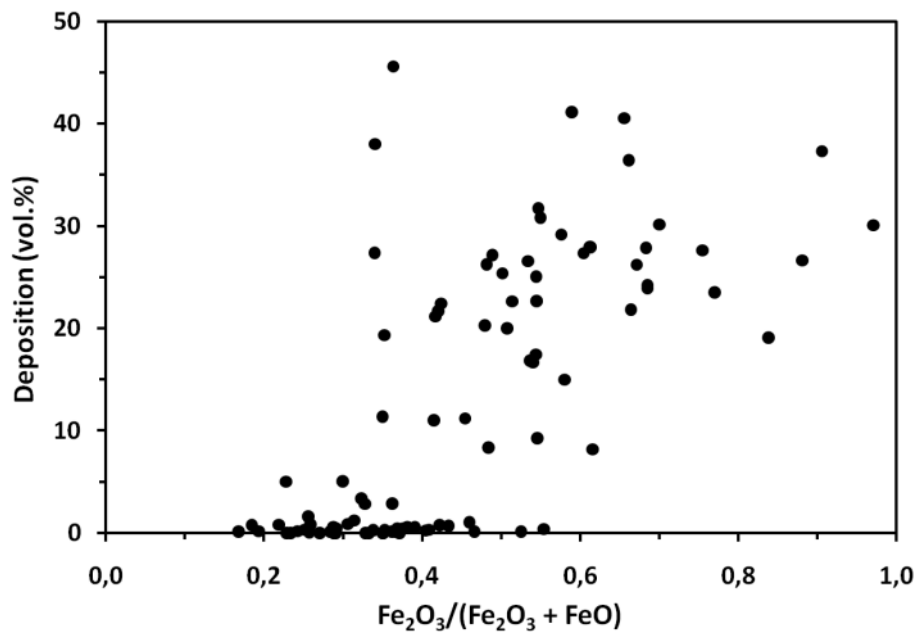


Figure 32. The amount of deposition versus the ratio between ferric iron and total iron content of the hyaloclastite tuff samples.

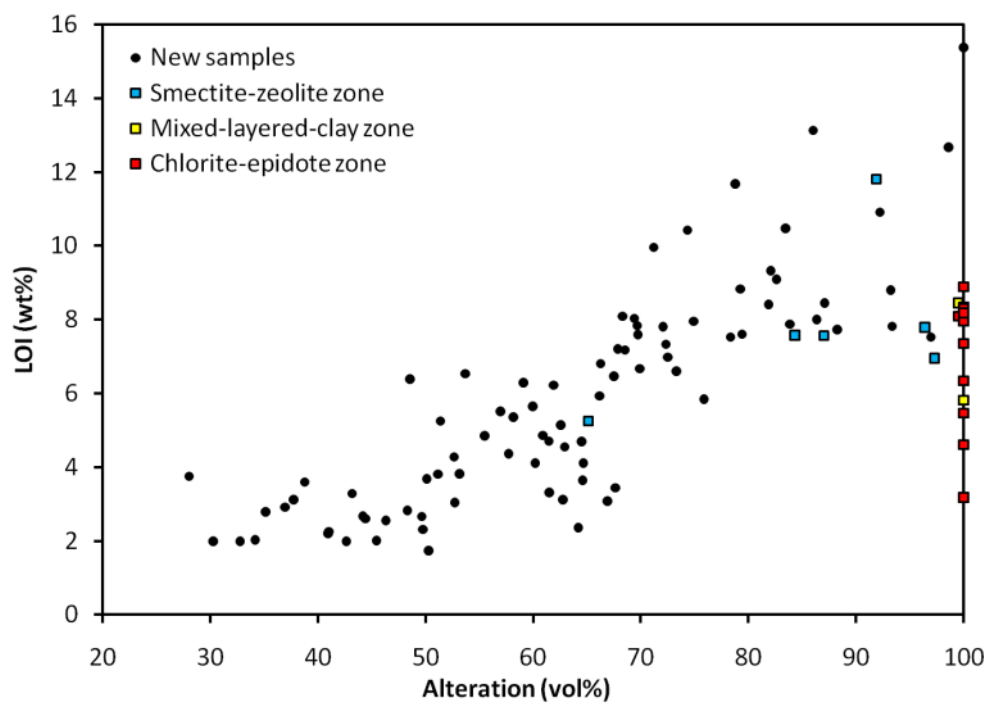


Figure 33. Loss on ignition versus the alteration of the hyaloclastite tuff samples. Solid circles represent new data and colored filled squares previously published data.

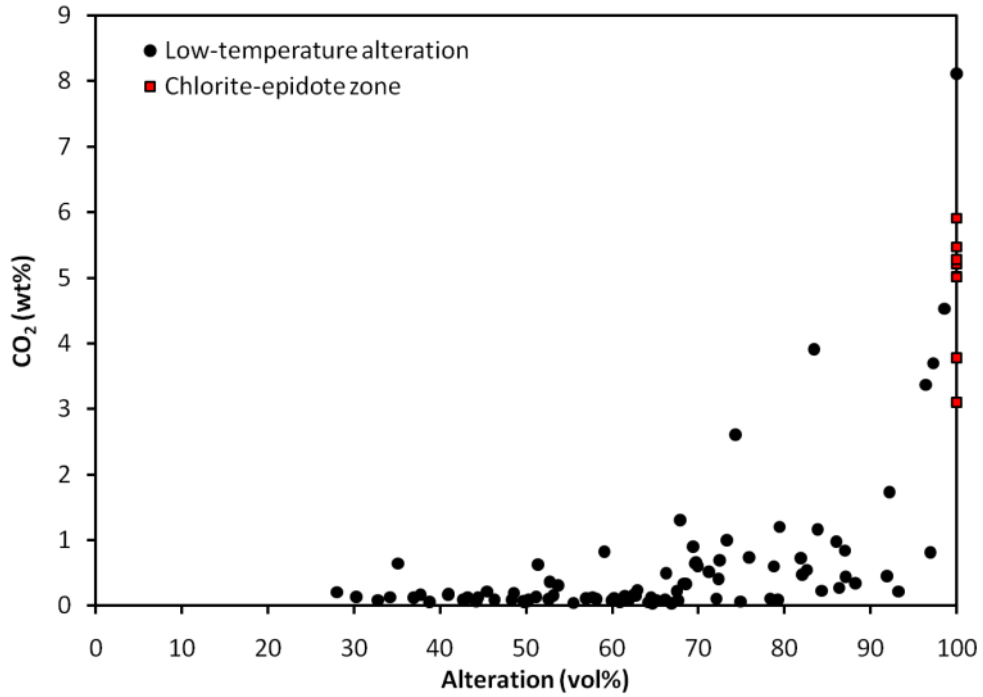


Figure 34. The CO₂ content versus the alteration of the hyaloclastite tuff samples. Solid circles represent new data and filled red squares previously published data.

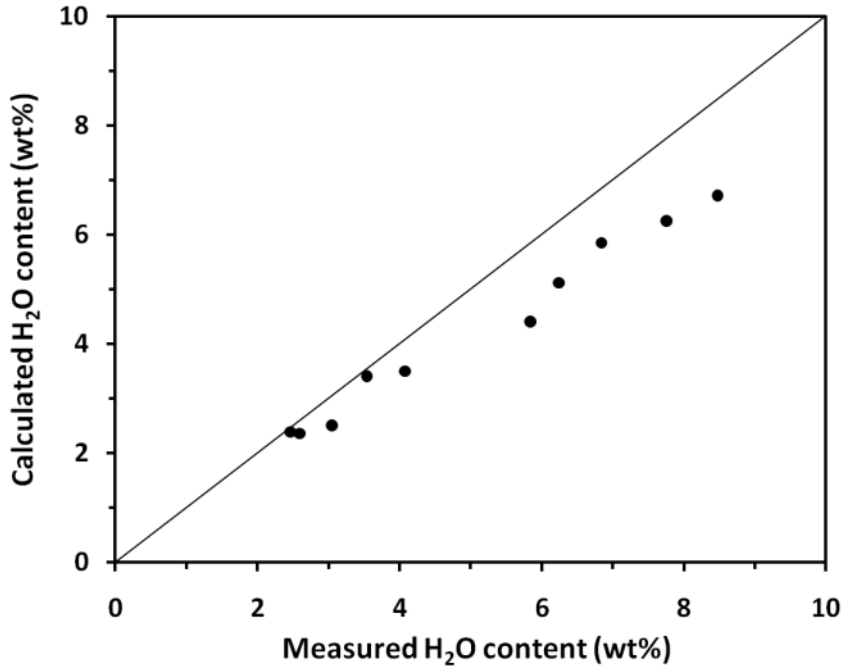


Figure 35. Measured H₂O content versus H₂O content calculated as LOI minus measured CO₂ content of the hyaloclastite tuff samples.

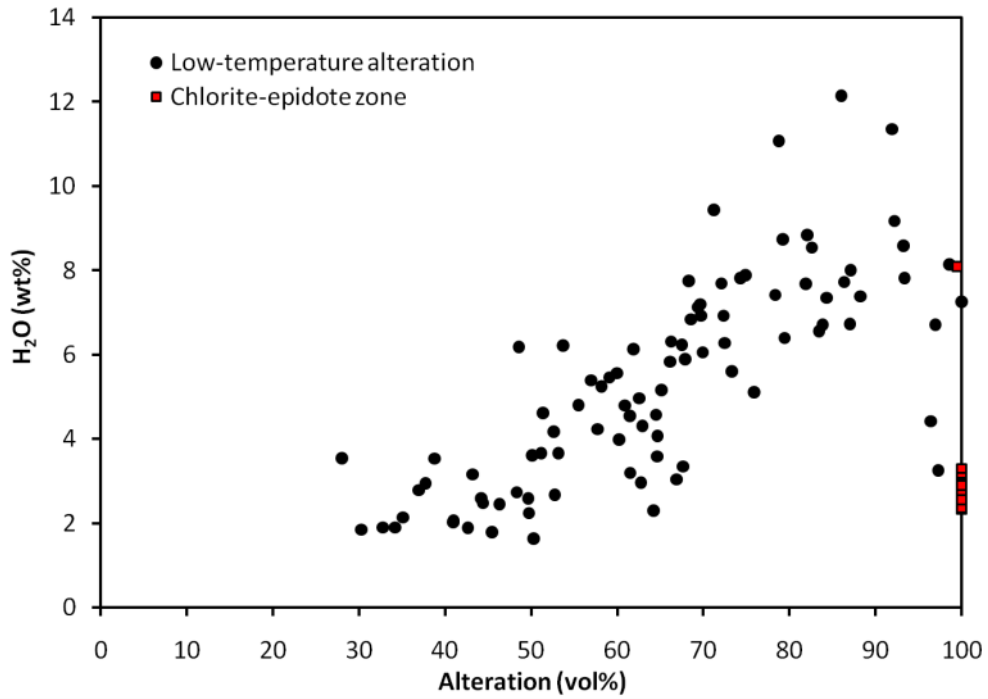


Figure 36. *H₂O content versus alteration of the hyaloclastite tuff samples. Filled circles represent new sample and filled red squares previously published data that are also more altered than the new samples.*

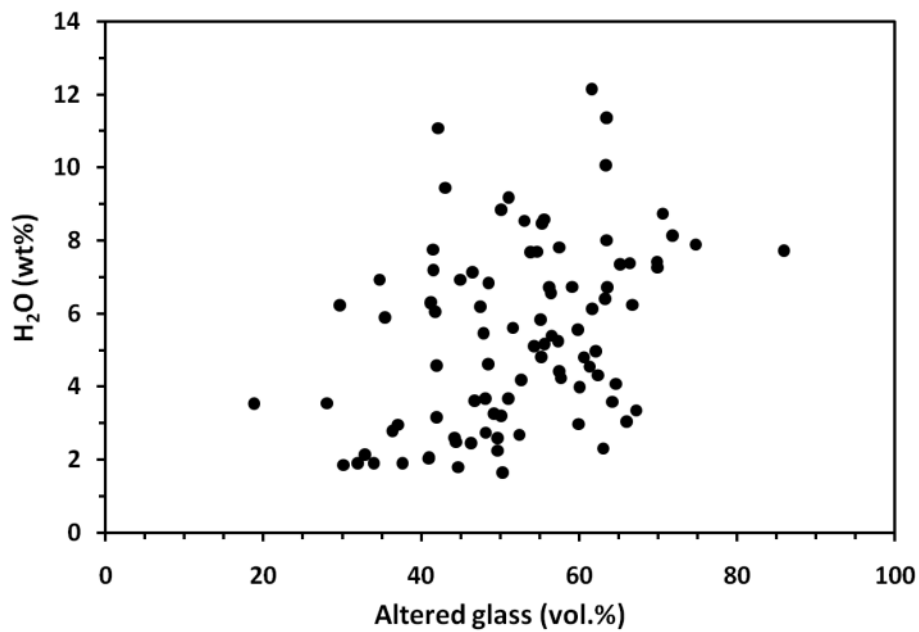


Figure 37. *H₂O content versus the amount of altered glass in the hyaloclastite tuff samples.*

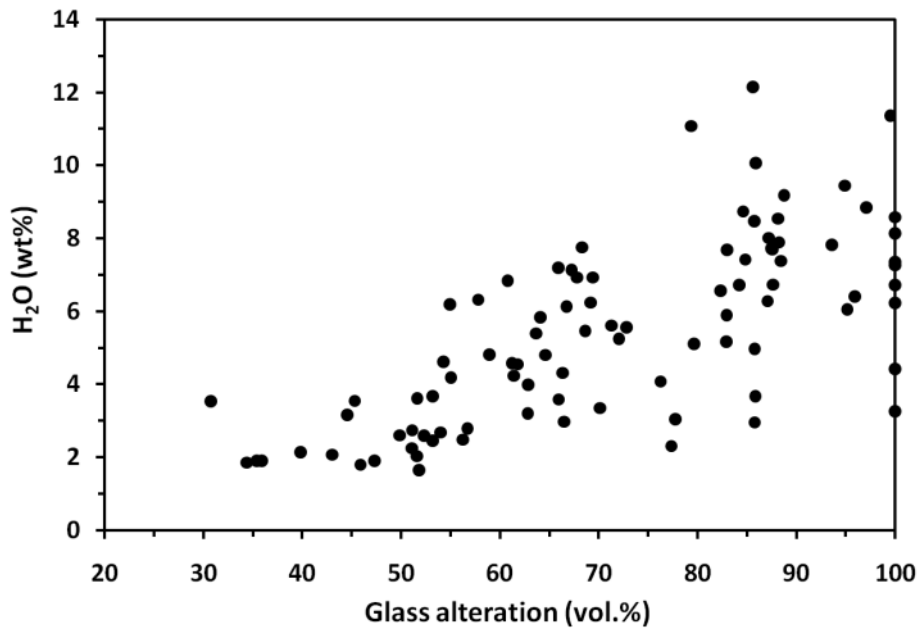


Figure 38. *H₂O content versus the amount of altered glass as a proportion of total glass in the hyaloclastite tuff samples.*

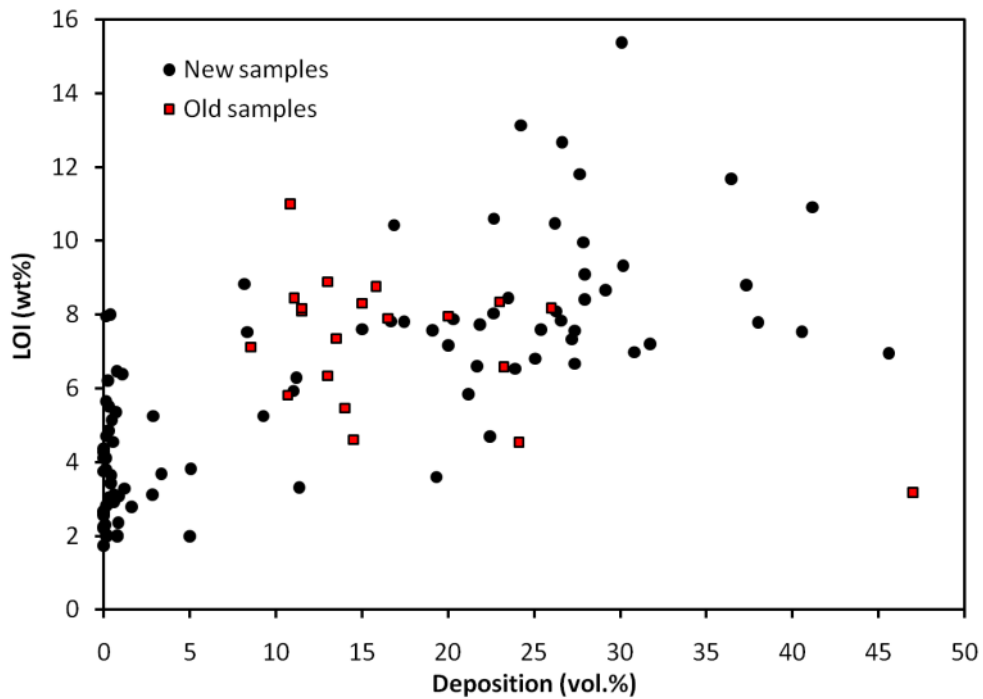


Figure 39. *Loss on ignition versus the amount of deposition of secondary minerals. Solid circles represent new data and filled red squares previously published data.*

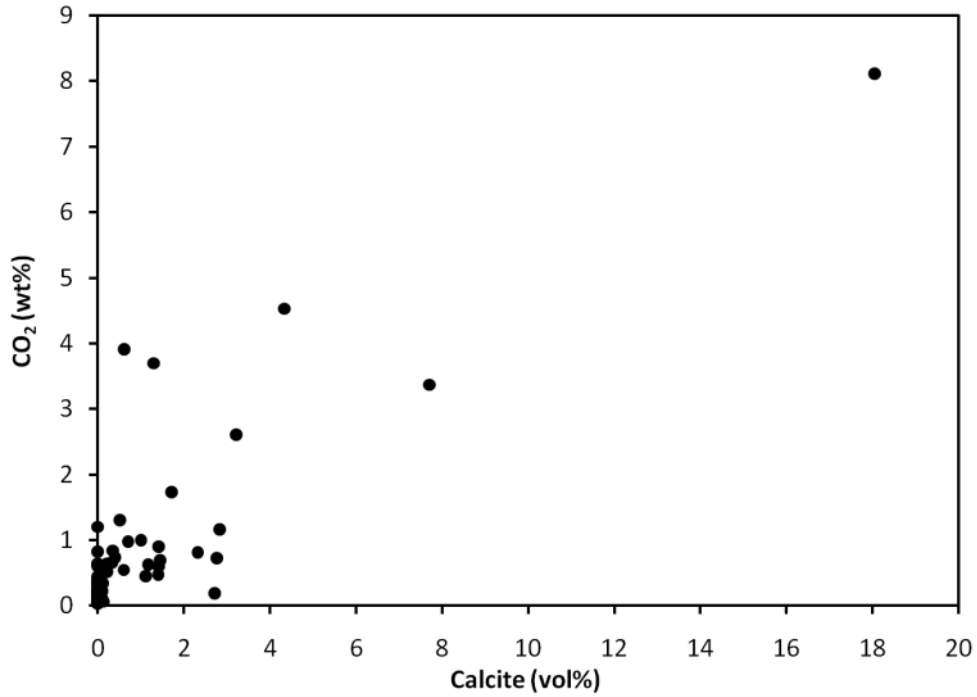


Figure 40. CO₂ content versus the amount of calcite deposition in the hyaloclastite tuff samples.

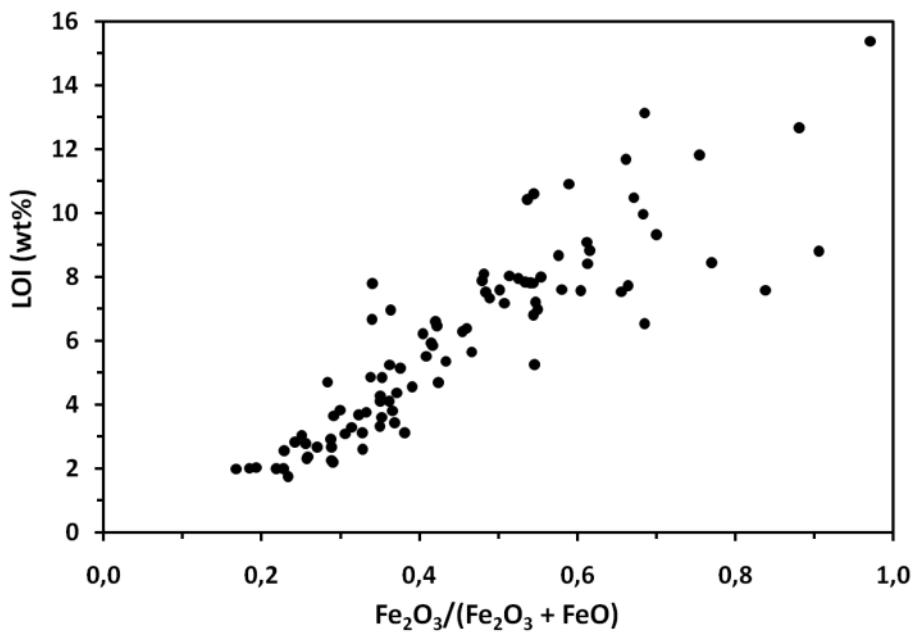


Figure 41. Loss on ignition versus the molar ratio between ferric iron and total iron content of the hyaloclastite formations.

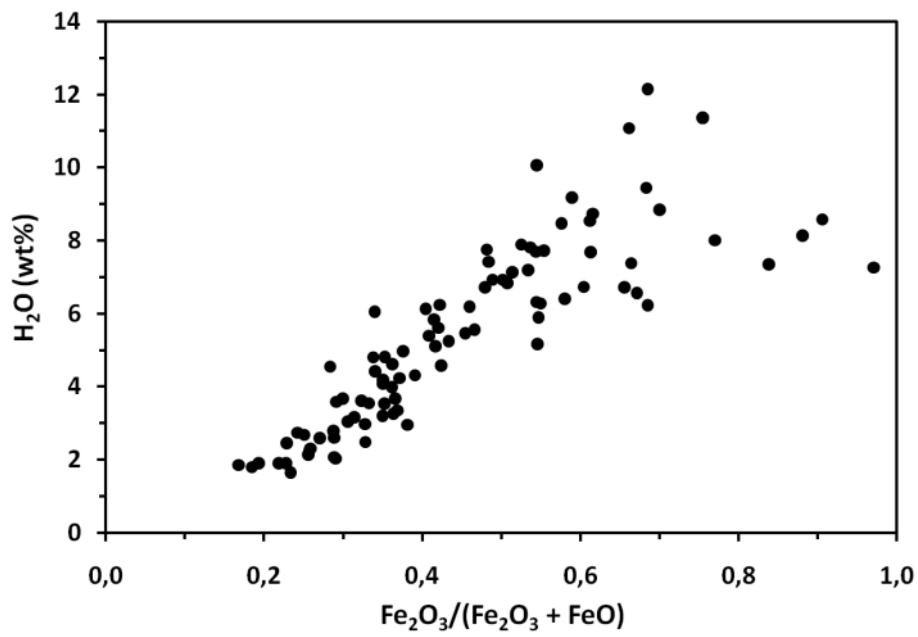


Figure 42. H_2O content versus the molar ratio between ferric iron and total iron content of the hyaloclastite formations.

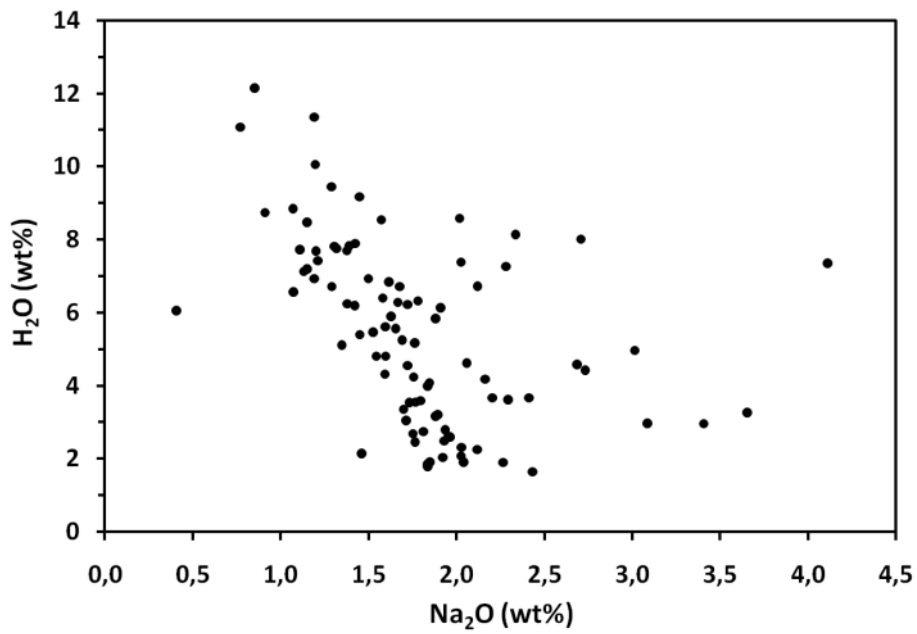


Figure 43. H_2O content versus Na_2O content of the hyaloclastite formations.

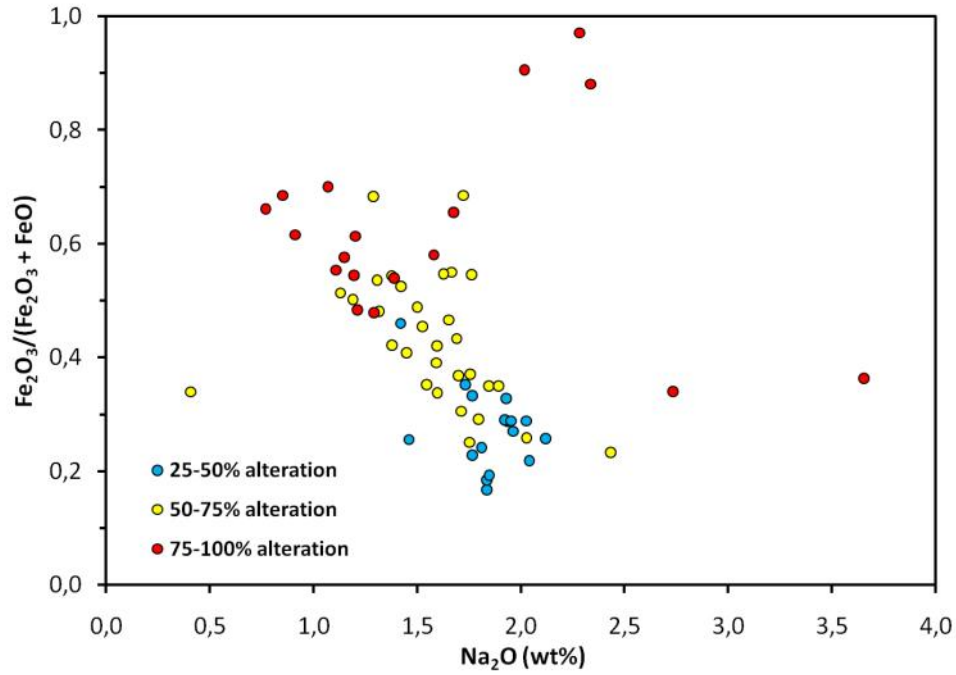


Figure 44. Molar ratio of ferric iron content and total iron content versus Na_2O content of the hyaloclastite tuff samples. Classified according to the degree of alteration. Only tholeiitic samples have been included.

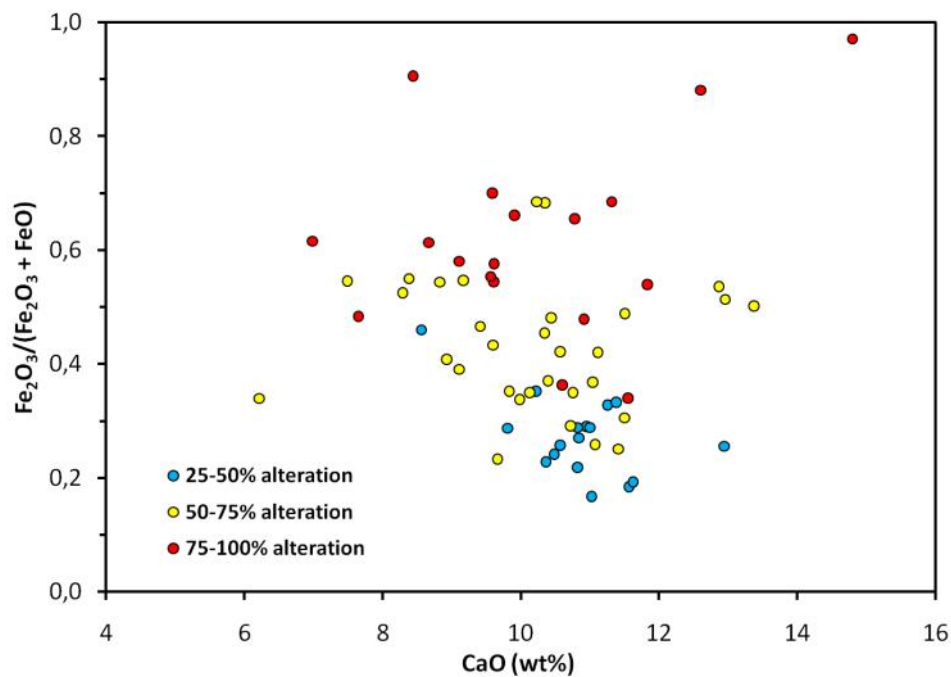


Figure 45. Molar ratio of ferric iron content and total iron content versus the CaO content of the hyaloclastite tuff samples. Classified according to the degree of alteration. Only tholeiitic samples have been included.

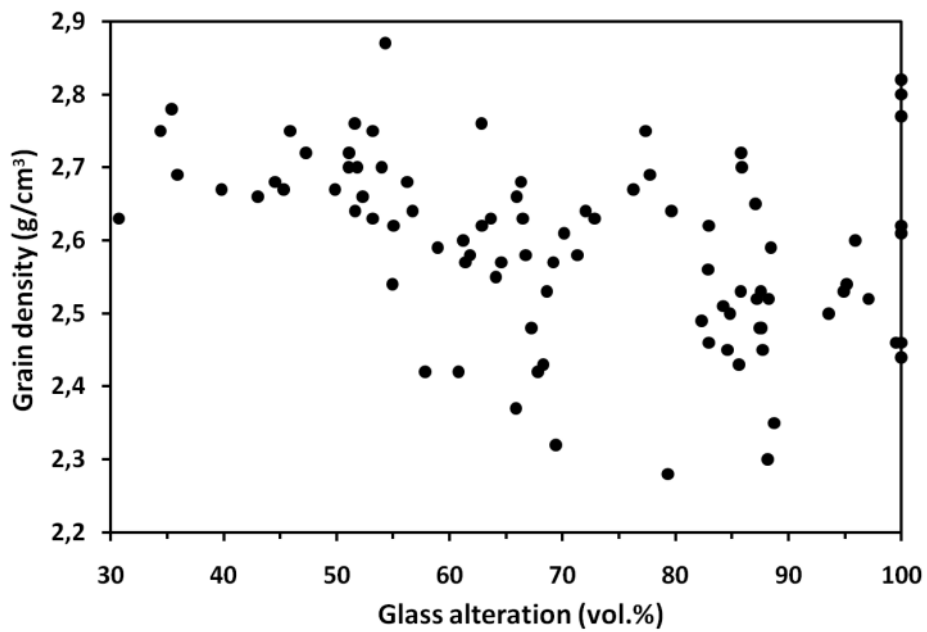


Figure 46. Grain density versus the extent of glass alteration of the hyaloclastite tuff samples.

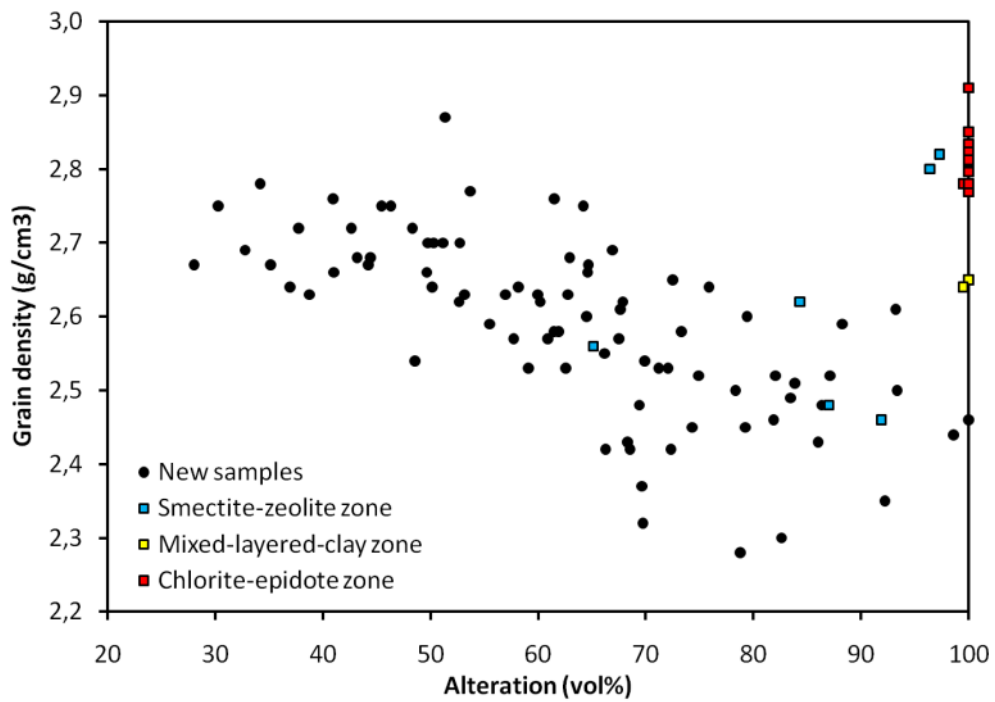


Figure 47. Grain density versus the alteration of the hyaloclastite tuff samples. Solid circles represent new data and colored filled squares represent previously published data.

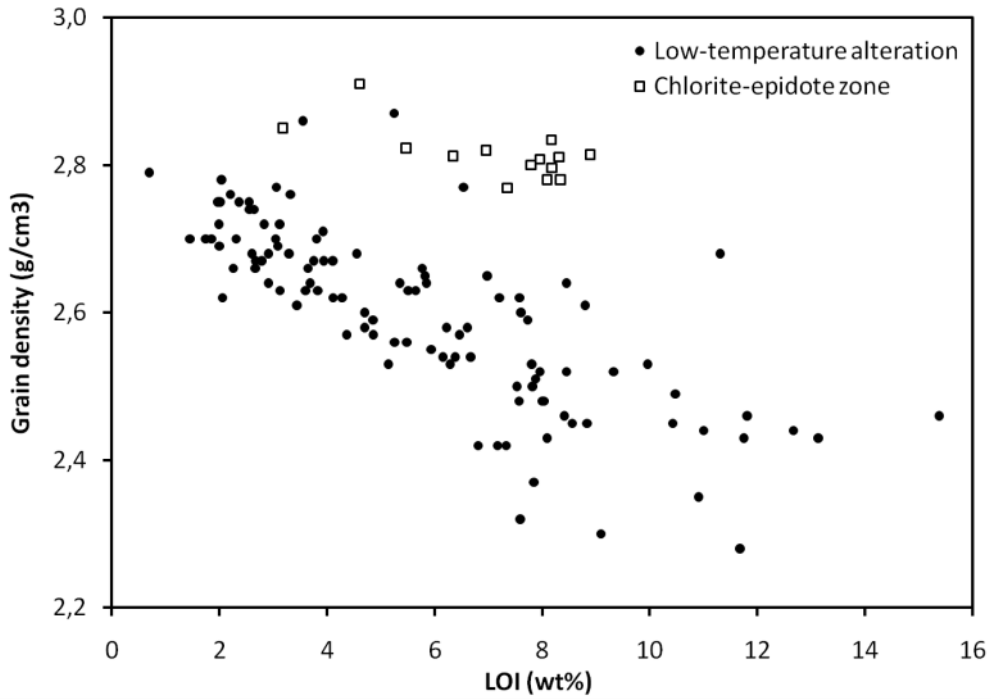


Figure 48. Grain density versus loss on ignition of the hyaloclastite tuff samples. Solid circles represent new data and open squares previously published data.

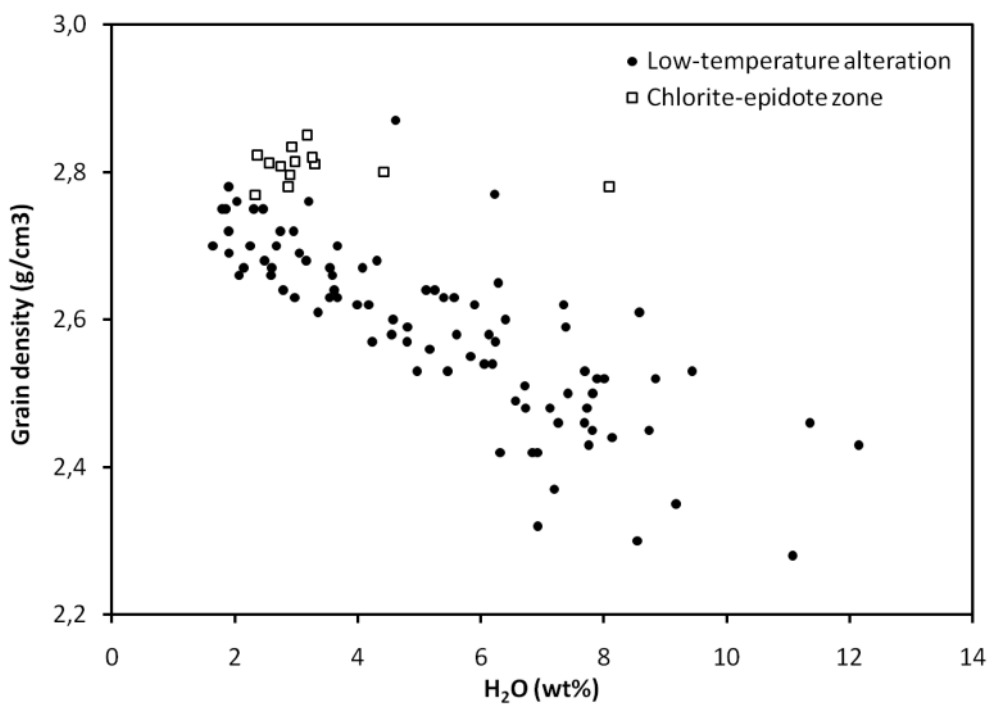


Figure 49. Grain density versus H₂O content of the hyaloclastite tuff samples. Filled circles represent new data and open squares previously published data.

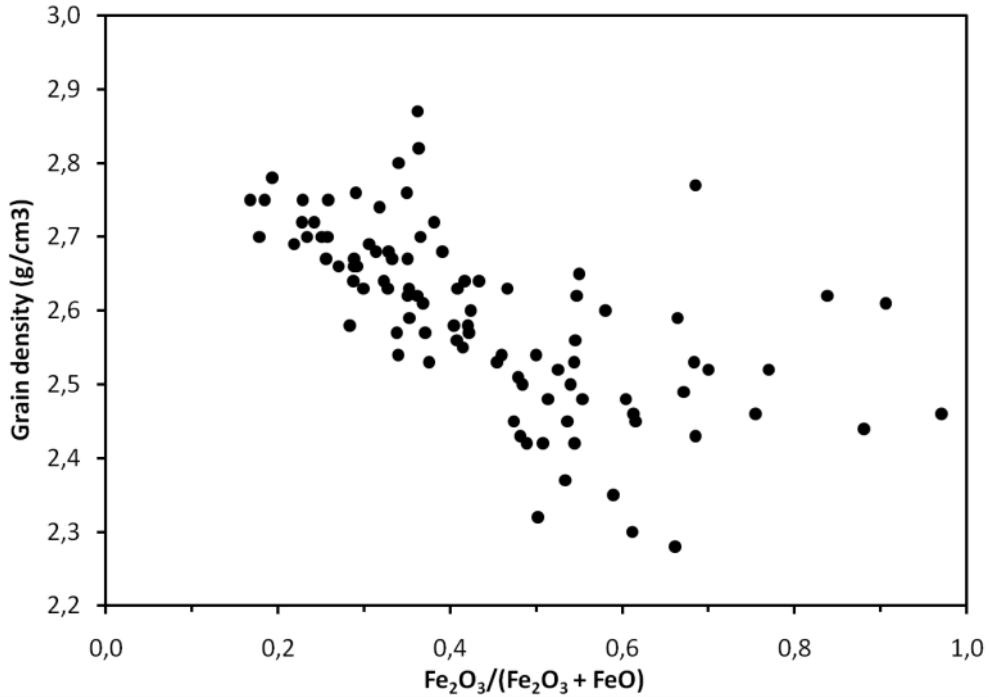


Figure 50. Grain density versus the molar ratio of ferric iron content and total iron content of the hyaloclastite formations.

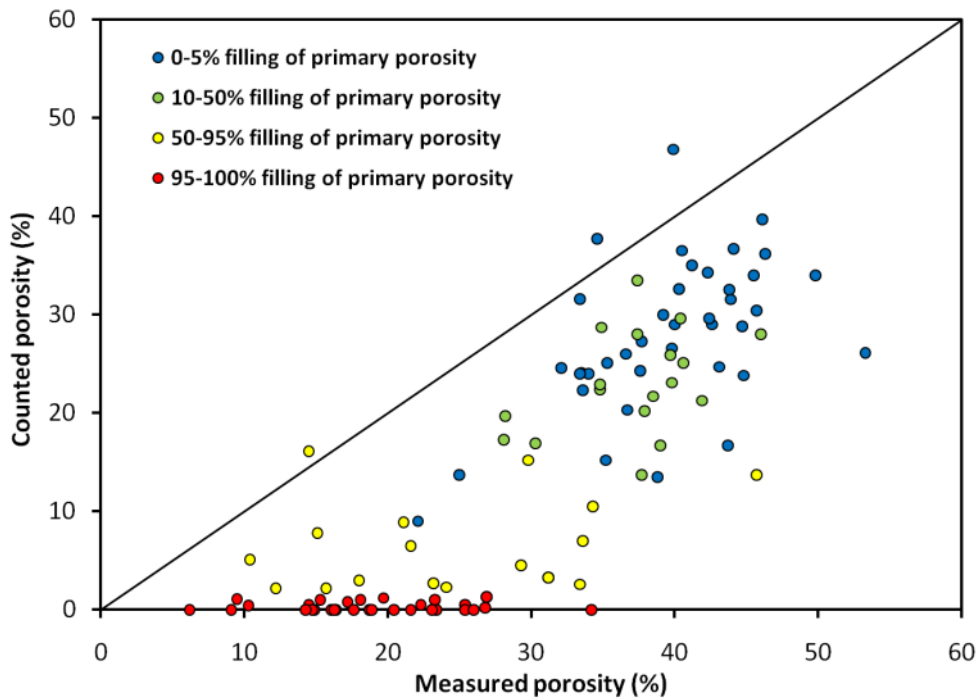


Figure 51. Porosity determined by point counting in thin sections versus porosity measured in air in drill cores of the hyaloclastite tuff samples. The diagonal line indicates equal counted and measured porosity.

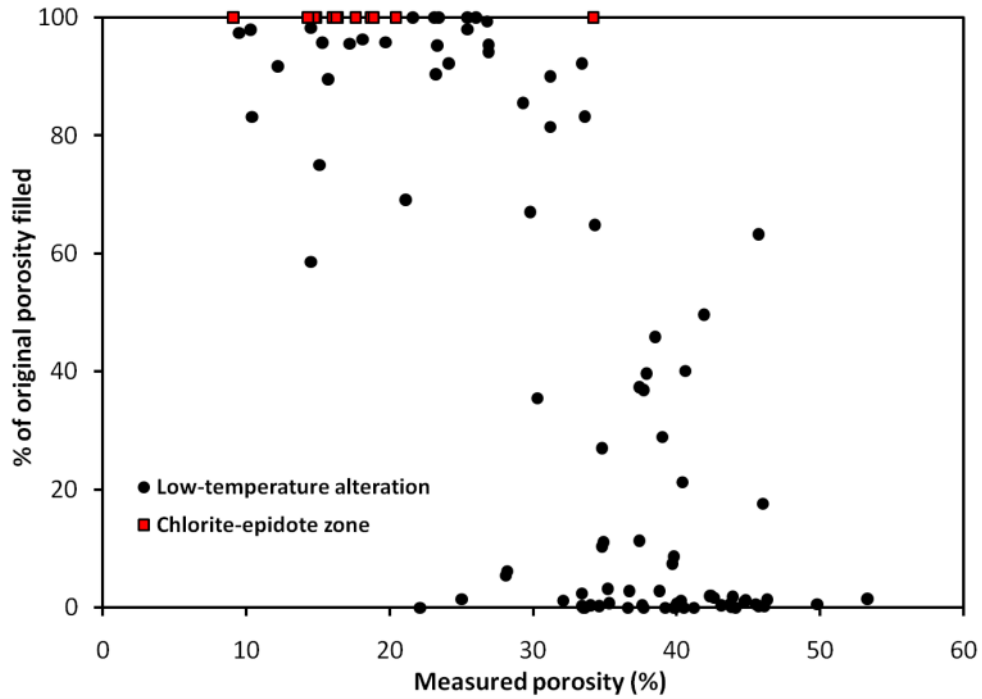


Figure 52. *Infilling of primary porosity determined by point counting versus measured porosity of the hyaloclastite tuff samples.*

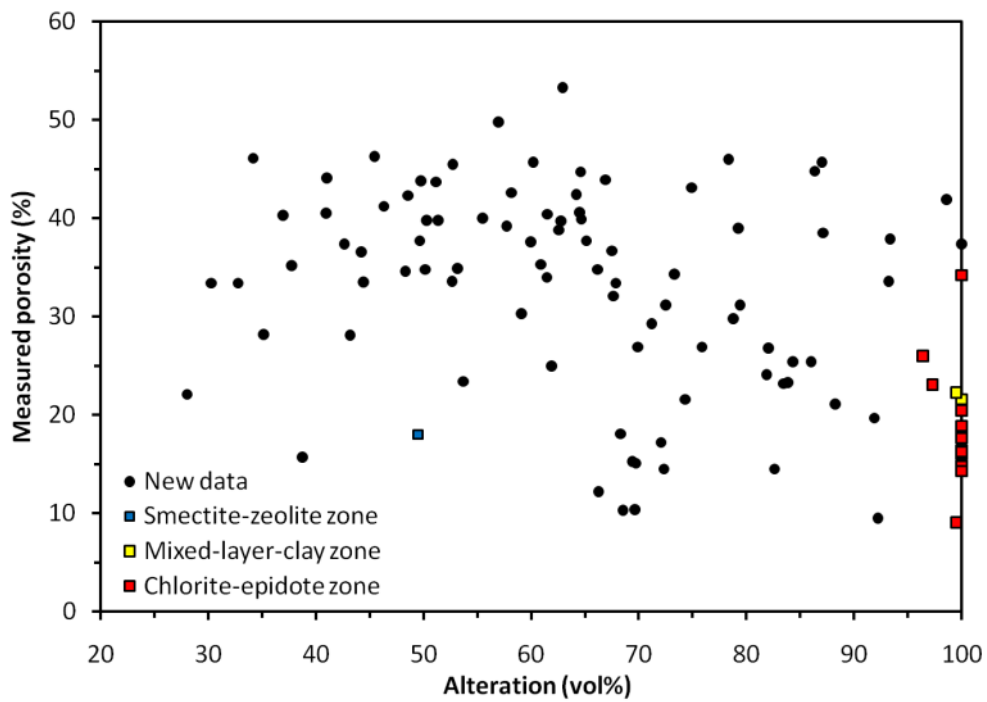


Figure 53. *Porosity measured in drill cores versus the extent of alteration of the hyaloclastite tuff samples.*

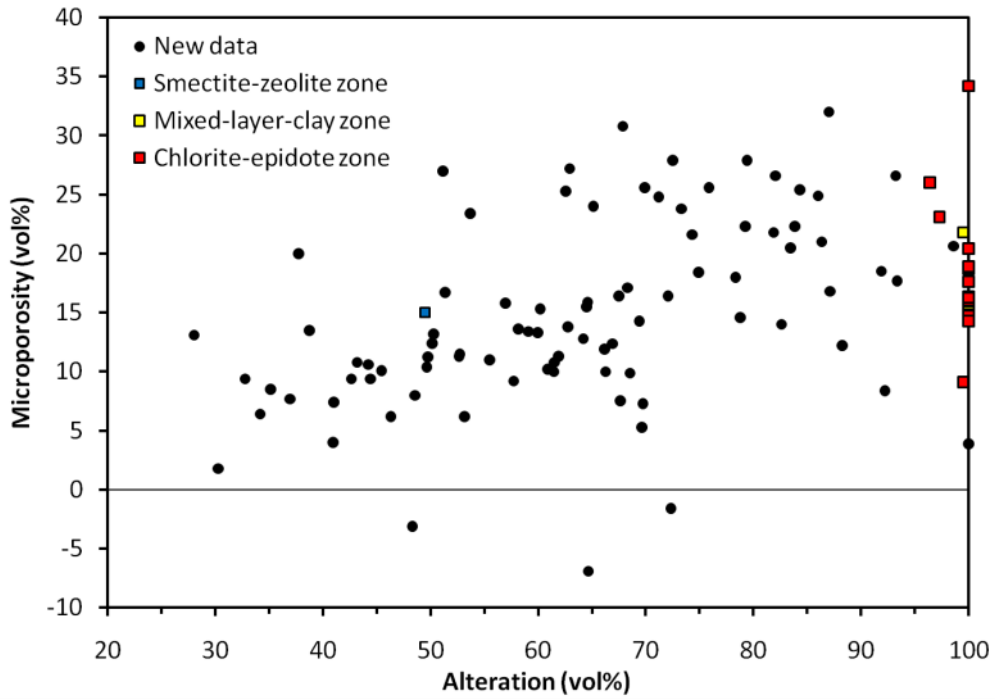


Figure 54. *Micro porosity versus alteration of the hyaloclastite tuff samples. See text for definition of micro porosity.*

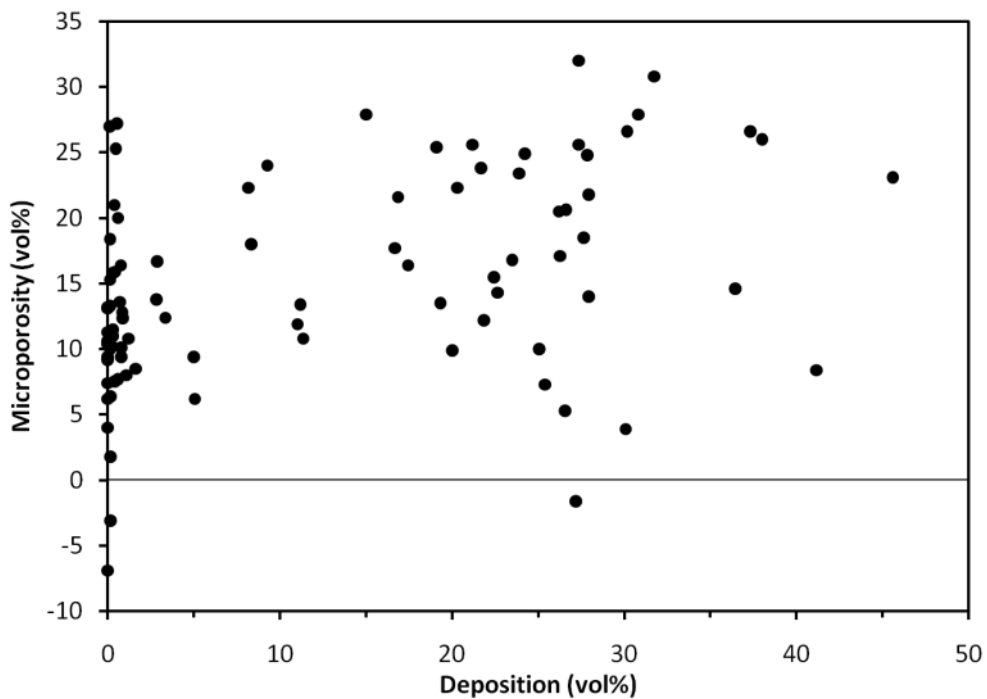


Figure 55. *Micro porosity versus the amount of deposition of secondary minerals in the hyaloclastite tuff samples.*

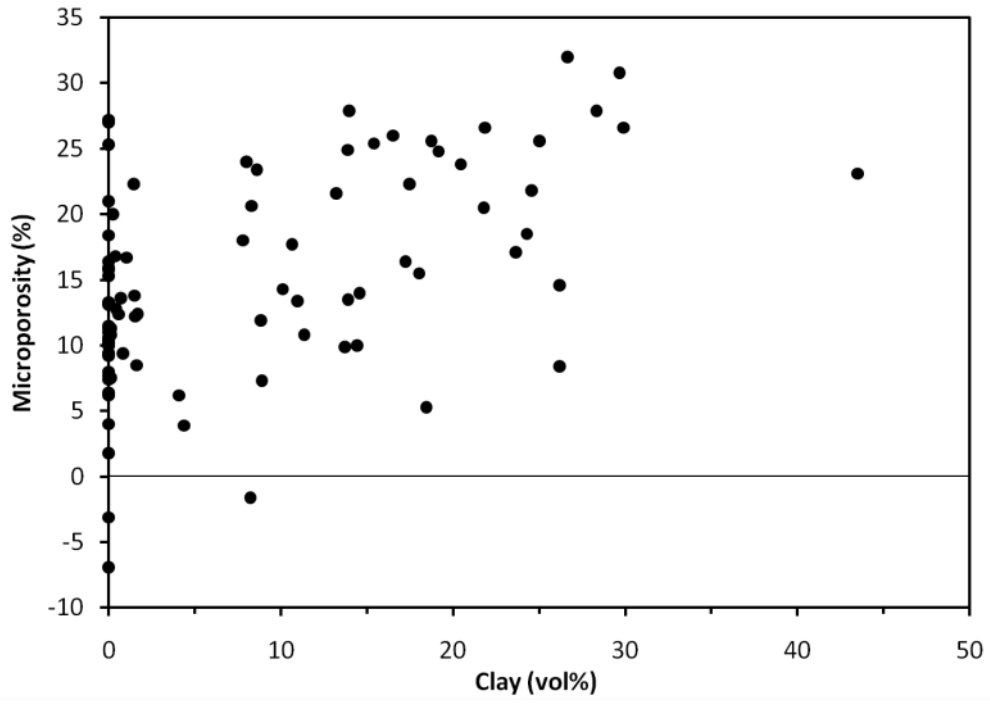


Figure 56. *Micro porosity versus the amount of clay in the hyaloclastite tuff samples.*

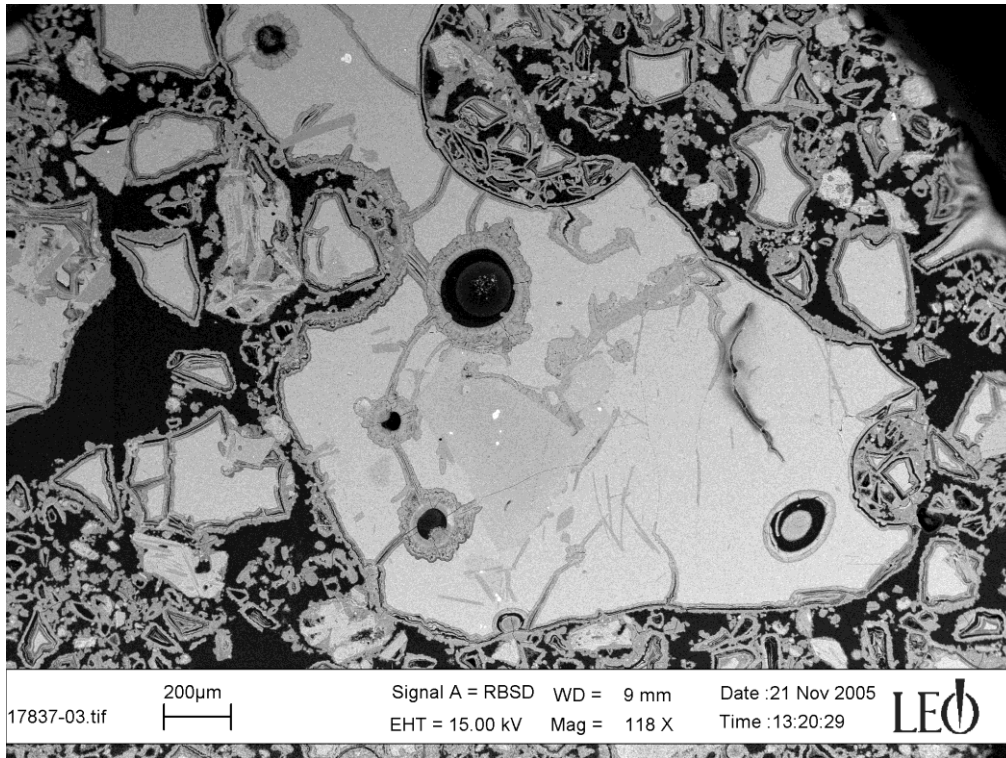


Figure 57. BEI photograph of palagonitized hyaloclastite tuff. The big glass particle is highly fractured with many of the fractures partly or wholly filled with palagonite.

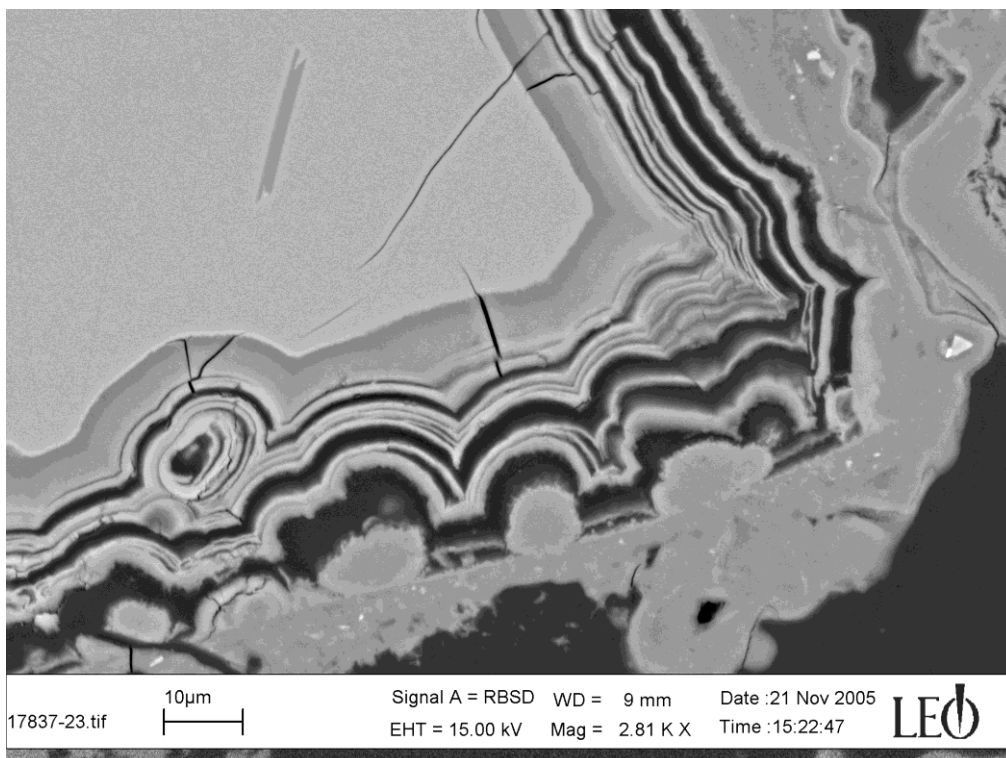


Figure 58. Close-up view of a sideromelane glass particle rimmed with layered palagonite. Open micro fractures are seen extending from the palagonite into the sideromelane glass.

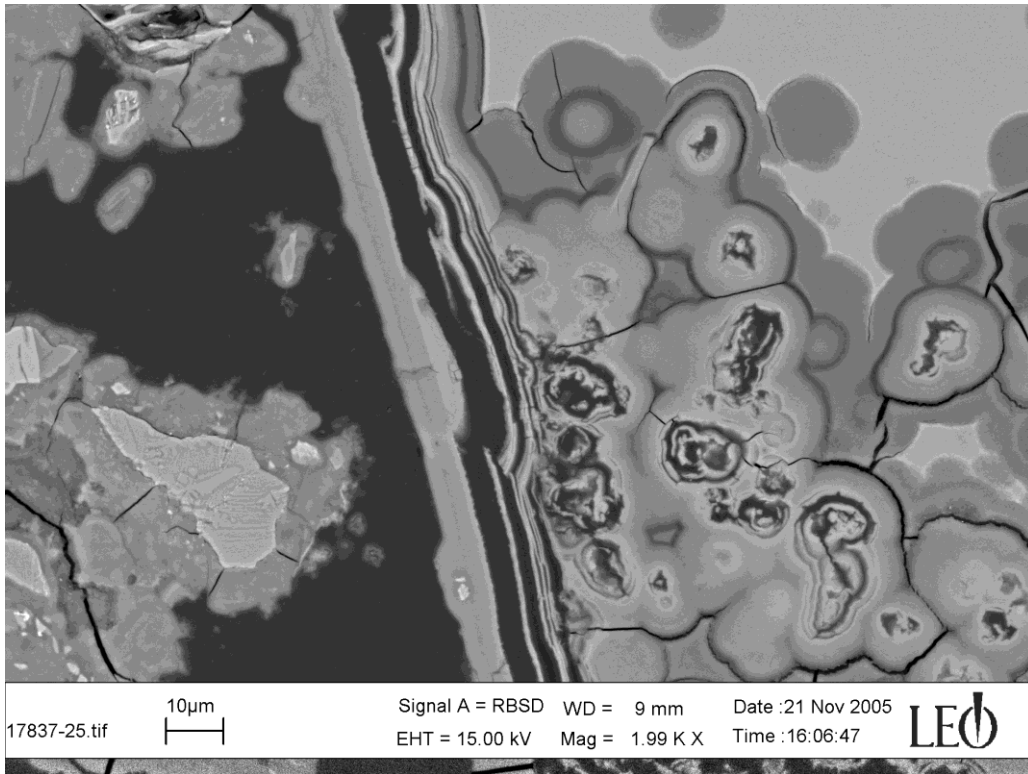


Figure 59. BEI photograph of palagonitized basaltic glass. The palagonite is highly fractured without the fractures extending into the glass.

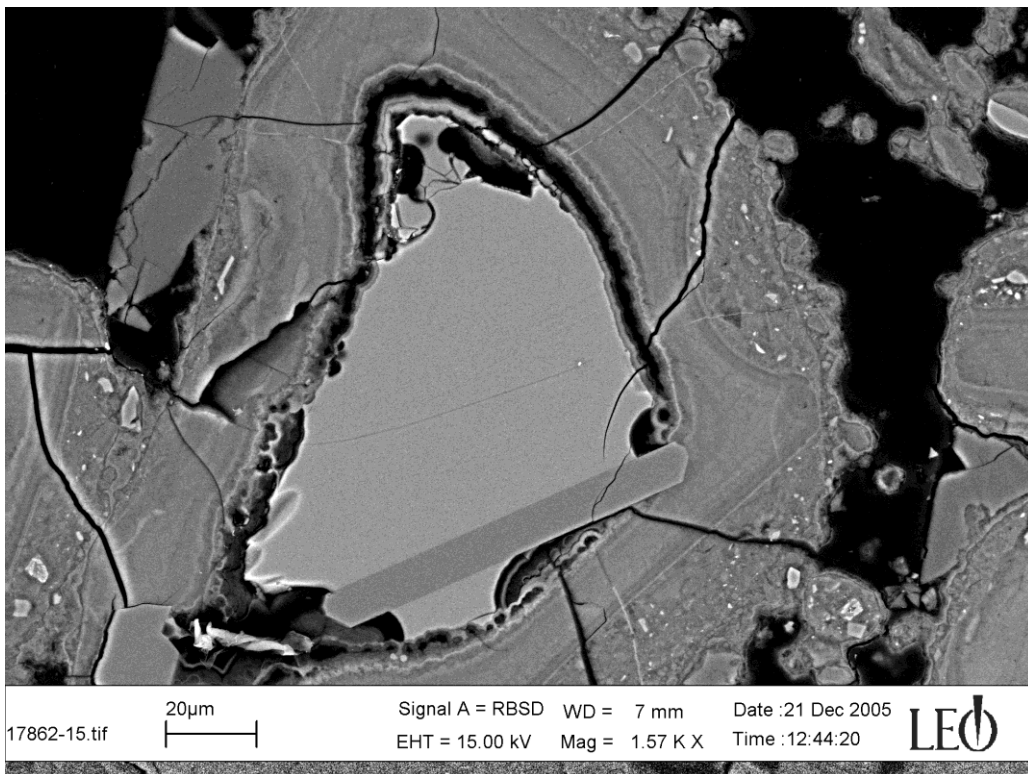


Figure 60. BEI photograph of a palagonitized sideromelane glass particle. Notice micro fractures, some open and other filled with palagonite. Fractures are seen penetrating both palagonite and fresh glass (along with an unaltered plagioclase phenocryst).

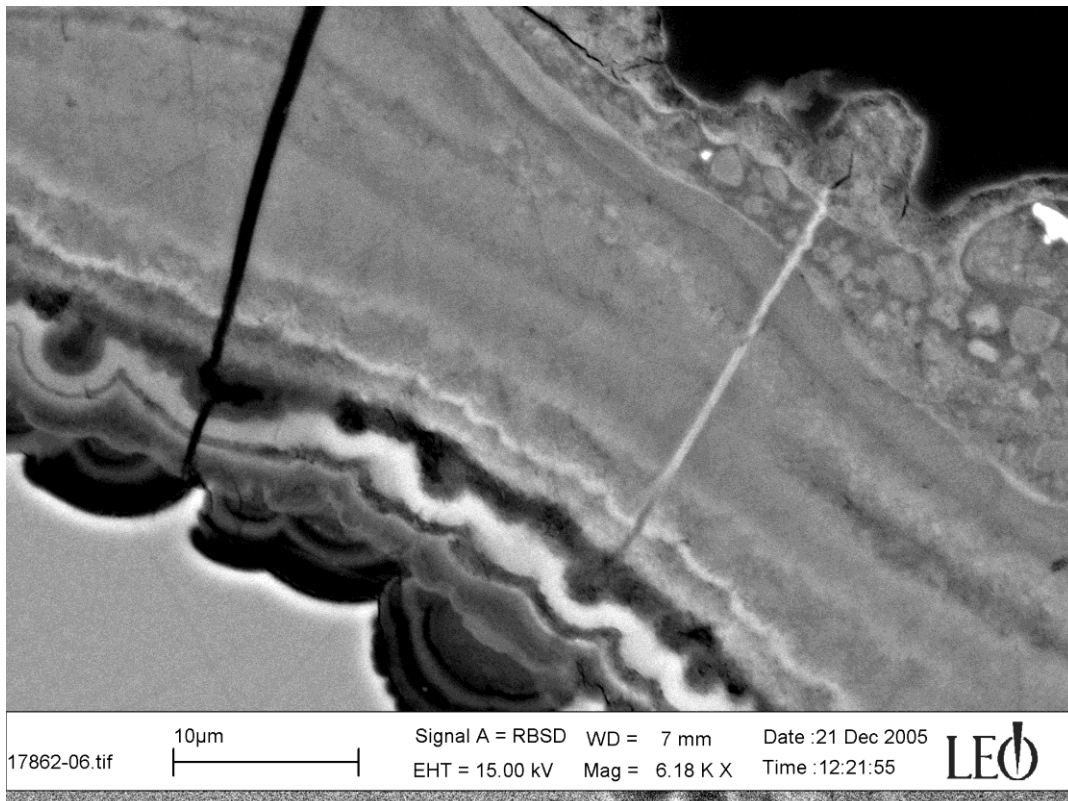


Figure 61. Close-up view of a palagonitized glass particle. Notice micro fractures in palagonite, one filled and the other open.

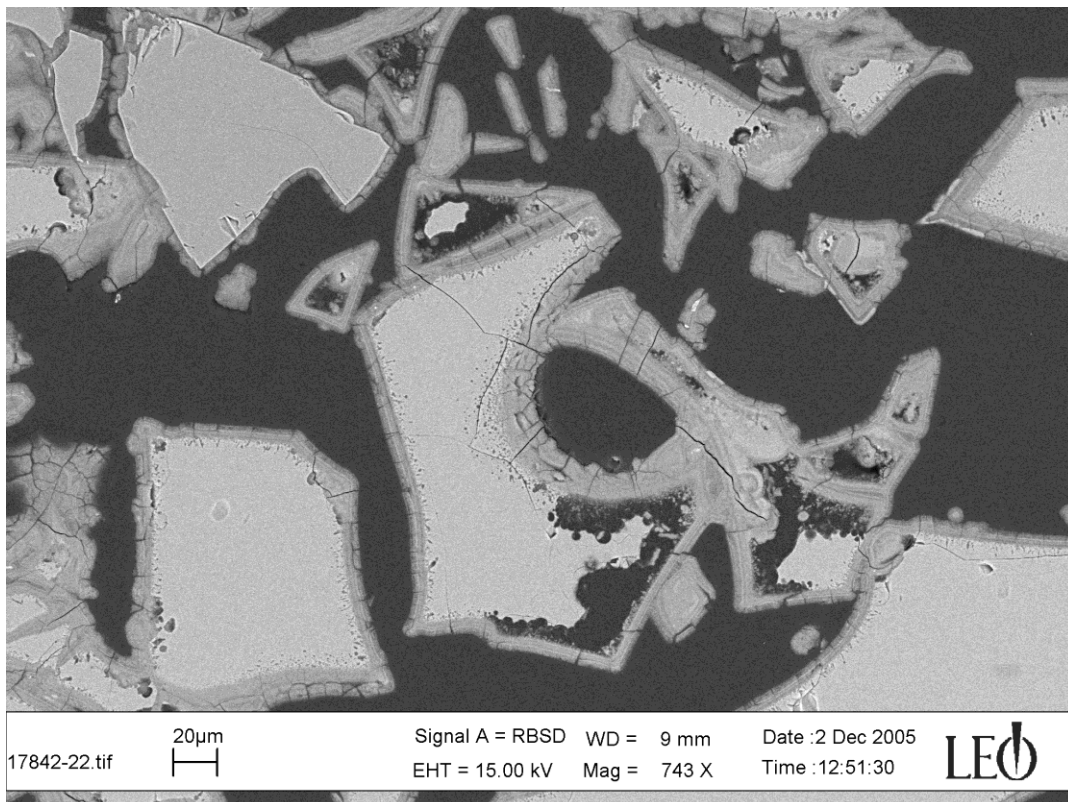


Figure 62. BEI photograph of palagonitized hyaloclastite tuff. Notice tubules on the rims of the fresh glass cores.

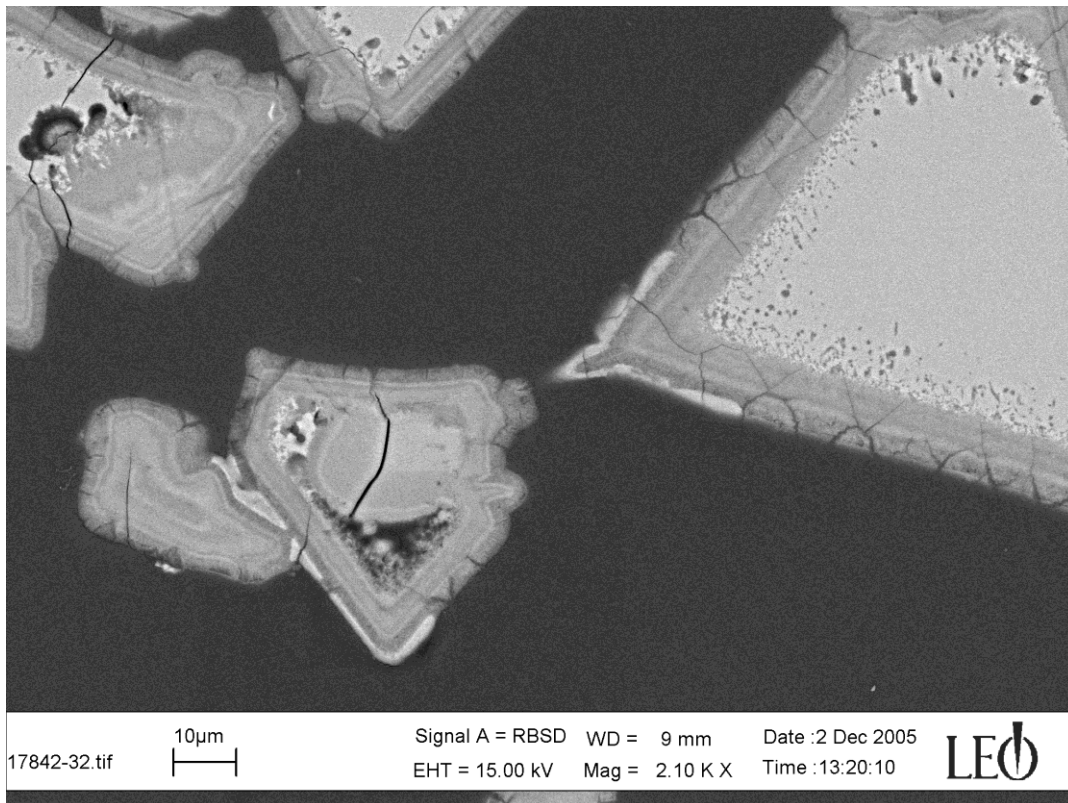


Figure 63. BEI photographs of a few palagonitized glass particles. Notice tubules on the rims of the fresh glass cores. Also notice micro fractures.

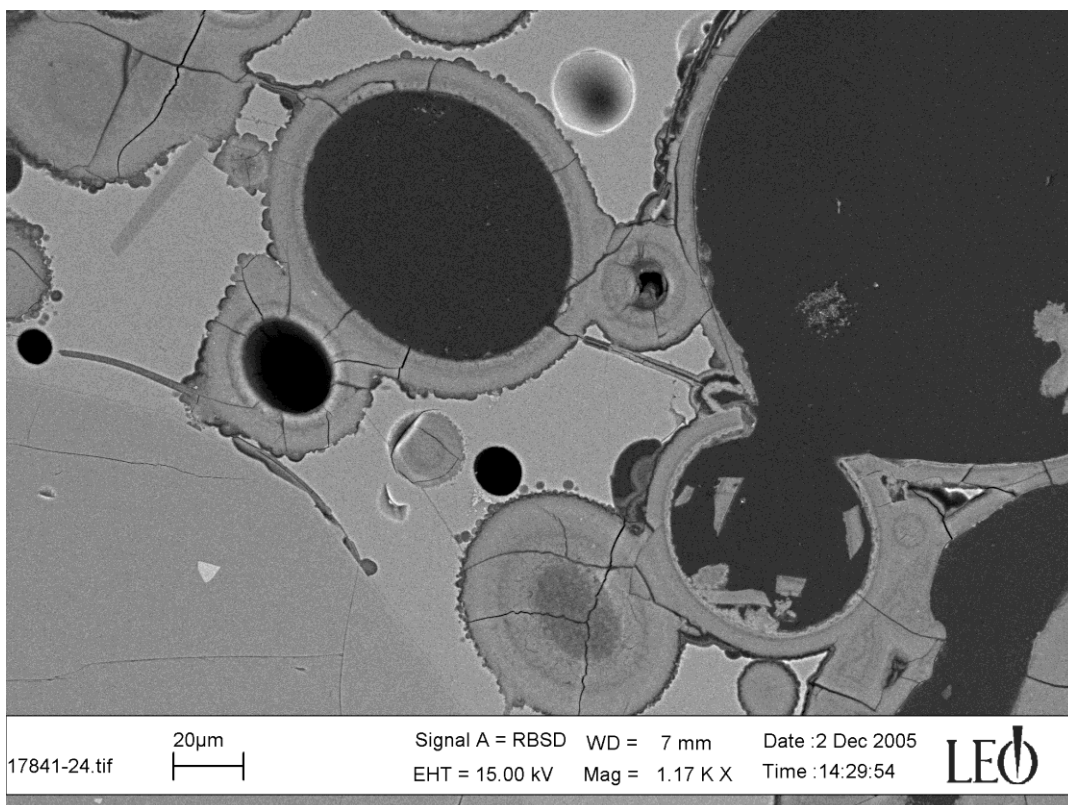


Figure 64. BEI photograph of hyaloclastite tuff. Notice pits between palagonite rinds and fresh glass. Also notice micro fractures, some lined with palagonite.

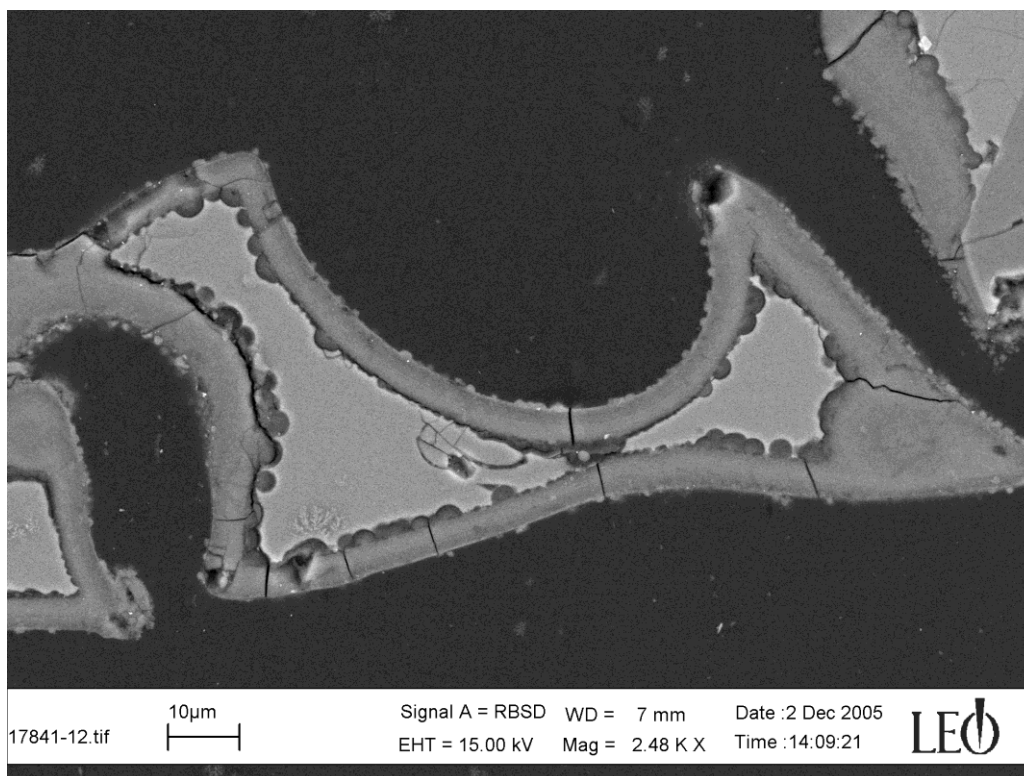


Figure 65. BEI photograph of a palagonitized glass particle. Notice pits between sideromelane and palagonite.

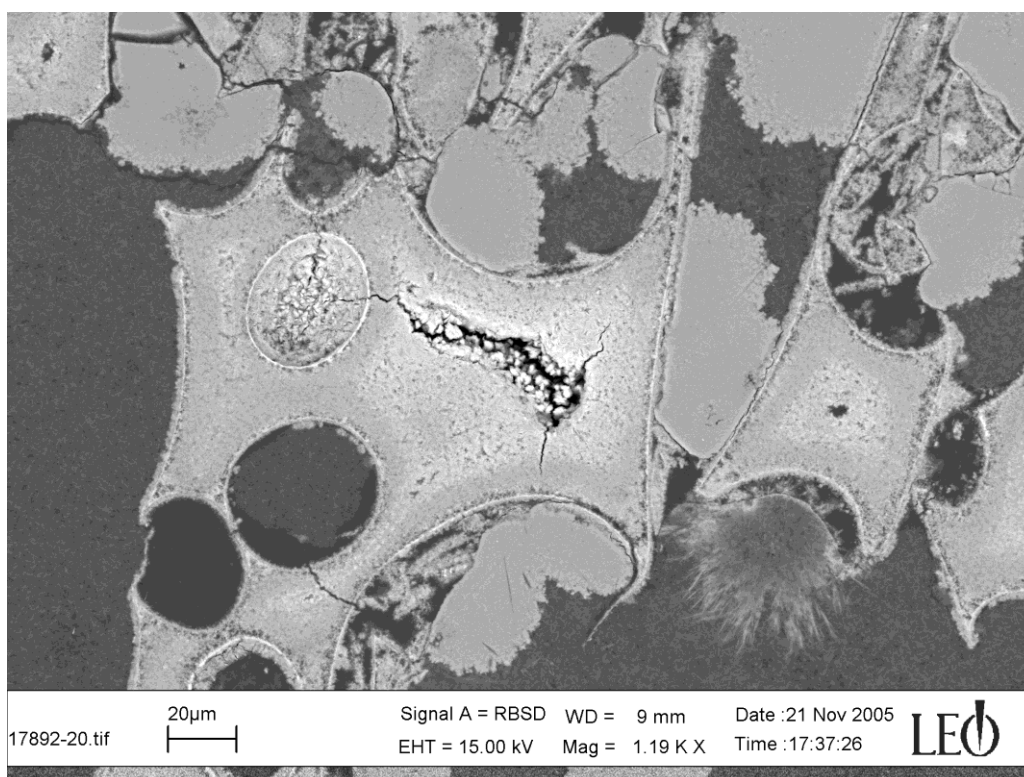


Figure 66. BEI photograph of a highly altered hyaloclastite tuff sample. The original glass particles have been replaced by smectite and the primary pores are partly filled with secondary minerals.

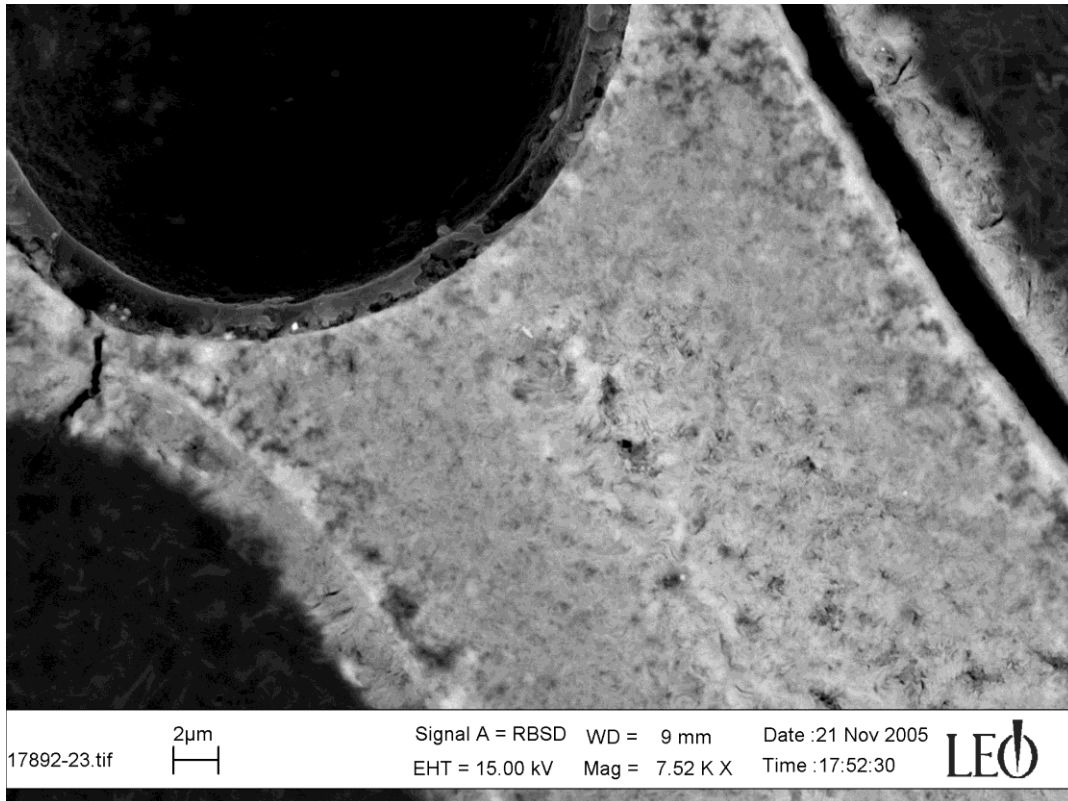


Figure 67. *Close-up view of a particle in a hyaloclastite tuff sample where the original sideromelane glass has been replaced by smectite. Notice the high porosity of the smectite.*

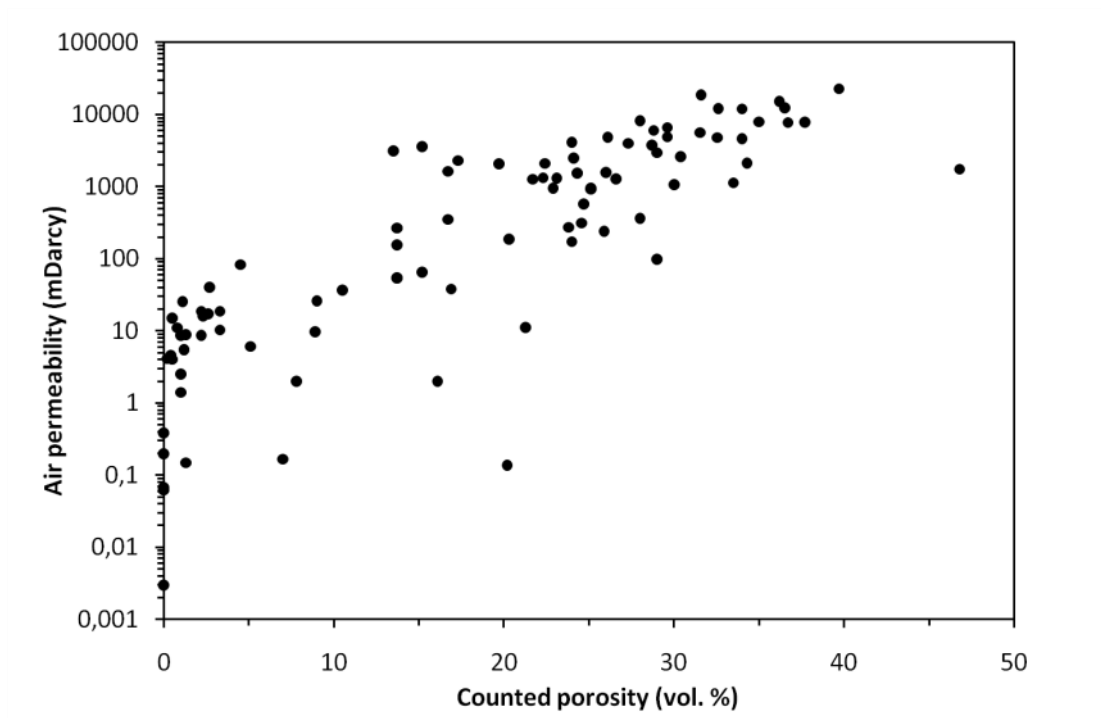


Figure 68. Air permeability versus porosity determined by point counting in thin sections in the hyaloclastite tuff samples.

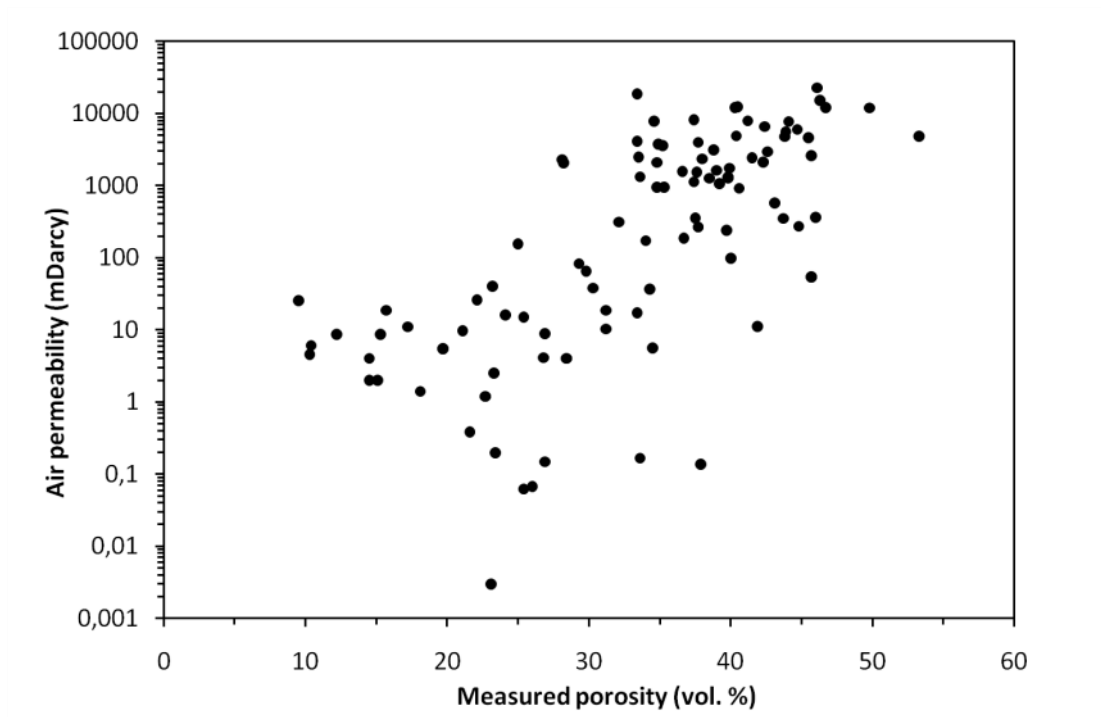


Figure 69. Air permeability and measured porosity of the hyaloclastite tuff samples.

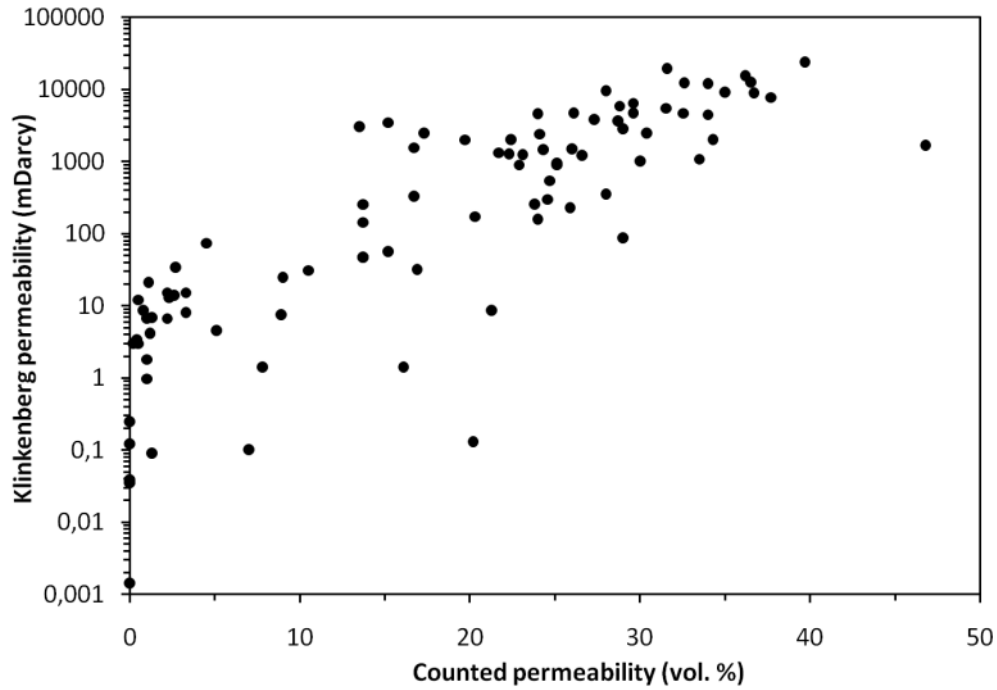


Figure 70. *Klinkenberg air permeability versus porosity determined by point counting in thin sections in the hyaloclastite tuff samples.*

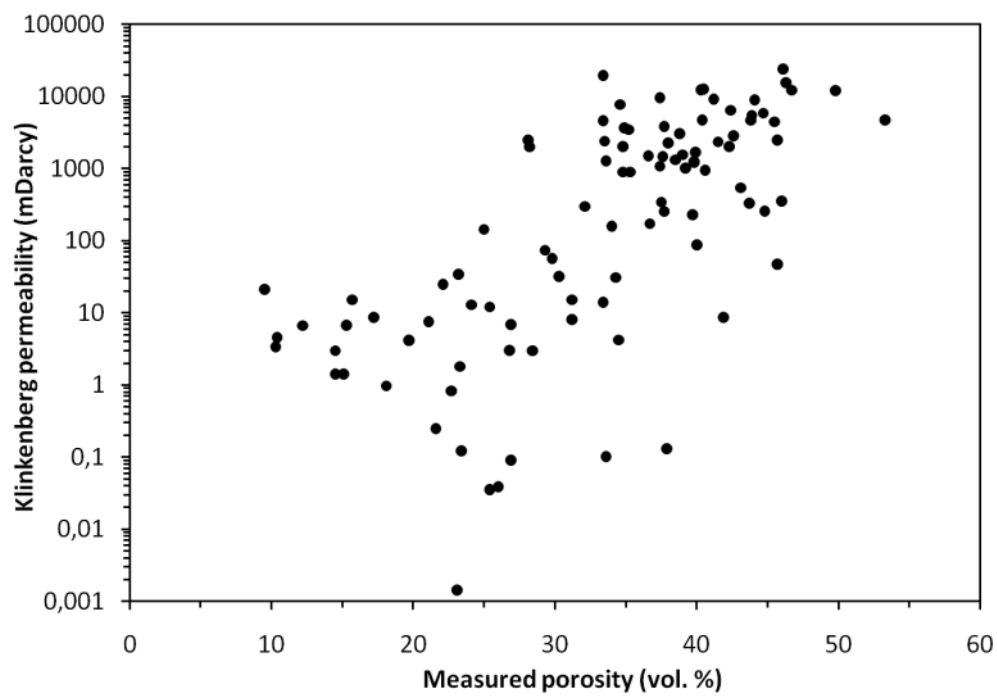


Figure 71. *Klinkenberg air permeability and measured porosity in the hyaloclastite tuff samples.*

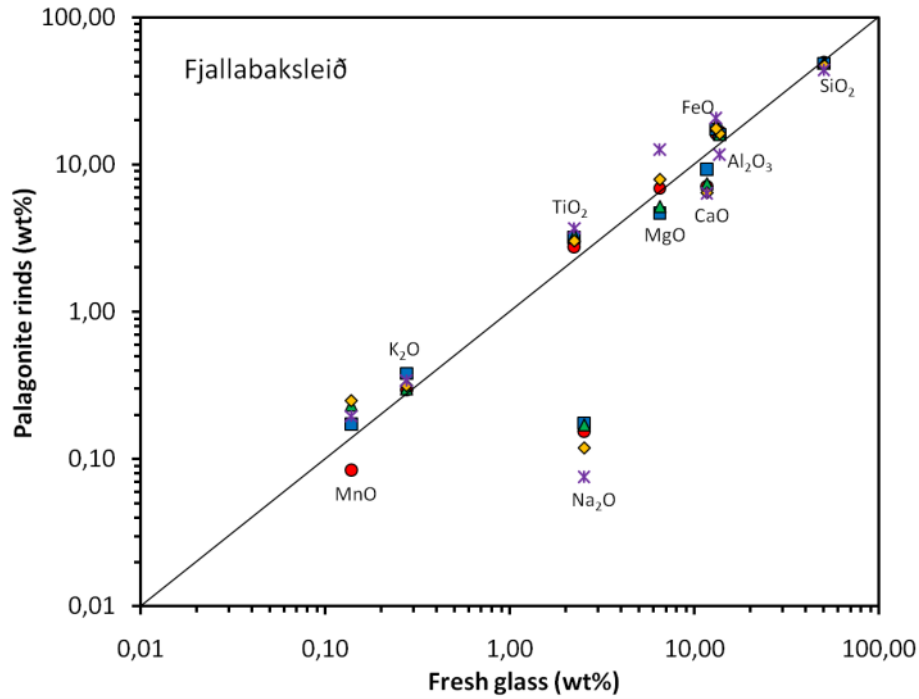


Figure 72. Comparison of the concentrations of 9 different oxides in fresh glass (1 spot analysis) and palagonite rinds (5 spot analyses) in a hyaloclastite tuff formation at Fjallabaksleið. Notice the logarithmic scales.

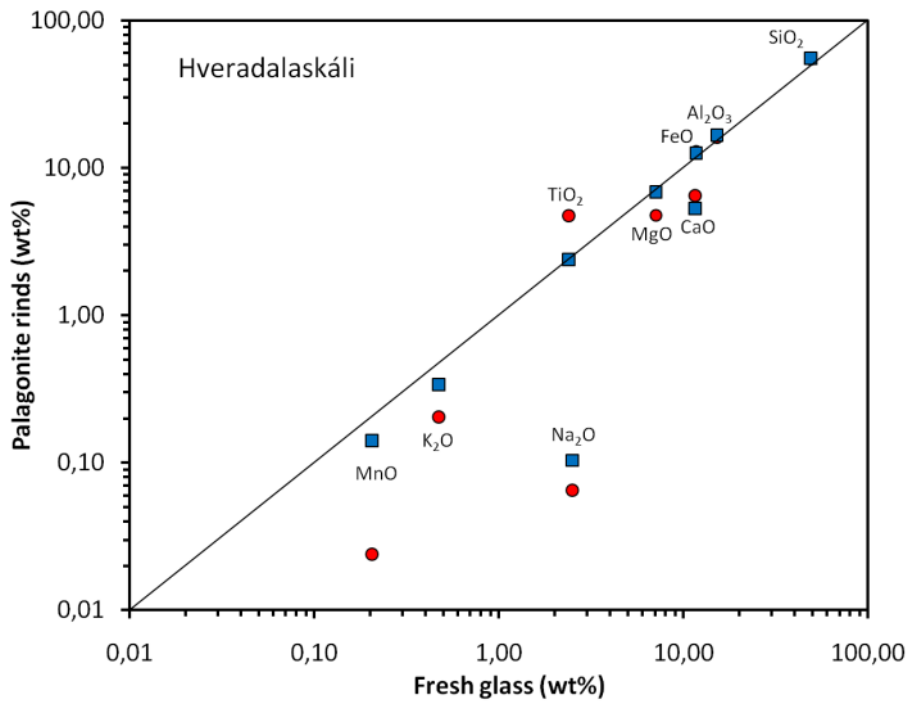


Figure 73. Comparison of the concentrations of 9 different oxides in fresh glass (1 spot analysis) and palagonite rinds (2 spot analyses) in a hyaloclastite tuff formation at Hveradalaskáli. Notice the logarithmic scales.

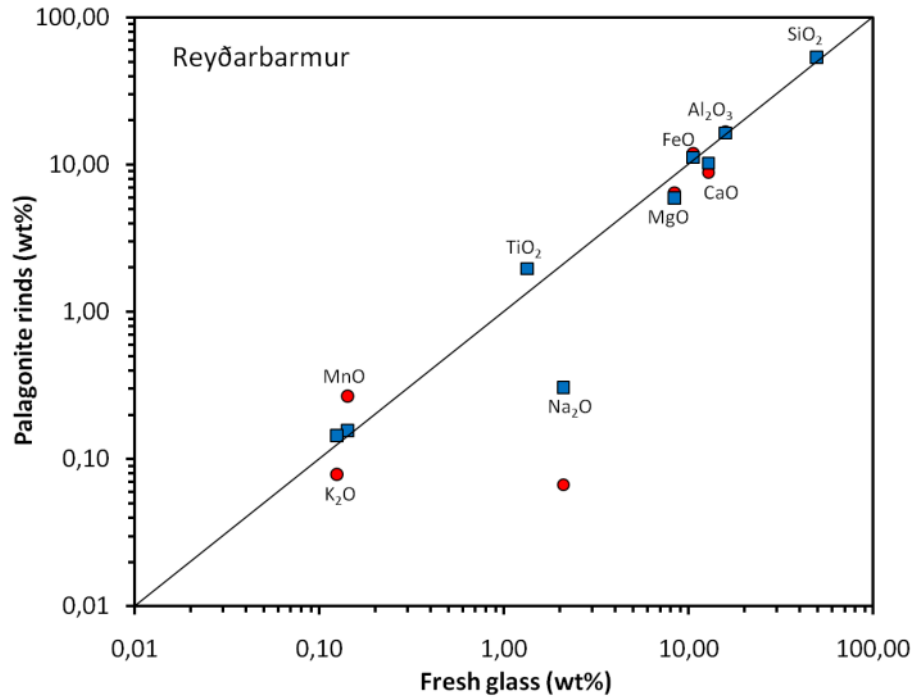


Figure 74. Comparison of the concentrations of 9 different oxides in fresh glass (1 spot analysis) and palagonite rinds (2 spot analyses) in a hyaloclastite tuff formation at Reyðarbarmur. Notice the logarithmic scales.

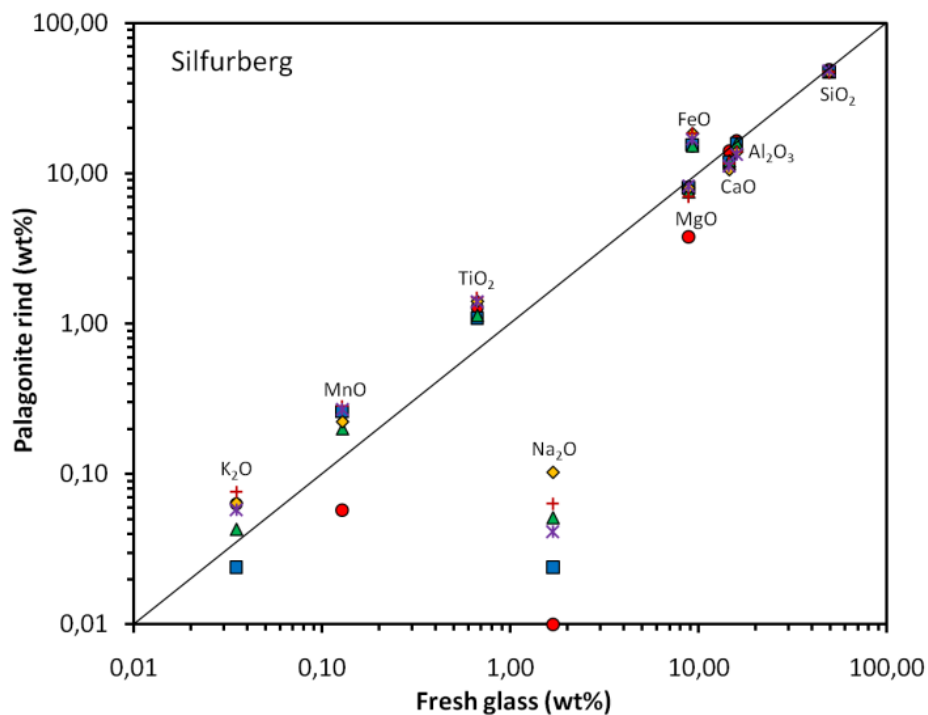


Figure 75. Comparison of the concentrations of 9 different oxides in fresh glass (1 spot analysis) and palagonite rinds (6 spot analyses) in a hyaloclastite tuff formation at Silfurberg. Notice the logarithmic scales.

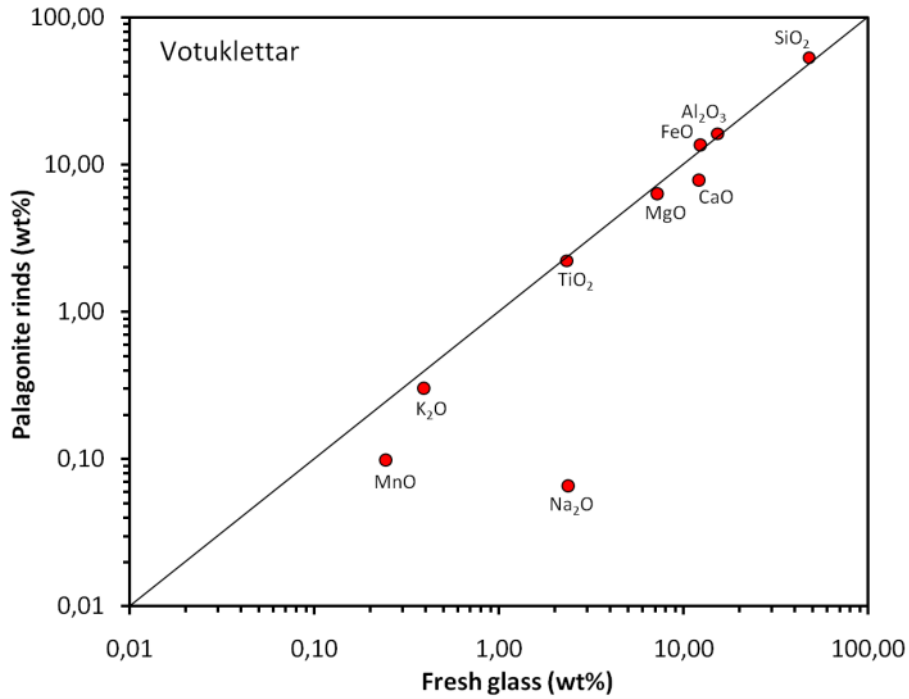


Figure 76. Comparison of the concentrations of 9 different oxides in fresh glass and in palagonite rind in a hyaloclastite tuff formation at Votuklettur. Notice the logarithmic scales.

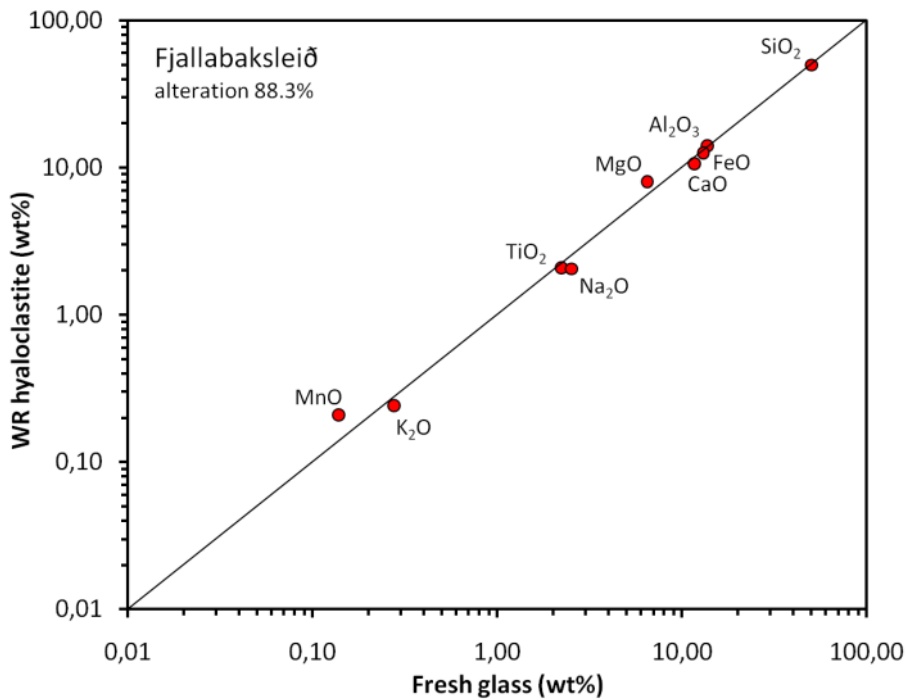


Figure 77. Comparison of a whole-rock analysis of a hyaloclastite sample from Fjallabaksleið with an EMP analysis of fresh glass from the same formation. Notice the logarithmic scales.

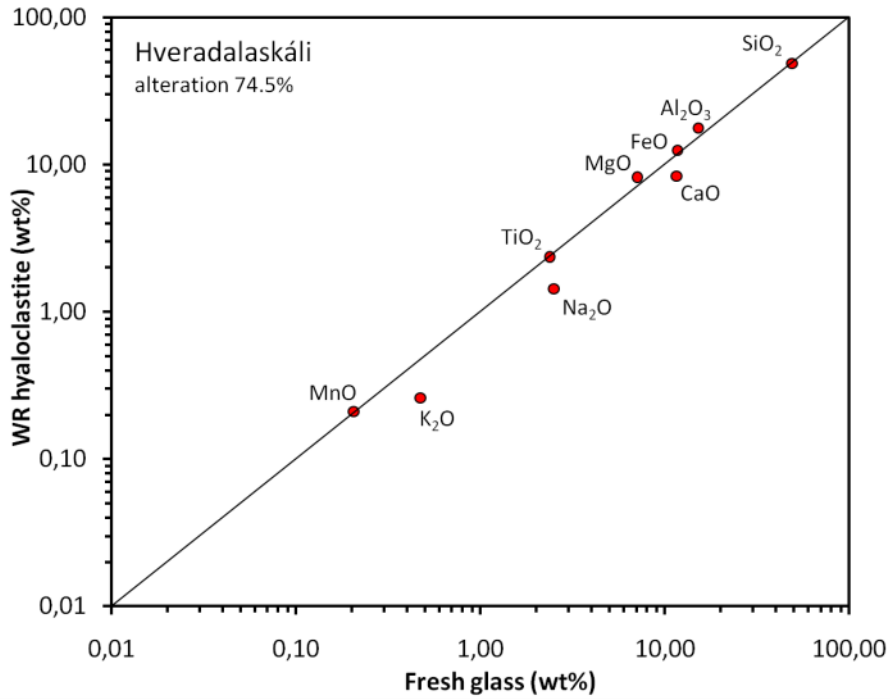


Figure 78. Comparison of a whole-rock analysis of a hyaloclastite sample from Hveradalaskáli with an EMP analysis of fresh glass from the same formation. Notice the logarithmic scales.

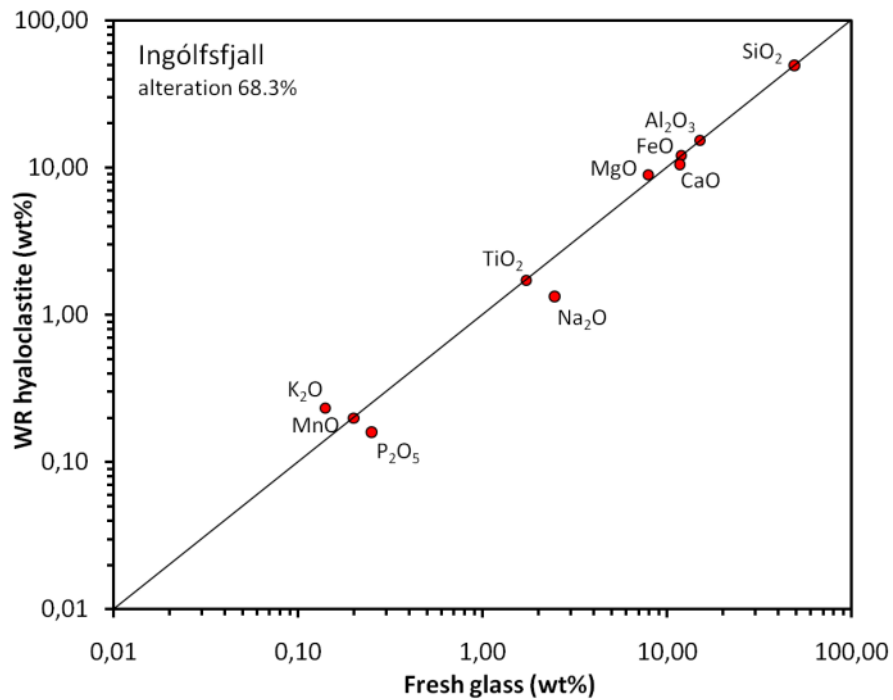


Figure 79. Comparison of a whole-rock analysis of a hyaloclastite sample from Ingólfssjall with an EMP analysis of fresh glass from the same formation. Notice the logarithmic scales.

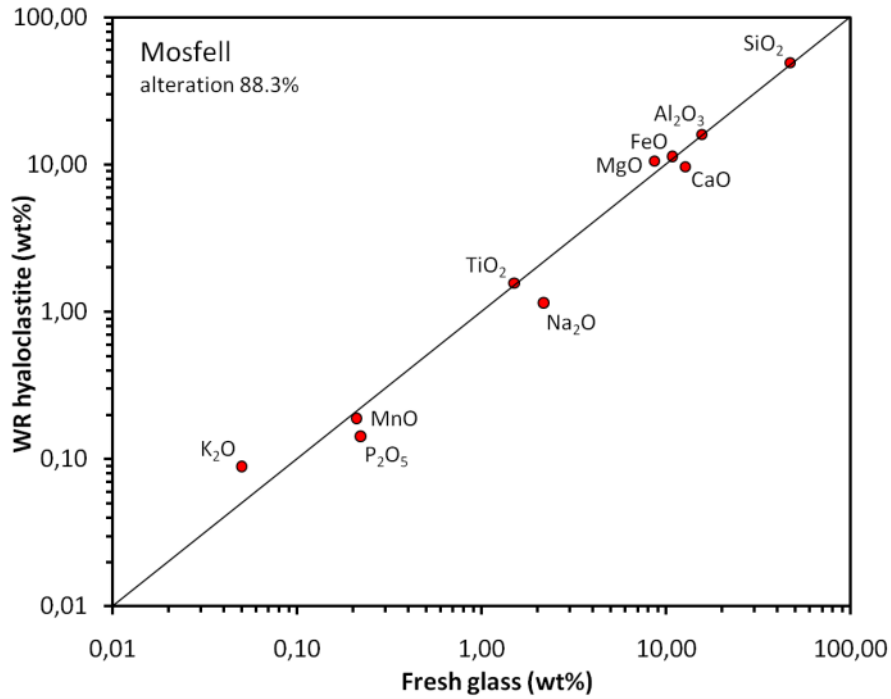


Figure 80. Comparison of a whole-rock analysis of a hyaloclastite sample from Mosfell with an EMP analysis of fresh glass from the same formation. Notice the logarithmic scales.

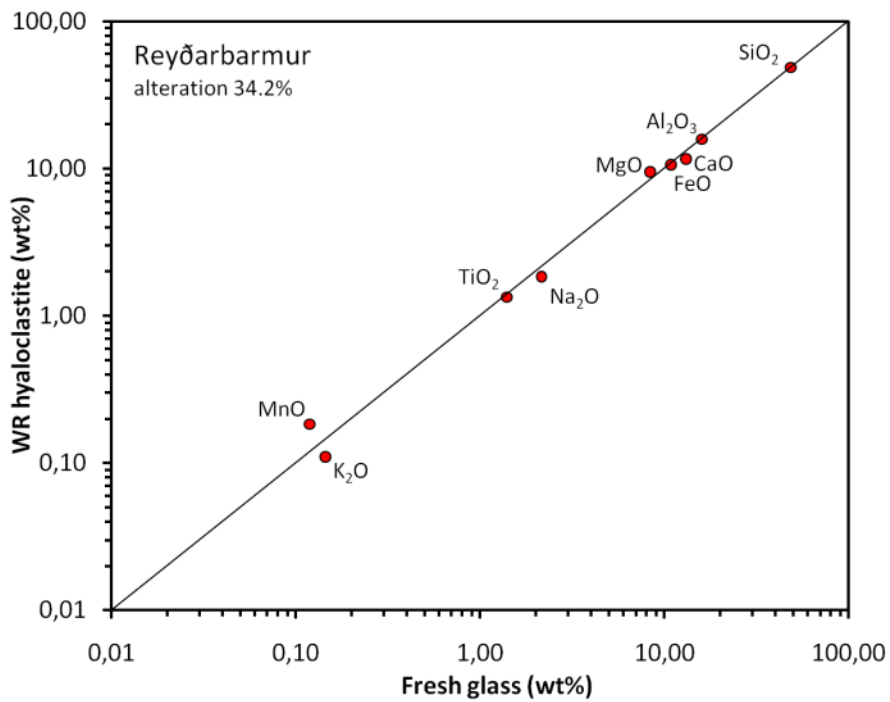


Figure 81. Comparison of a whole-rock analysis of a hyaloclastite sample from Reyðarbarmur with an EMP analysis of fresh glass from the same formation. Notice the logarithmic scales.

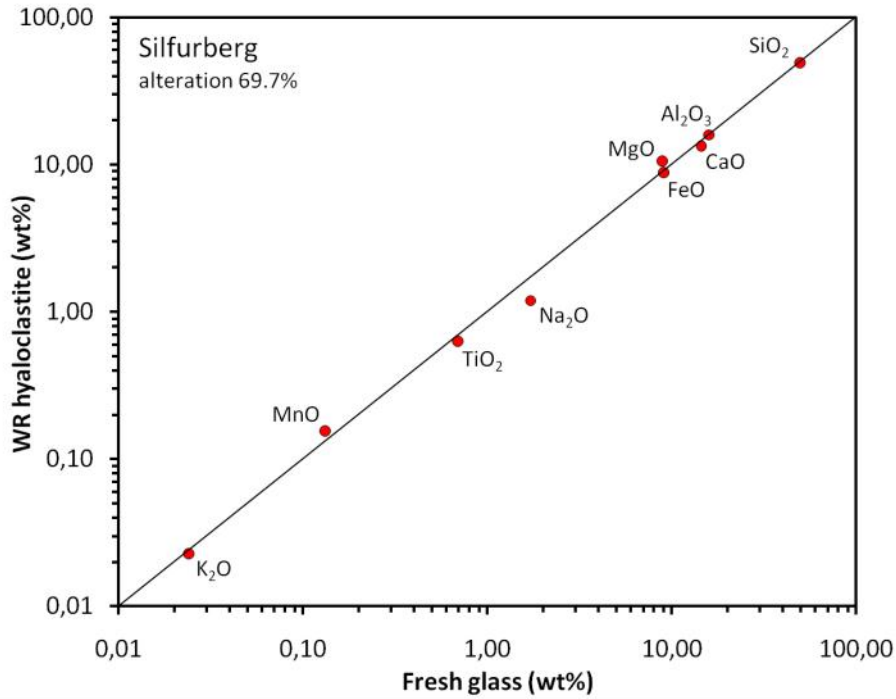


Figure 82. Comparison of a whole-rock analysis of a hyaloclastite sample from Silfurberg with an EMP analysis of fresh glass from the same formation. Notice the logarithmic scales.

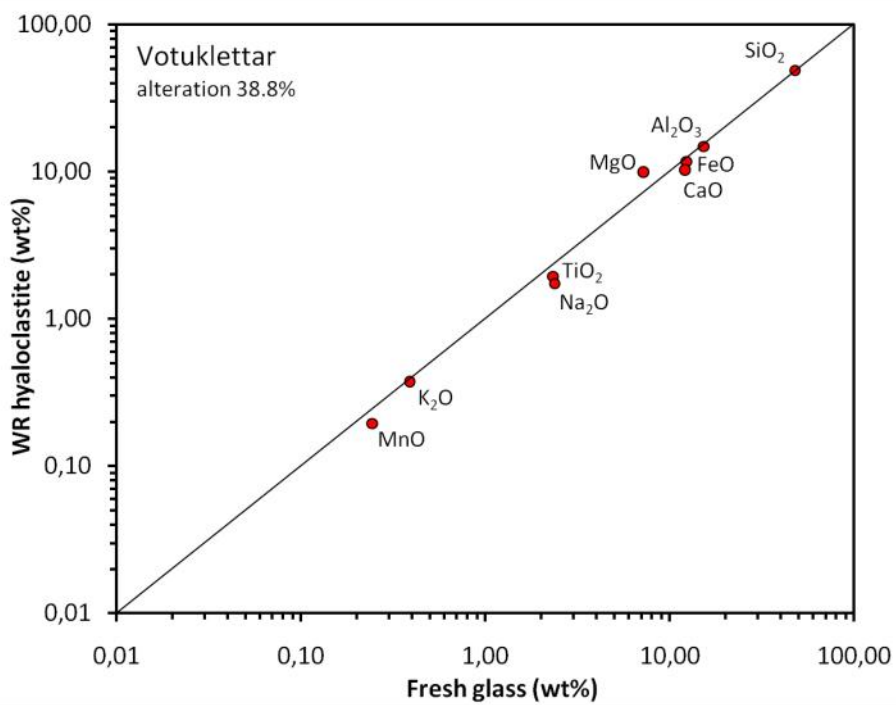


Figure 83. Comparison of a whole-rock analysis of a hyaloclastite sample from Votuklettur with an EMP analysis of fresh glass from the same formation. Notice the logarithmic scales.

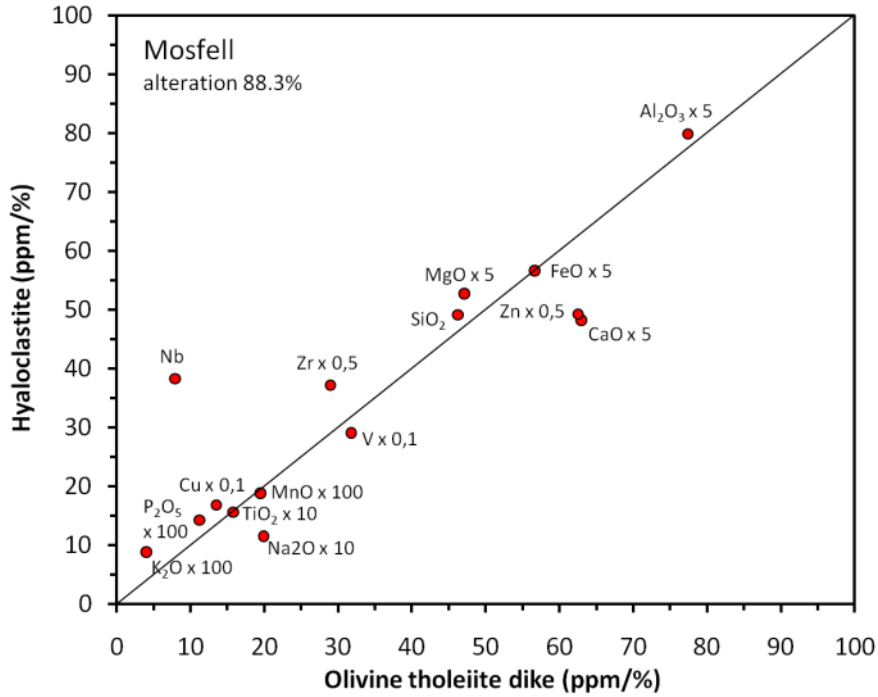


Figure 84. Comparison of the WR composition of a hyaloclastite sample and a related crystallized sample from Mosfell. Several major and minor oxides (wt%) and trace elements (ppm) have been included. Multiplication factors are used for most elements for clarity.

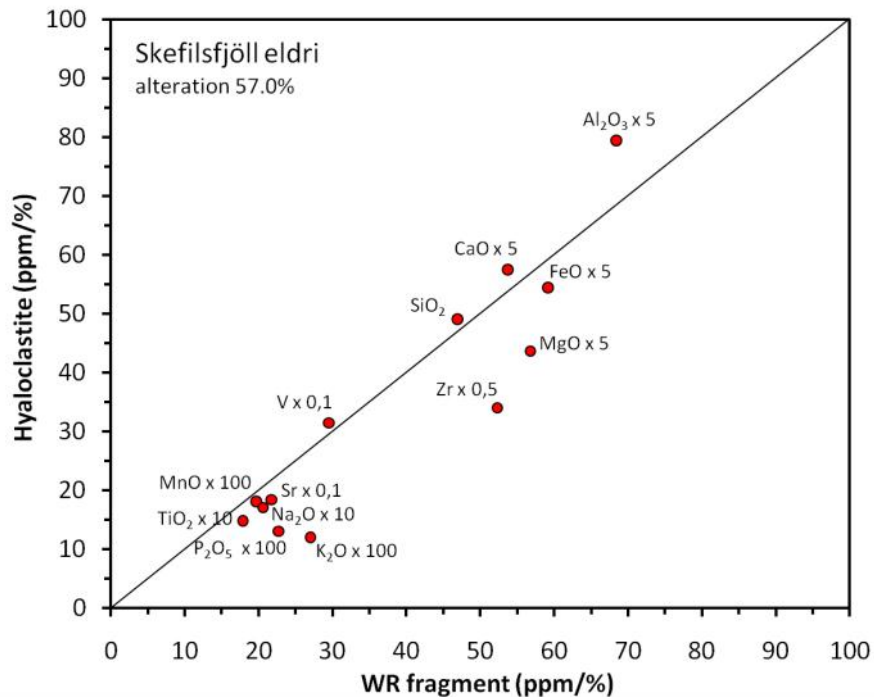


Figure 85. Comparison of the WR composition of a hyaloclastite sample and a related crystallized sample from Skefilsfjöll eldri. Several major and minor oxides (wt%) and trace elements (ppm) have been included. Multiplication factors are used for most elements for clarity.

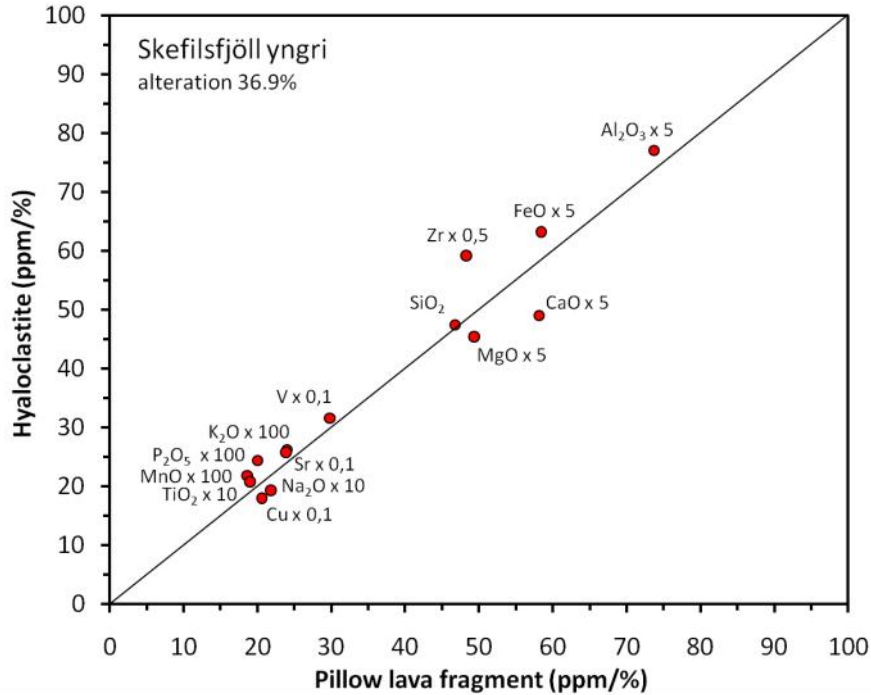


Figure 86. Comparison of the WR composition of a hyaloclastite sample and a related crystallized sample from Skefilsfjöll yngri. Several major and minor oxides (wt%) and trace elements (ppm) have been included. Multiplication factors are used for most elements for clarity.

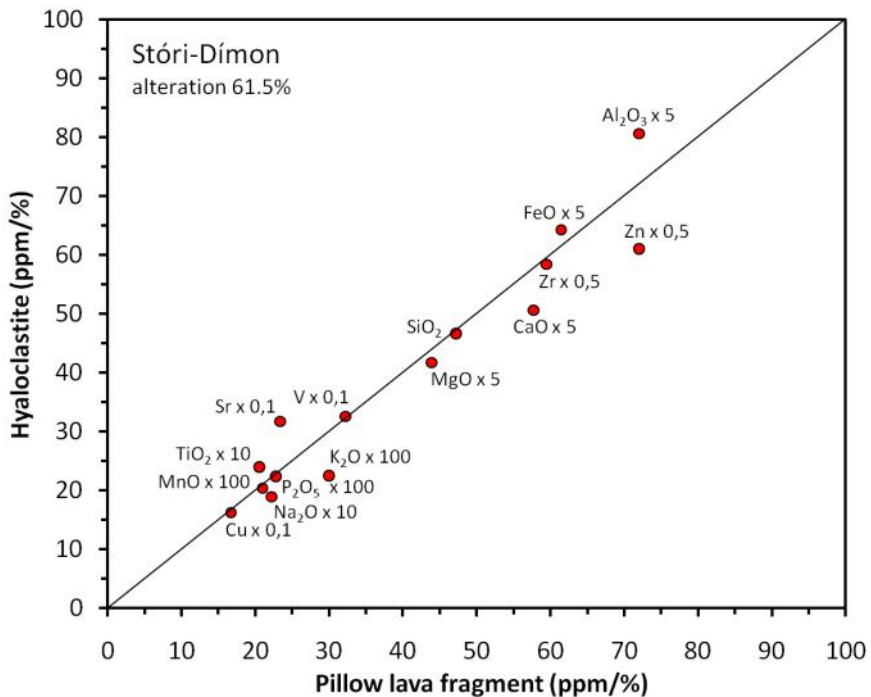


Figure 87. Comparison of the WR composition of a hyaloclastite sample and a related crystallized sample from Stóri-Dímon. Several major and minor oxides (wt%) and trace elements (ppm) have been included. Multiplication factors are used for most elements for clarity.

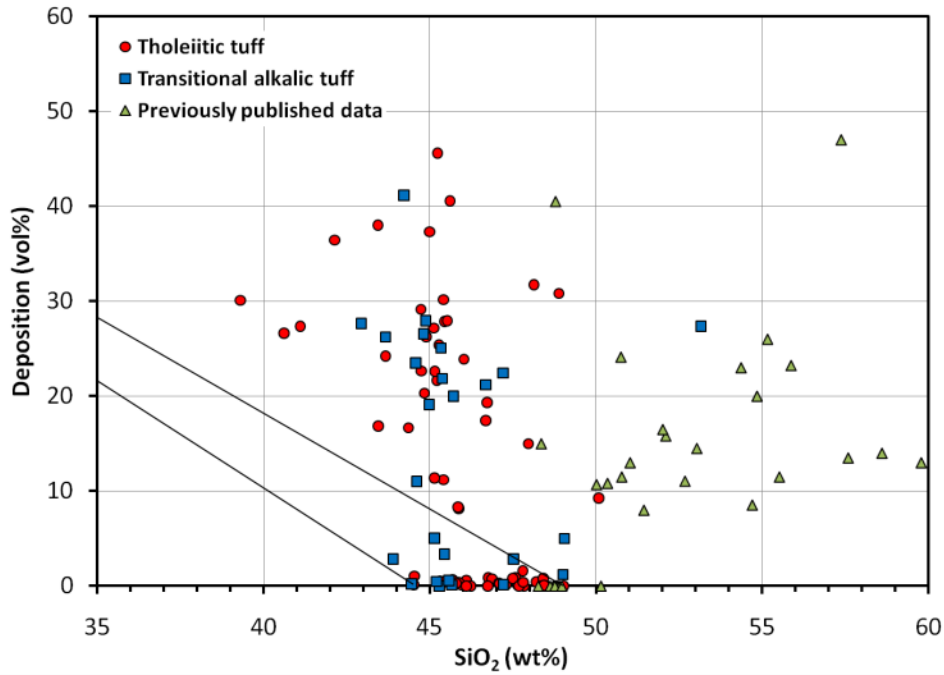


Figure 88. Deposition of secondary minerals versus SiO₂ content of the hyaloclastite tuff samples. The lines enclose an area of expected distribution if SiO₂ were immobile and simply diluted by the precipitation of secondary minerals (only relevant to tholeiitic samples from the WRZ).

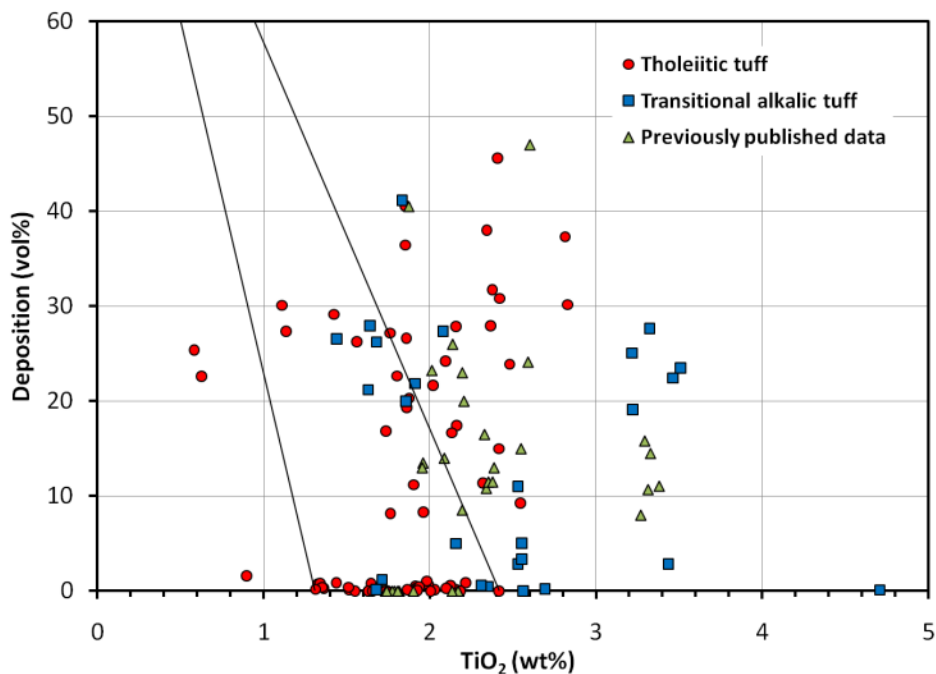


Figure 89. Deposition of secondary minerals versus TiO₂ content of the hyaloclastite tuff samples. The lines enclose an area of expected distribution if TiO₂ were immobile and simply diluted by the precipitation of secondary minerals (only relevant to tholeiitic samples from the WRZ).

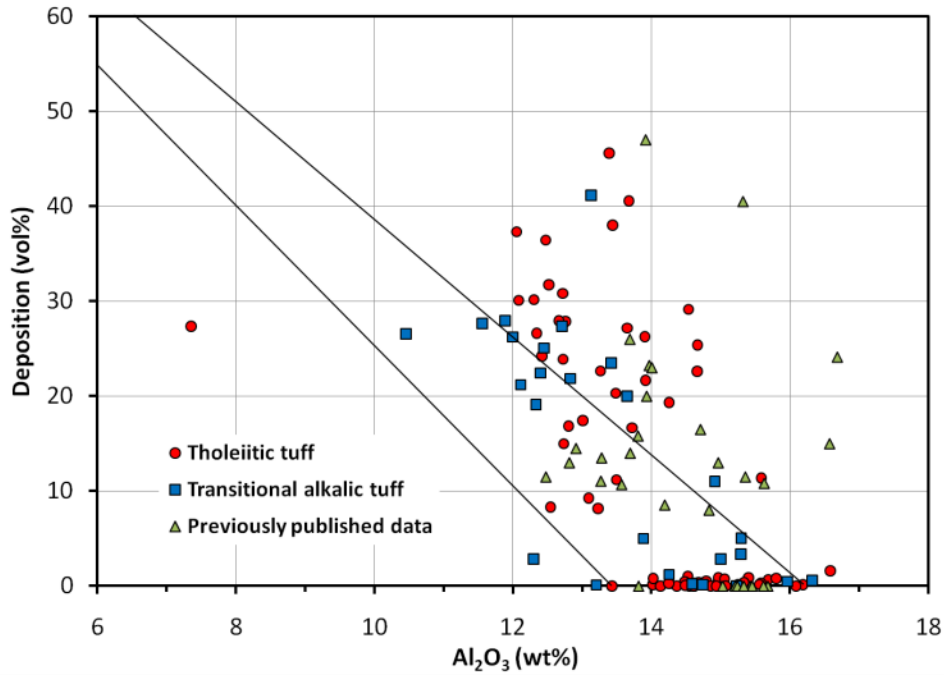


Figure 90. Deposition of secondary minerals versus Al_2O_3 content of the hyaloclastite tuff samples. The lines enclose an area of expected distribution if Al_2O_3 were immobile and simply diluted by the precipitation of secondary minerals (only relevant to tholeiitic samples from the WRZ).

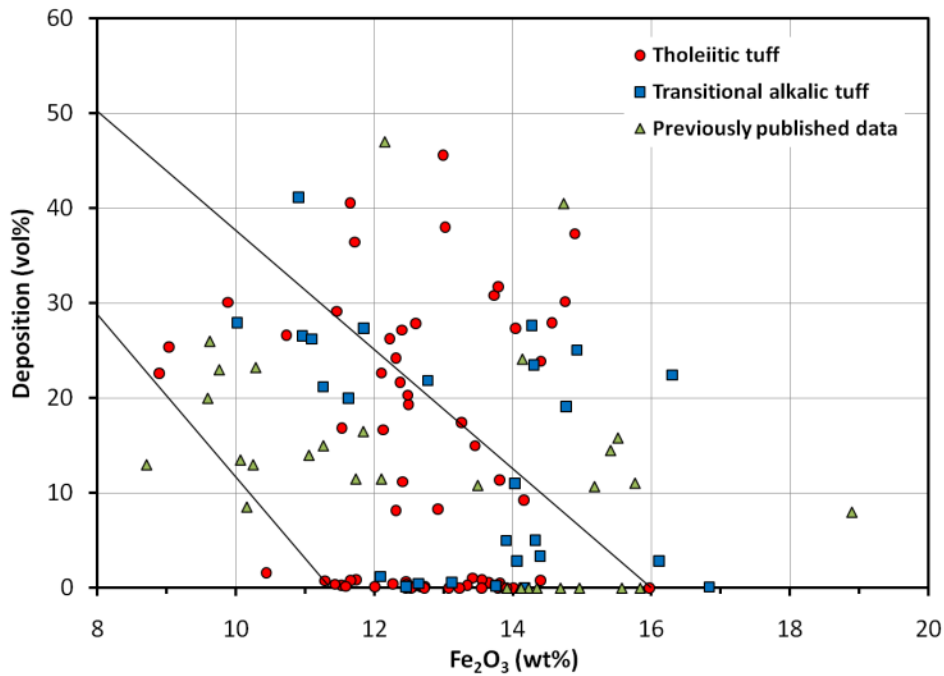


Figure 91. Deposition of secondary minerals versus Fe_2O_3 content of the hyaloclastite tuff samples. The lines enclose an area of expected distribution if Fe_2O_3 were immobile and simply diluted by the precipitation of secondary minerals (only relevant to tholeiitic samples from the WRZ).

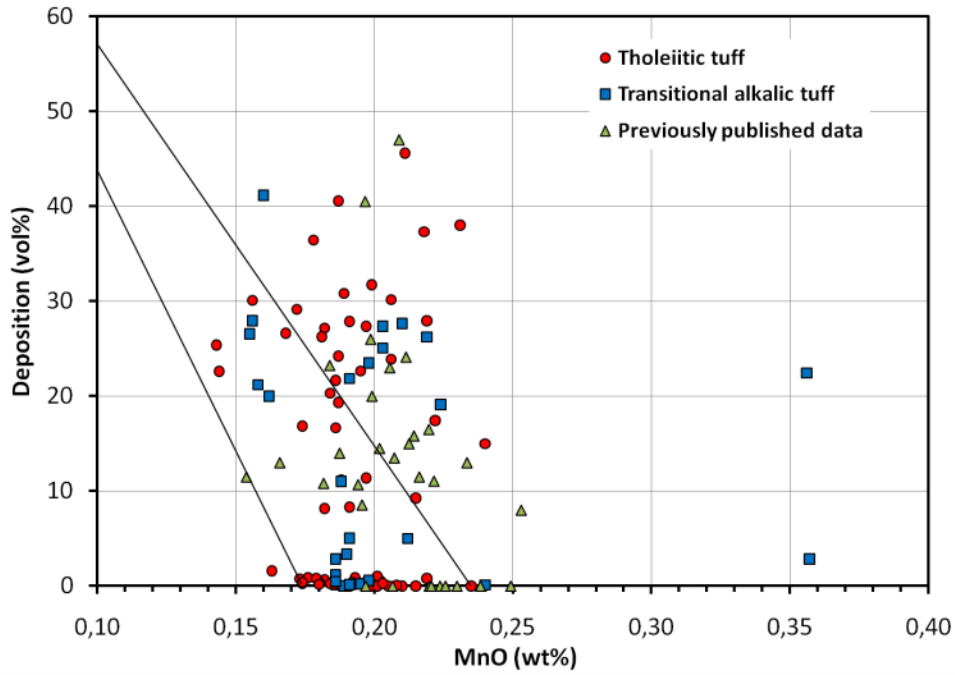


Figure 92. Deposition of secondary minerals versus MnO content of the hyaloclastite tuff samples. The lines enclose an area of expected distribution if MnO were immobile and simply diluted by the precipitation of secondary minerals (only relevant to tholeiitic samples from the WRZ).

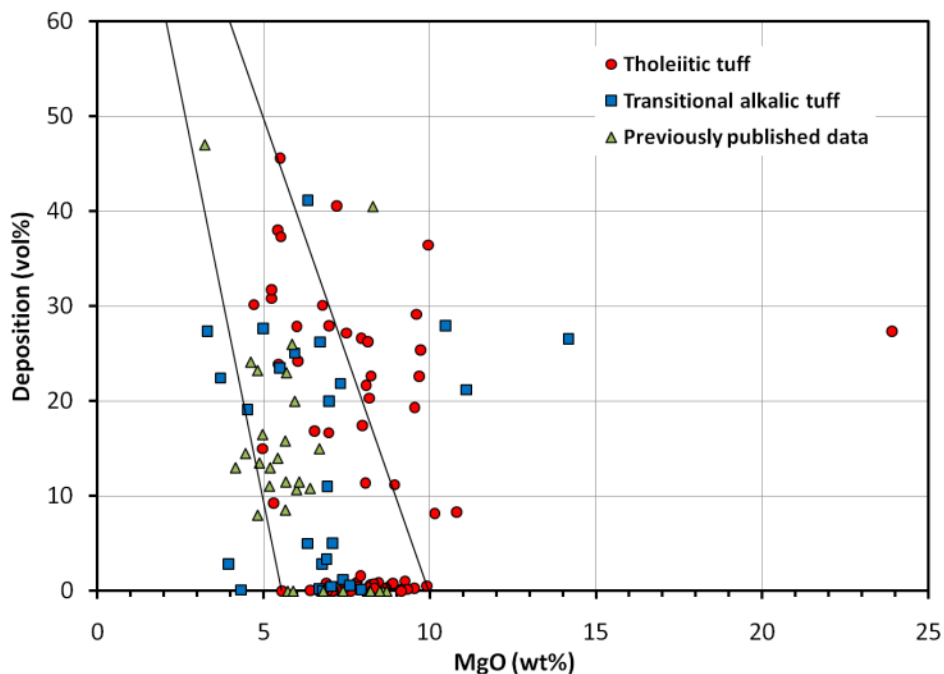


Figure 93. Deposition of secondary minerals versus MgO content of the hyaloclastite tuff samples. The lines enclose an area of expected distribution if MgO were immobile and simply diluted by the precipitation of secondary minerals (only relevant to tholeiitic samples from the WRZ).

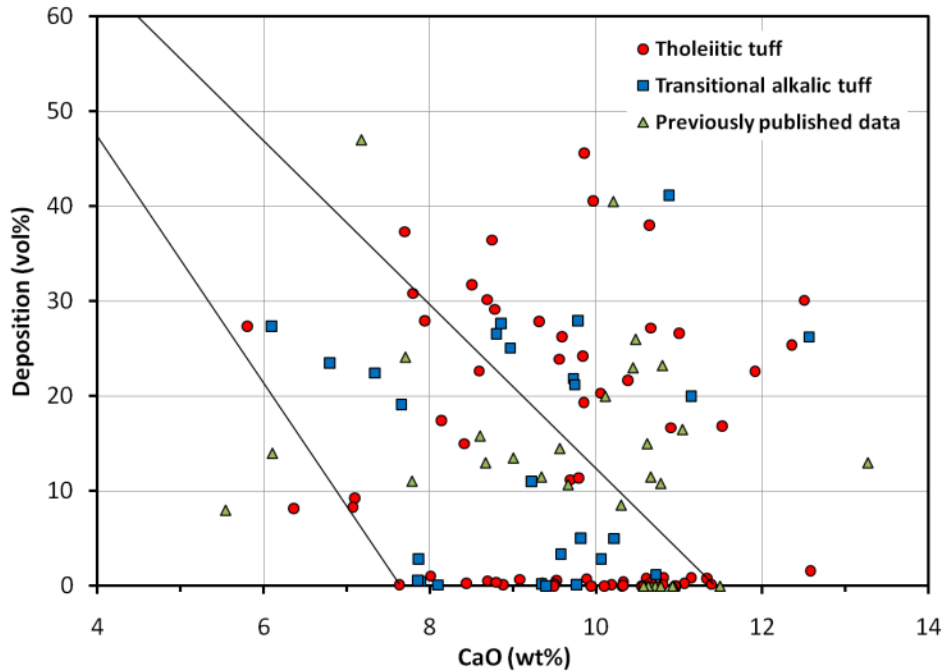


Figure 94. Deposition of secondary minerals versus CaO content of the hyaloclastite tuff samples. The lines enclose an area of expected distribution if CaO were immobile and simply diluted by the precipitation of secondary minerals (only relevant to tholeiitic samples from the WRZ).

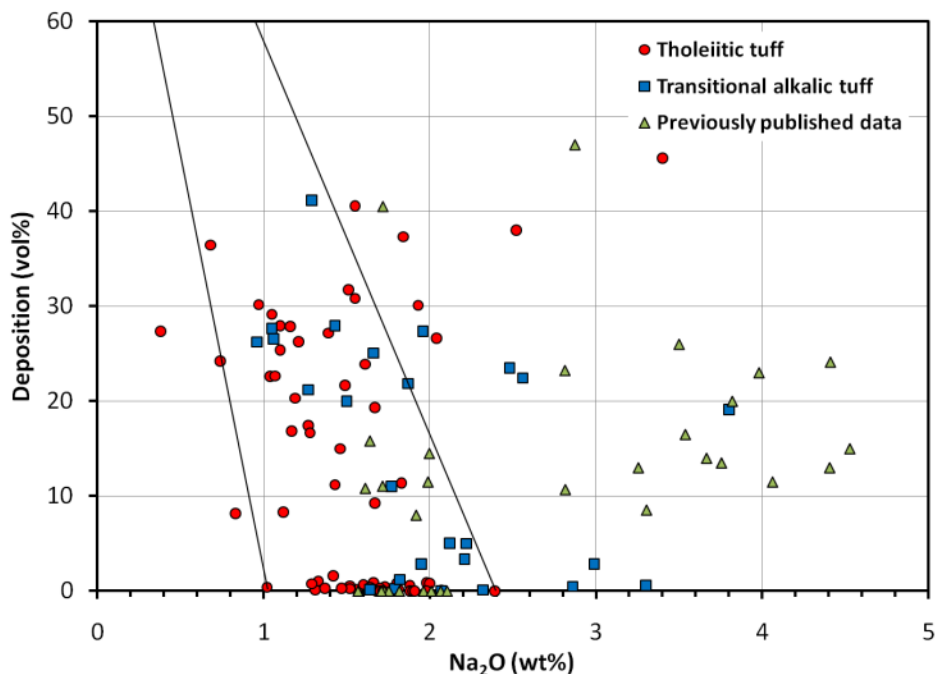


Figure 95. Deposition of secondary minerals versus Na₂O content of the hyaloclastite tuff samples. The lines enclose an area of expected distribution if Na₂O were immobile and simply diluted by the precipitation of secondary minerals (only relevant to tholeiitic samples from the WRZ).

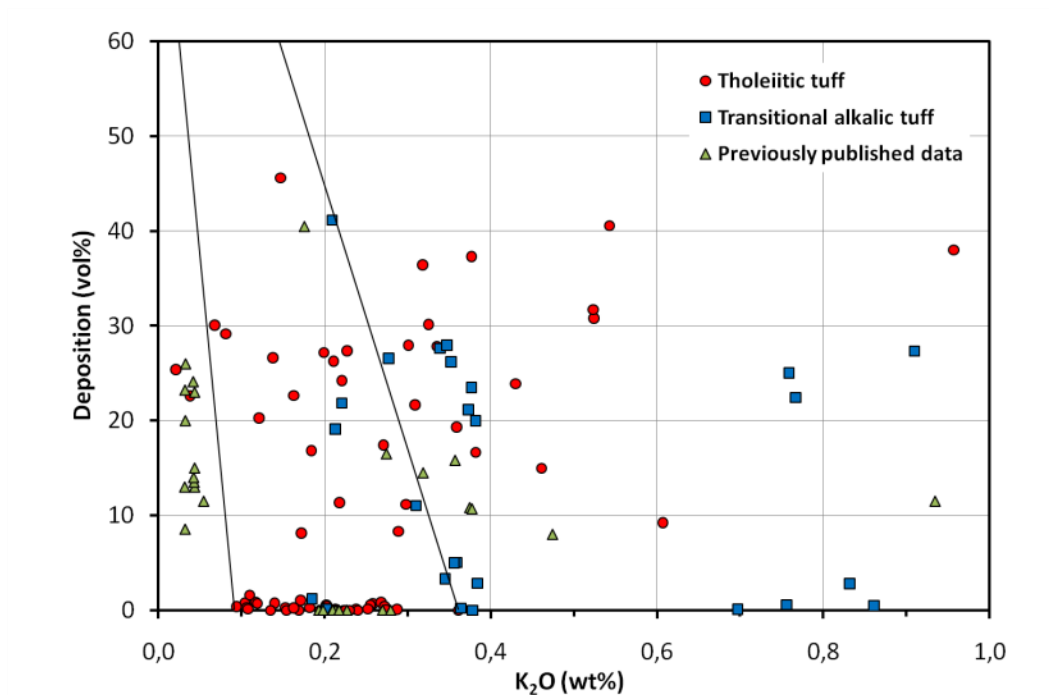


Figure 96. Deposition of secondary minerals versus K₂O content of the hyaloclastite tuff samples. The lines enclose an area of expected distribution if K₂O were immobile and simply diluted by the precipitation of secondary minerals (only relevant to tholeiitic samples from the WRZ).

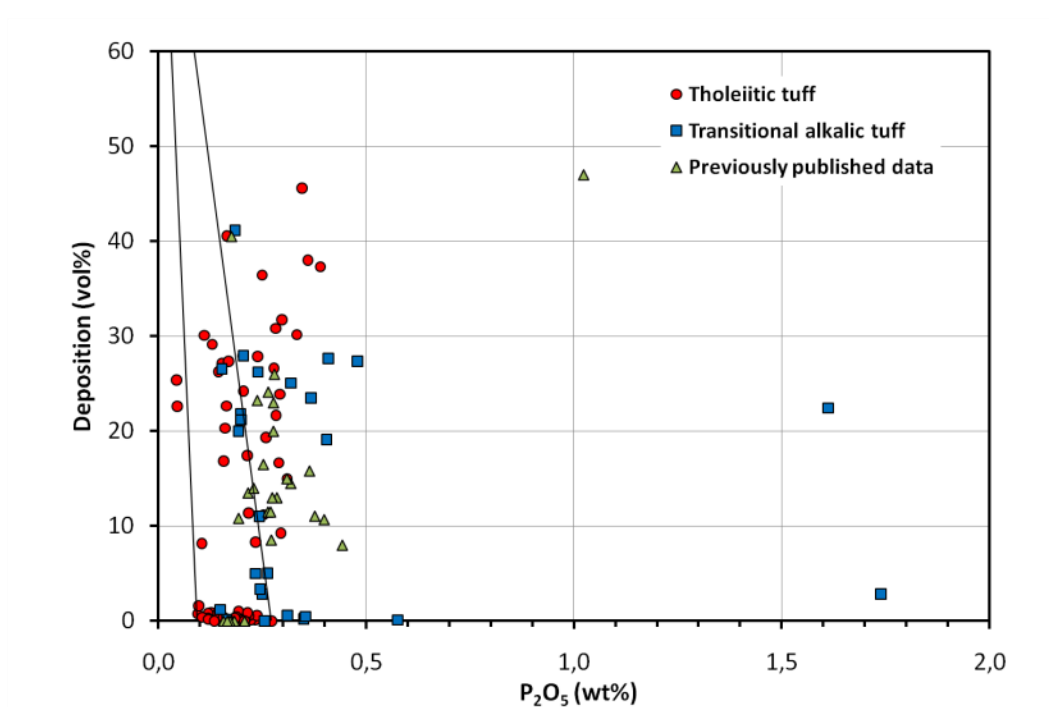


Figure 97. Deposition of secondary minerals versus P₂O₅ content of the hyaloclastite tuff samples. The lines enclose an area of expected distribution if P₂O₅ were immobile and simply diluted by the precipitation of secondary minerals (only relevant to tholeiitic samples from the WRZ).

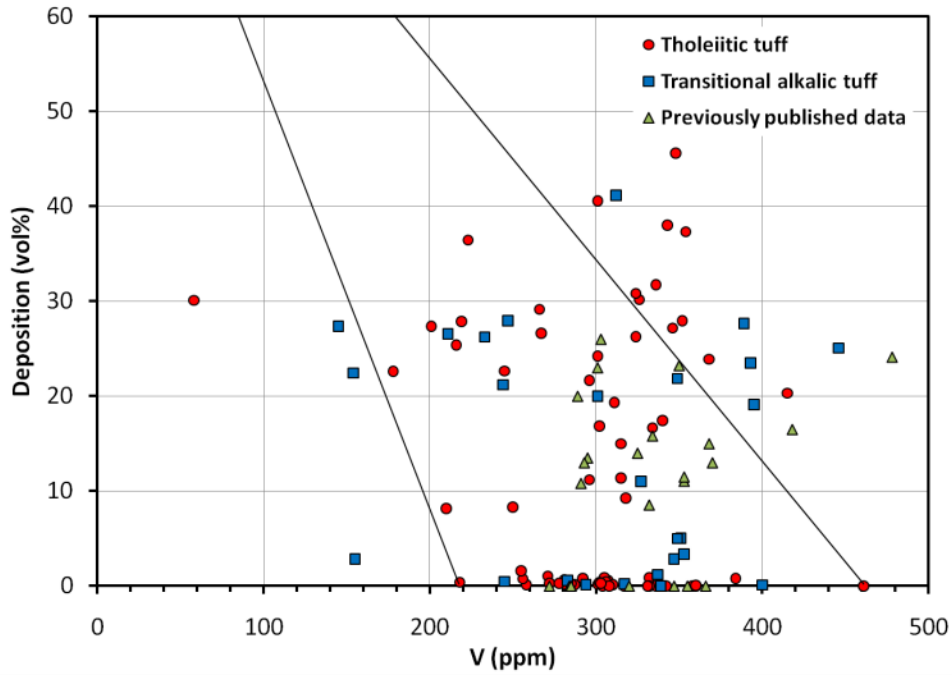


Figure 98. Deposition of secondary minerals versus the V content of the hyaloclastite tuff samples. The lines enclose an area of expected distribution if V were immobile and simply diluted by the precipitation of secondary minerals (only relevant to tholeiitic samples from the WRZ).

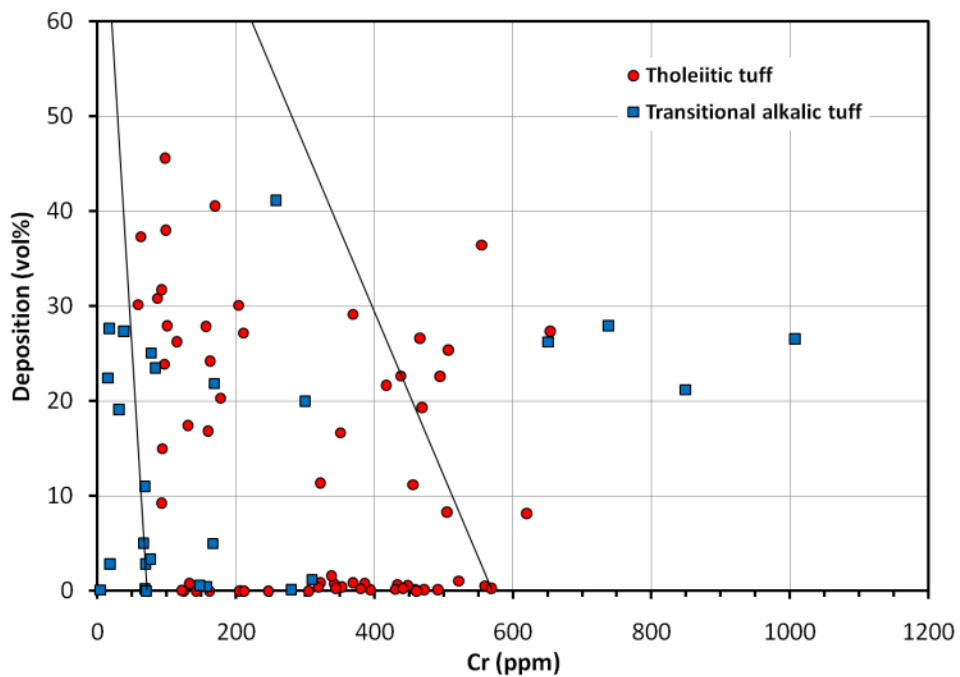


Figure 99. Deposition of secondary minerals versus Cr content of the hyaloclastite tuff samples. The lines enclose an area of expected distribution if Cr were immobile and simply diluted by the precipitation of secondary minerals (only relevant to tholeiitic samples from the WRZ).

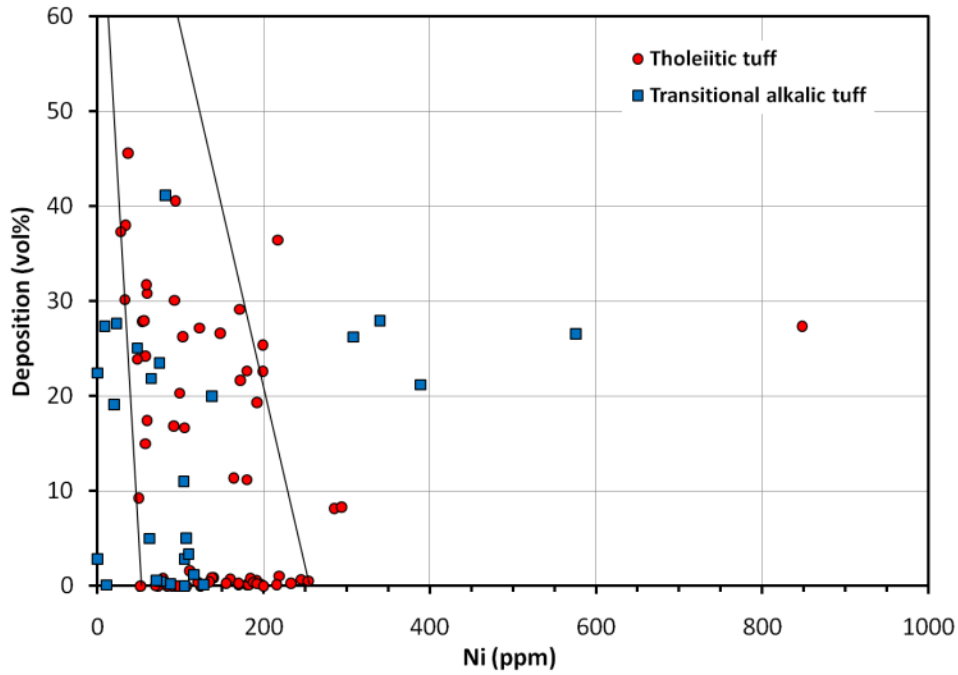


Figure 100. Deposition of secondary minerals versus Ni content of hyaloclastite tuff samples. The lines enclose an area of expected distribution if Ni were immobile and simply diluted by the precipitation of secondary minerals (only relevant to tholeiitic samples from the WRZ).

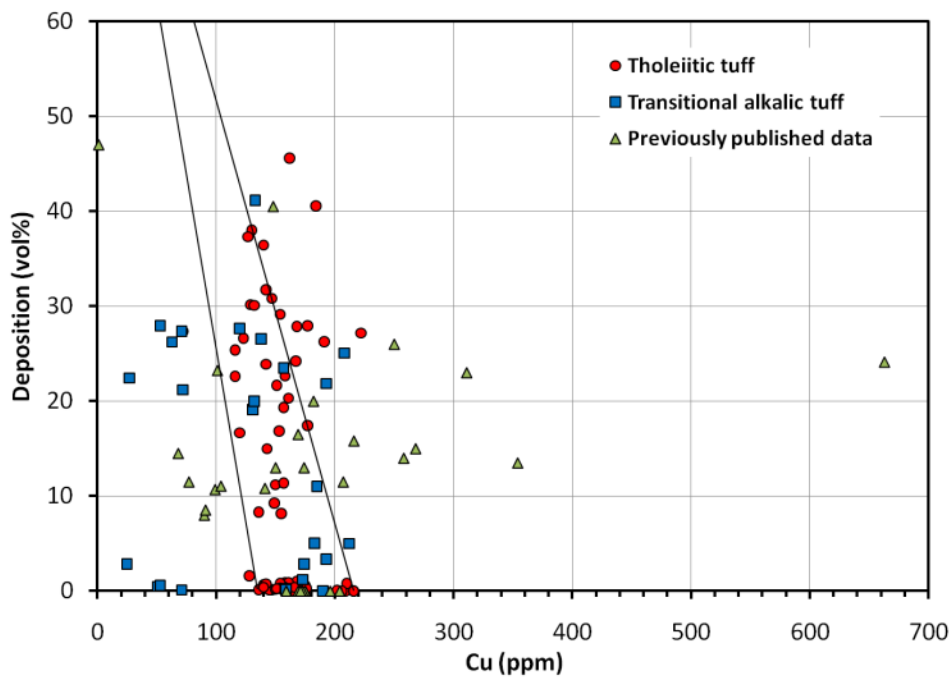


Figure 101. Deposition of secondary minerals versus Cu content of hyaloclastite tuff samples. The lines enclose an area of expected distribution if Cu were immobile and simply diluted by the precipitation of secondary minerals (only relevant to tholeiitic samples from the WRZ).

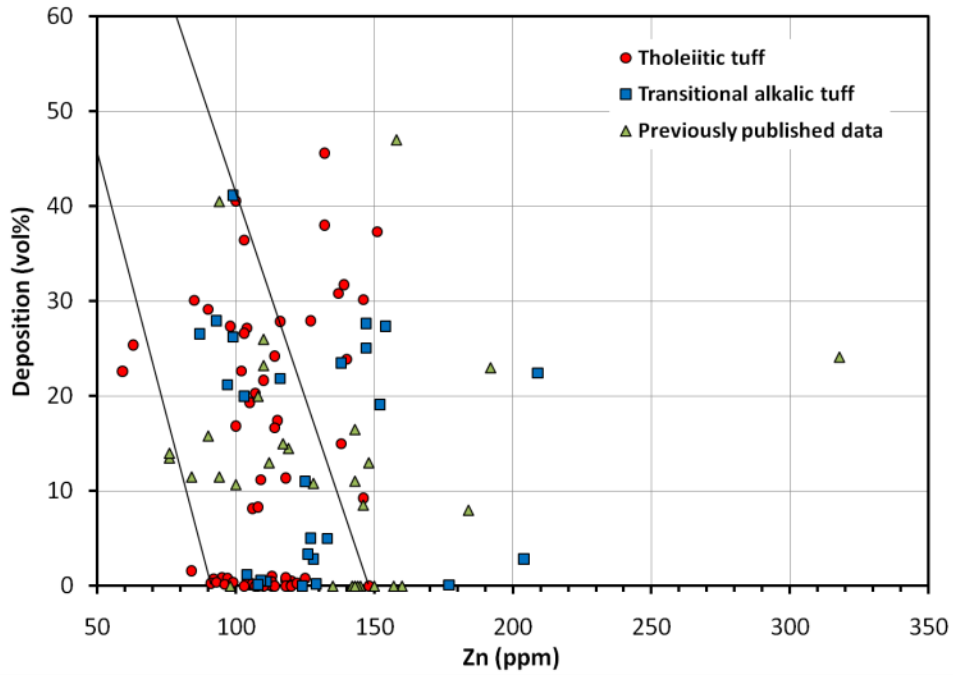


Figure 102. Deposition of secondary minerals versus Zn content of hyaloclastite tuff samples. The lines enclose an area of expected distribution if Zn were immobile and simply diluted by the precipitation of secondary minerals (only relevant to tholeiitic samples from the WRZ).

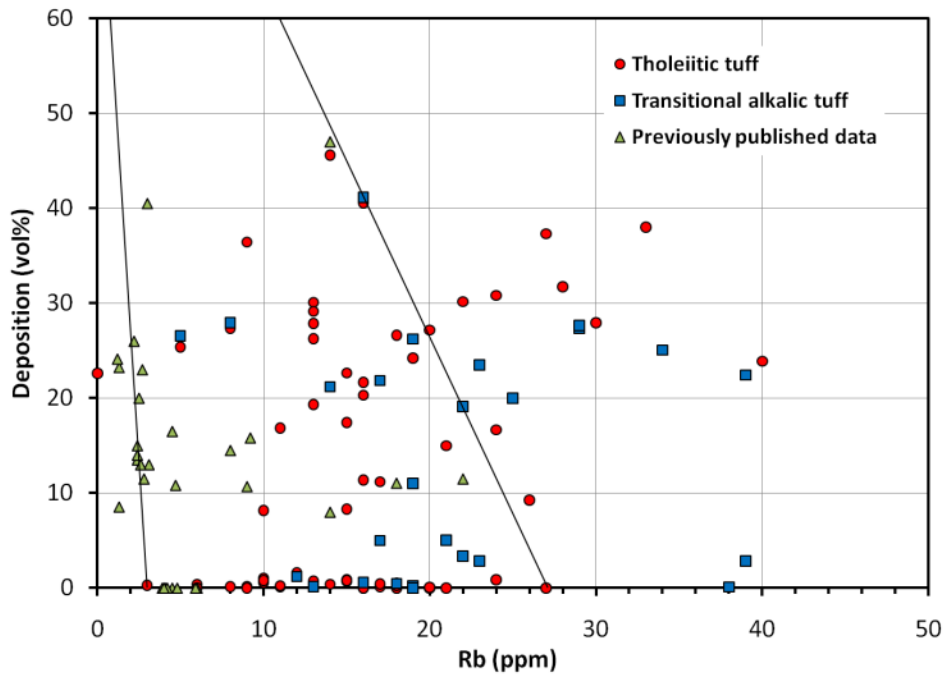


Figure 103. Deposition of secondary minerals versus Rb content of hyaloclastite tuff samples. The lines enclose an area of expected distribution if Rb were immobile and simply diluted by the precipitation of secondary minerals (only relevant to tholeiitic samples from the WRZ).

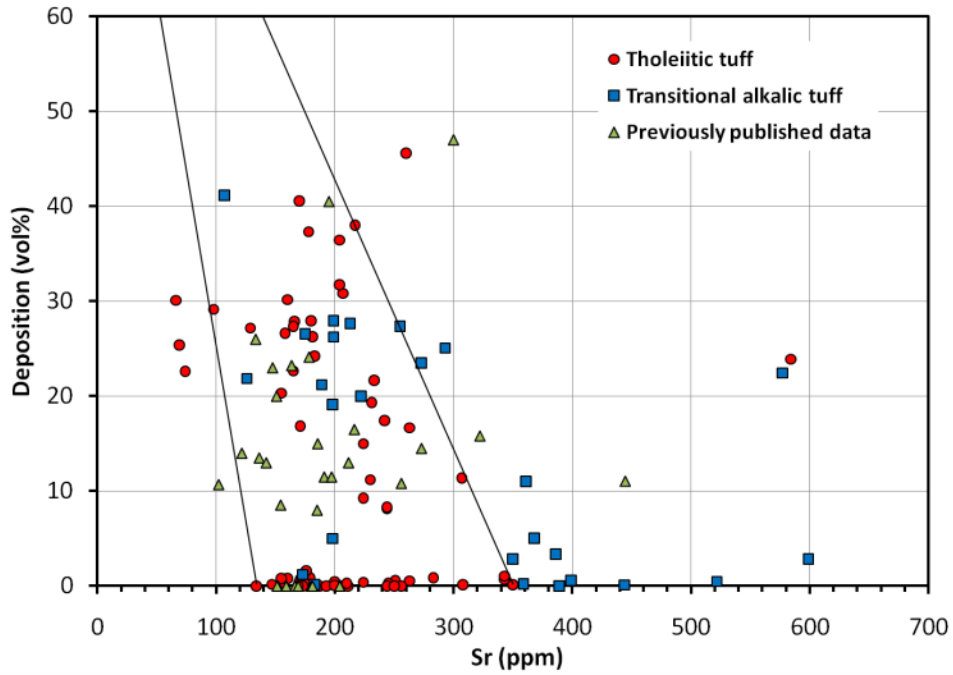


Figure 104. Deposition of secondary minerals versus Sr content of hyaloclastite tuff samples. The lines enclose an area of expected distribution if Sr were immobile and simply diluted by the precipitation of secondary minerals (only relevant to tholeiitic samples from the WRZ).

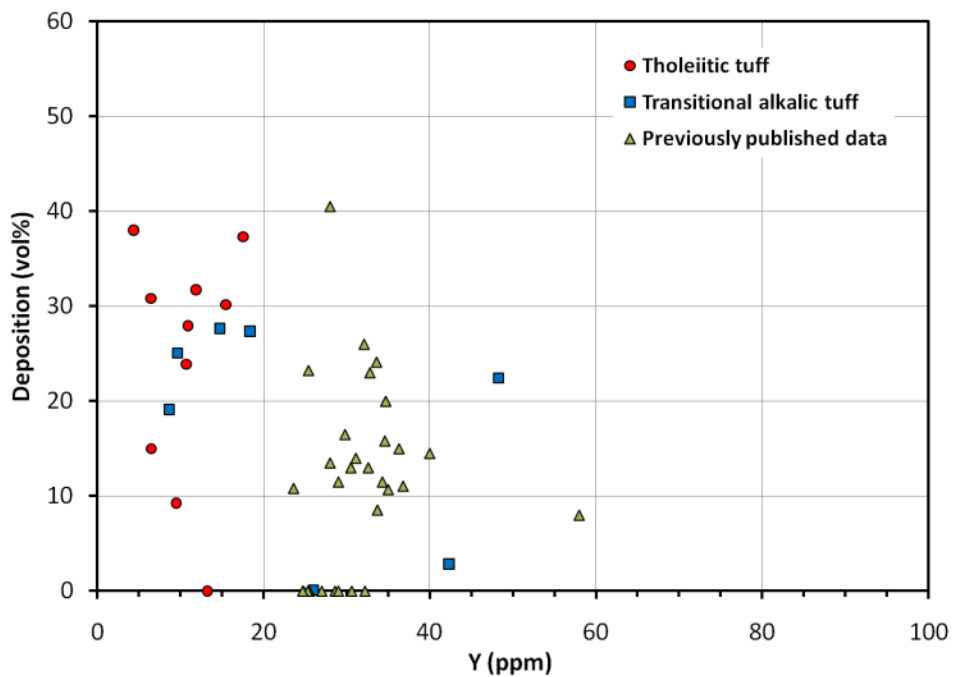


Figure 105. Deposition of secondary minerals versus Y content of the hyaloclastite tuff samples.

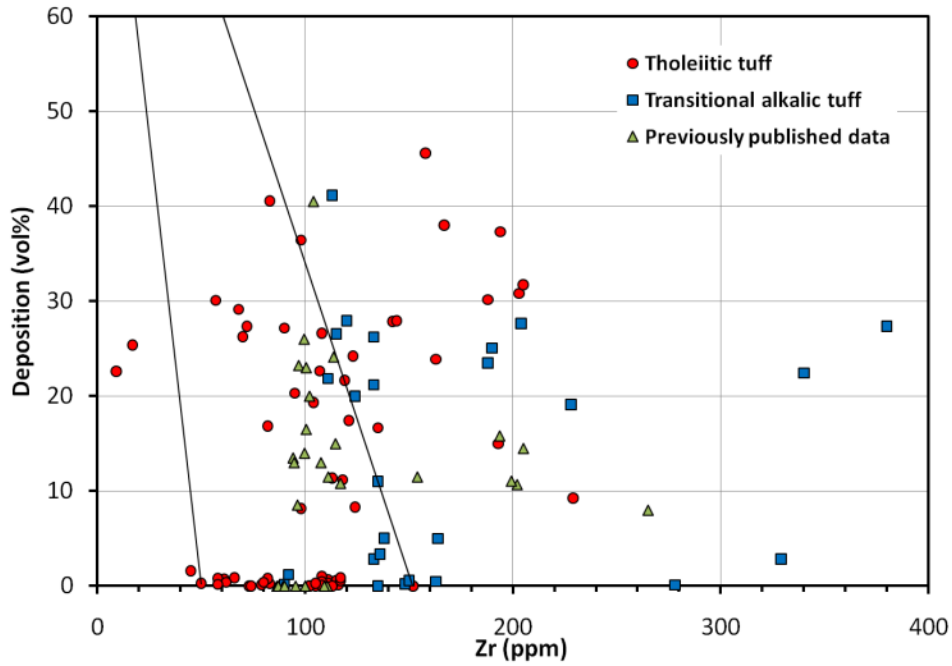


Figure 106. Deposition of secondary minerals versus Zr content of the hyaloclastite tuff samples. The lines enclose an area of expected distribution if Zr were immobile and simply diluted by the precipitation of secondary minerals (only relevant to tholeiitic samples from the WRZ).

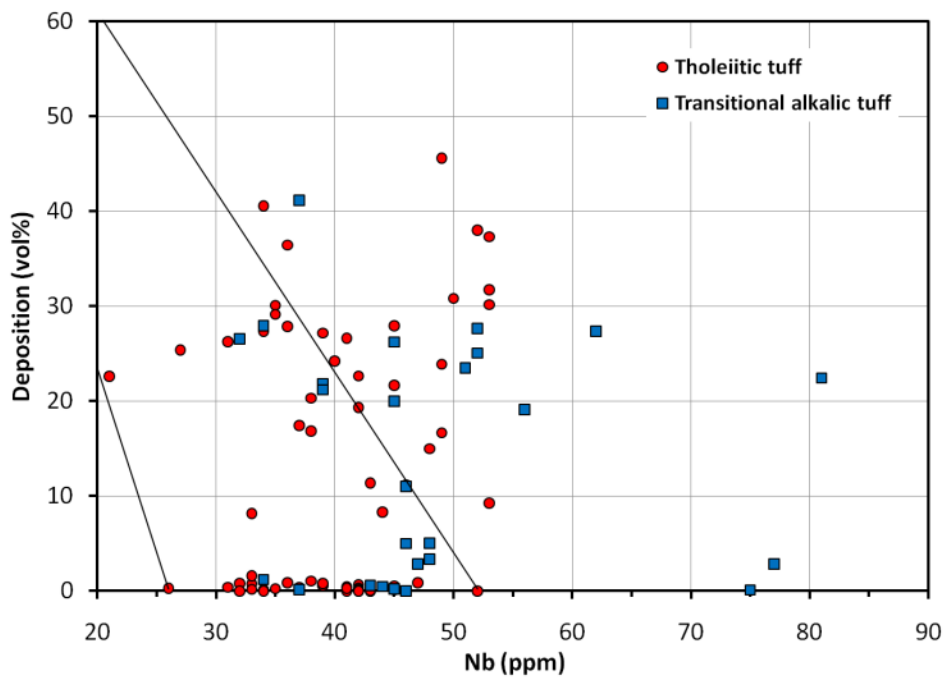


Figure 107. Deposition of secondary minerals versus Nb content of the hyaloclastite tuff samples. The lines enclose an area of expected distribution if Nb were immobile and simply diluted by the precipitation of secondary minerals (only relevant to tholeiitic samples from the WRZ).

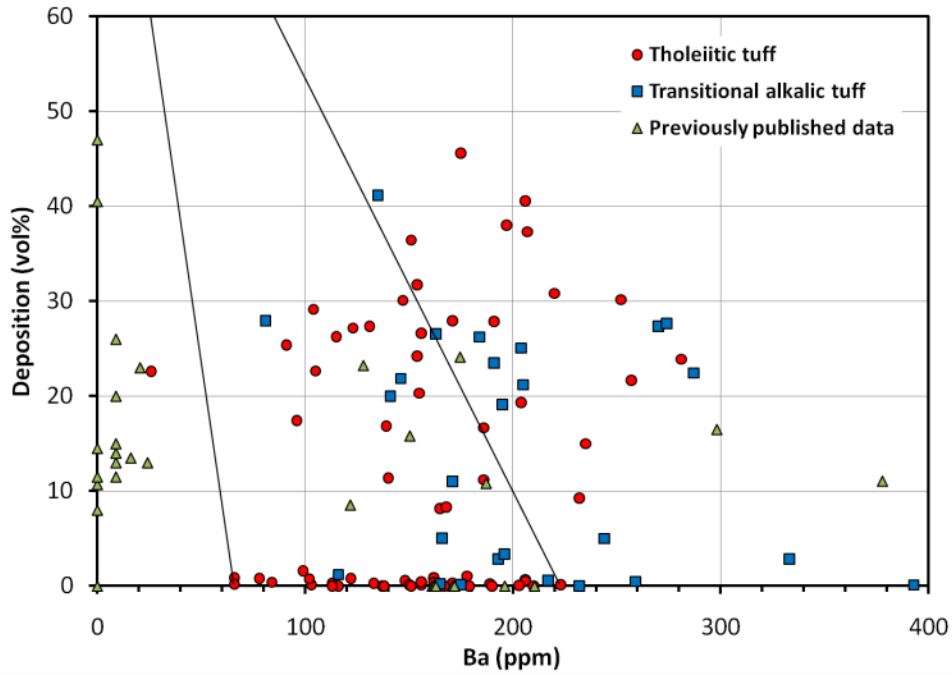


Figure 108. Deposition of secondary minerals versus Ba content of the hyaloclastite tuff samples. The lines enclose an area of expected distribution if Ba were immobile and simply diluted by the precipitation of secondary minerals (only relevant to tholeiitic samples from the WRZ).

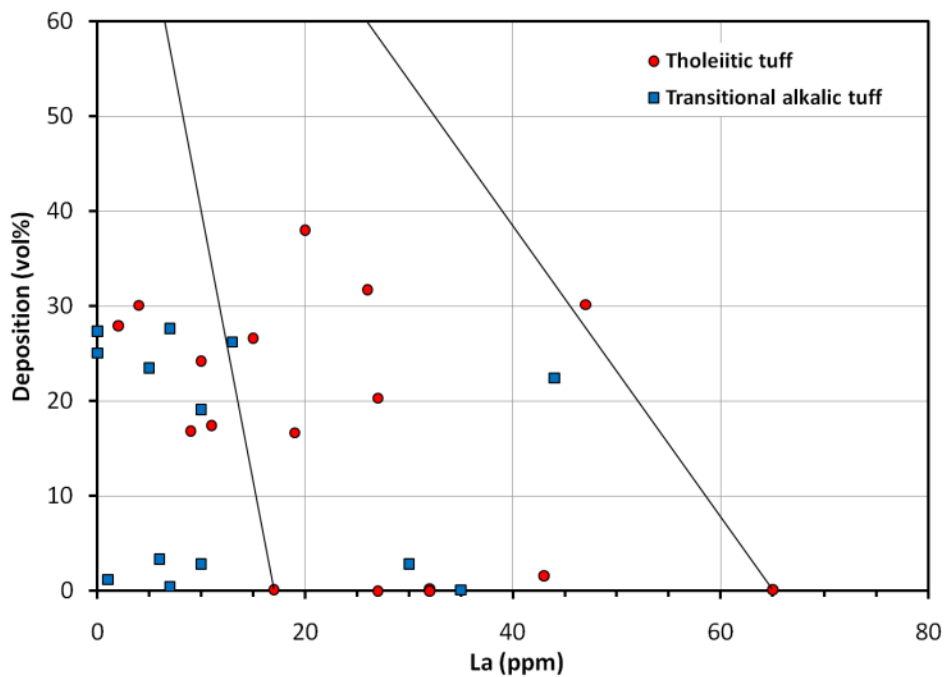


Figure 109. Deposition of secondary minerals versus La content of the hyaloclastite tuff samples. The lines enclose an area of expected distribution if La were immobile and simply diluted by the precipitation of secondary minerals (only relevant to tholeiitic samples from the WRZ).

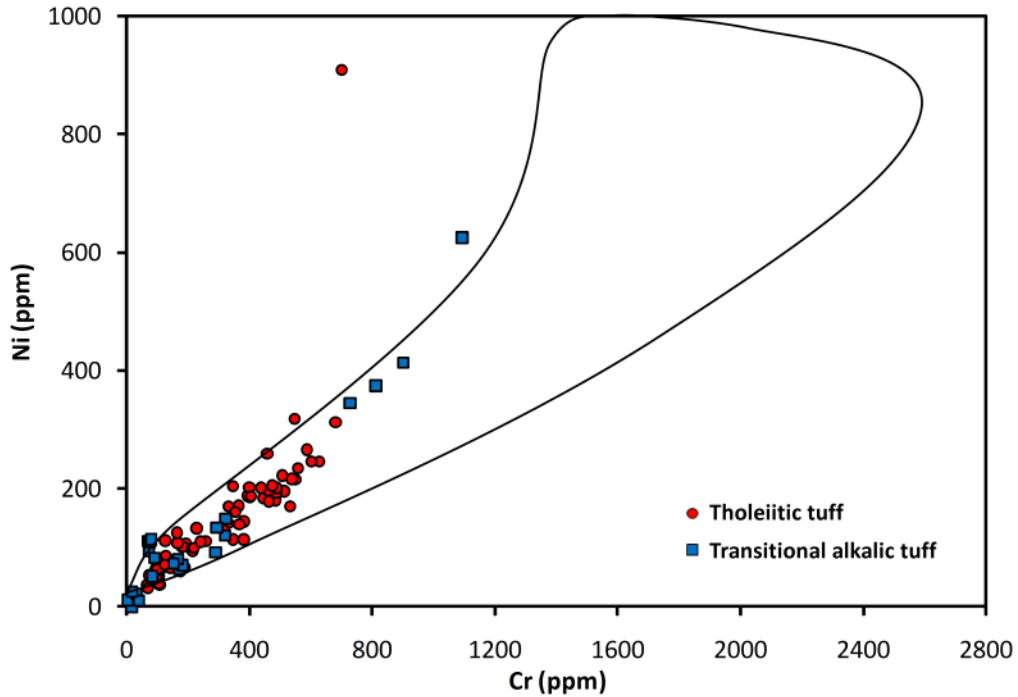


Figure 110. *The relationship between the Ni and Cr contents of the hyaloclastite tuff samples. Outlined area denotes the range of Holocene lavas from the WRZ.*

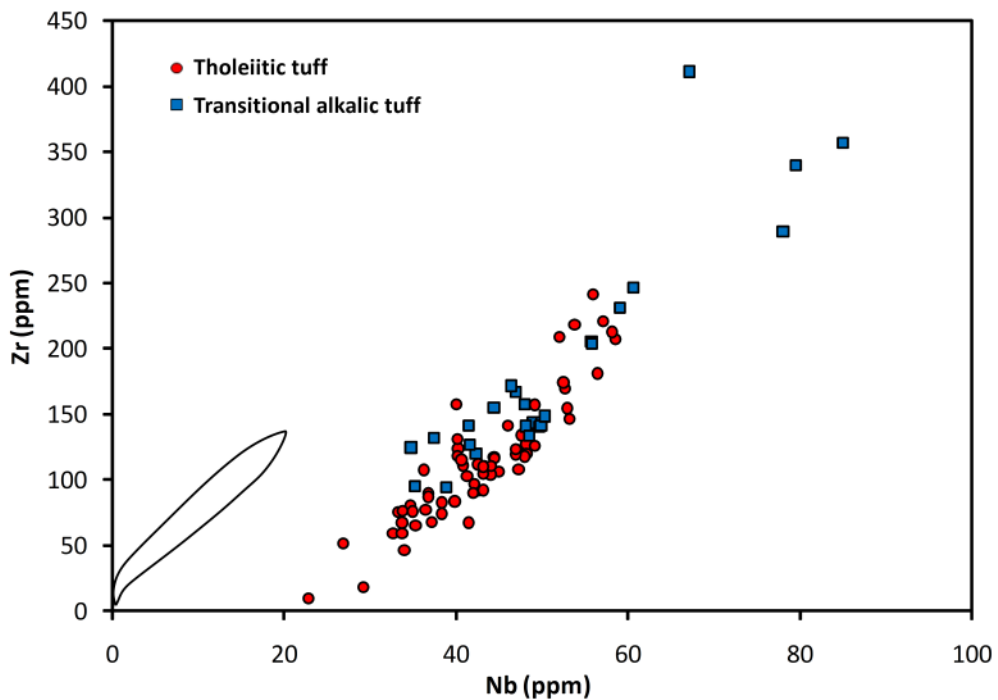


Figure 111. *The relationship between the Zr and Nb contents of the hyaloclastite tuff samples. Outlined area denotes the range of Holocene lavas from the WRZ. The offset between the tuff samples and the range of the Holocene samples is apparently caused by a systematic error in the Nb analyses of the tuff samples.*

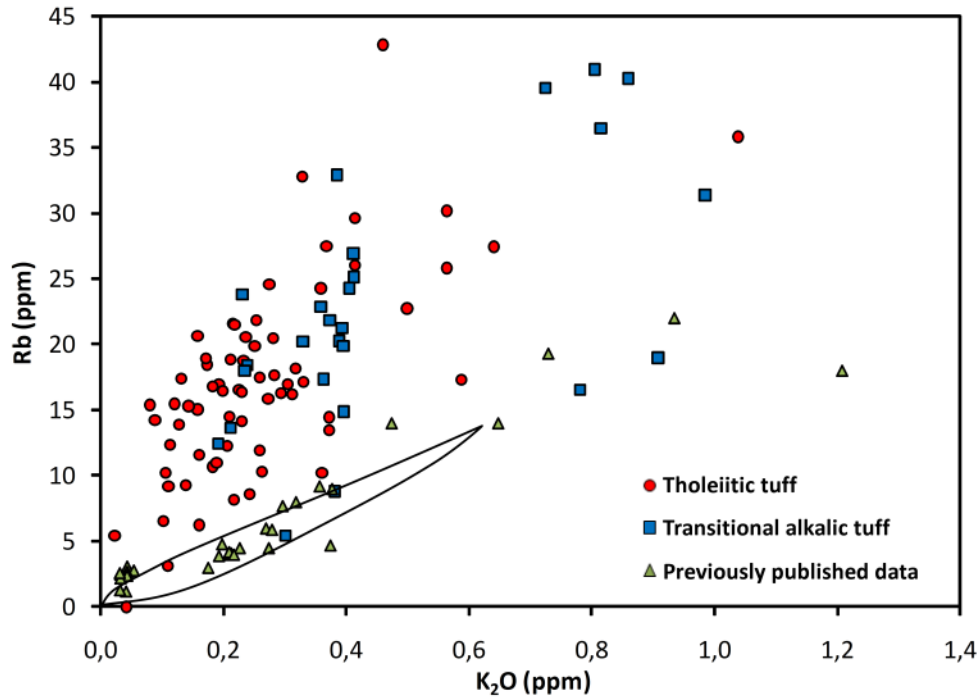


Figure 112. The relationship between the Rb and K₂O contents of the hyaloclastite tuff samples. Outlined area denotes the range of Holocene lavas from the WRZ.

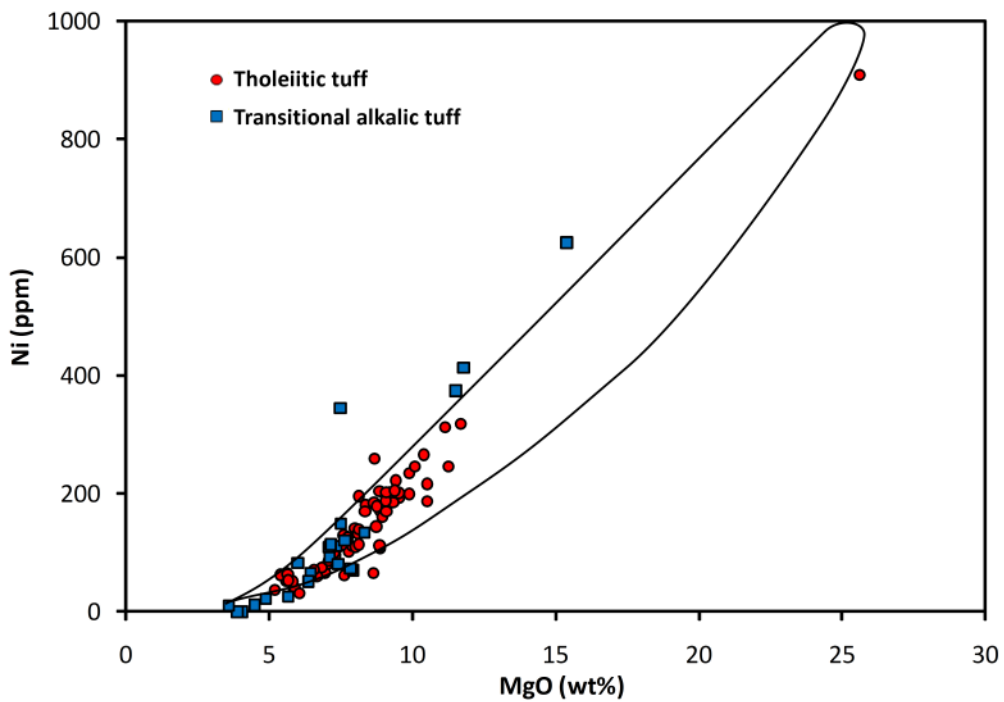


Figure 113. The relationship between the Ni and MgO contents of the hyaloclastite tuff samples. Outlined area denotes the range of Holocene lavas from the WRZ.

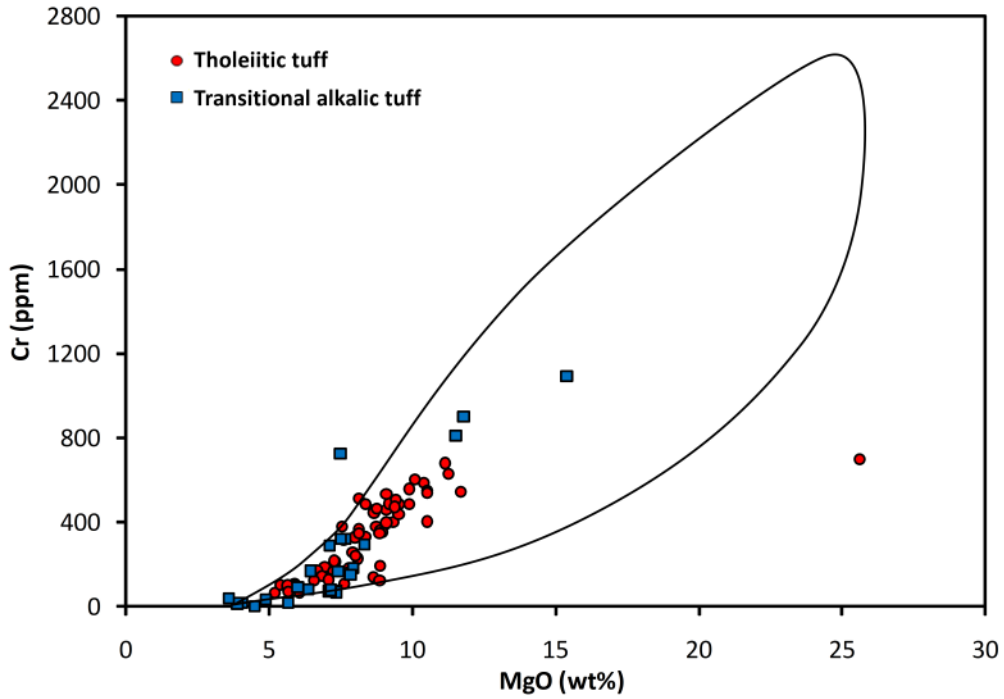


Figure 114. The relationship between the Cr and MgO contents of the hyaloclastite tuff samples. Outlined area denotes the range of Holocene lavas from the WRZ.

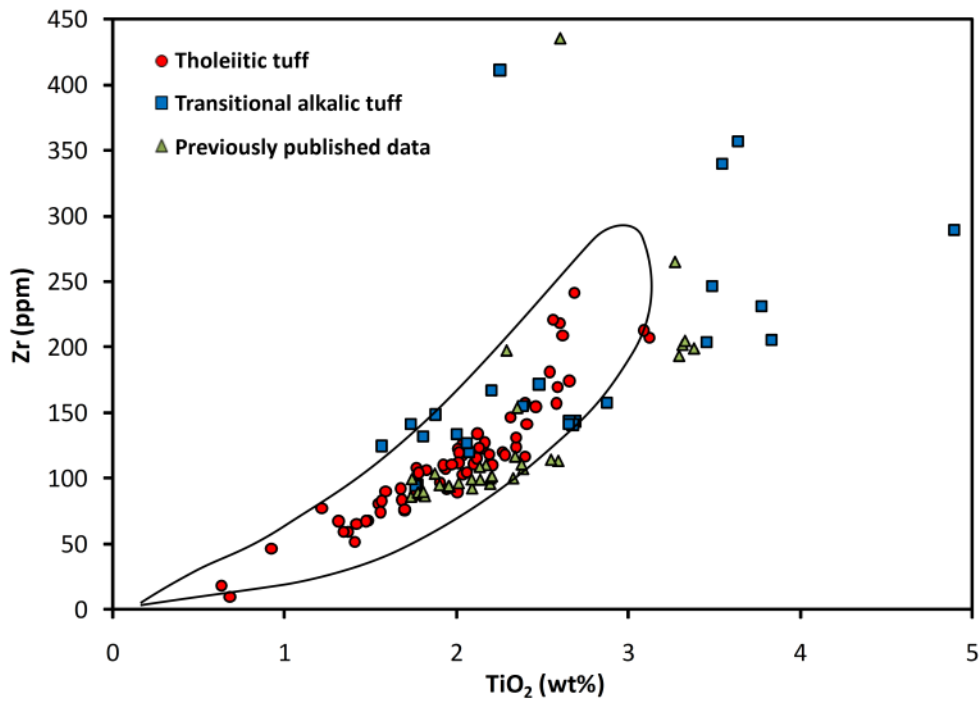


Figure 115. The relationship between the Zr and TiO₂ contents of the hyaloclastite tuff samples. Outlined area denotes the range of Holocene lavas from the WRZ.

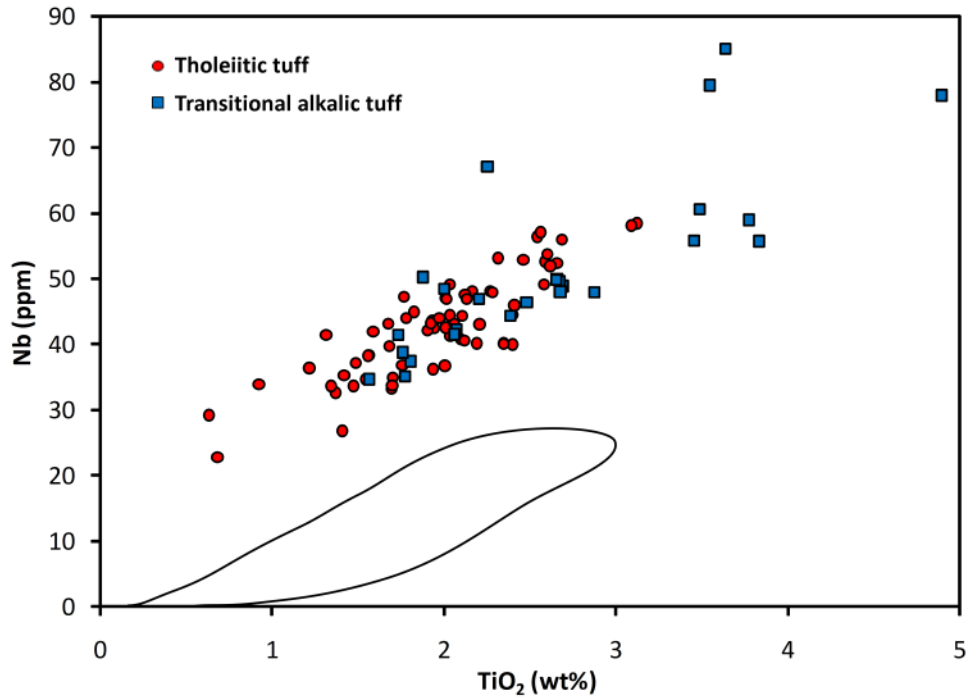


Figure 116. *The relationship between the Nb and TiO₂ contents of the hyaloclastite tuff samples. Outlined area denotes the range of Holocene lavas from the WRZ. The offset between the tuff samples and the range of the Holocene samples is apparently caused by a systematic error in the Nb analyses of the tuff samples.*

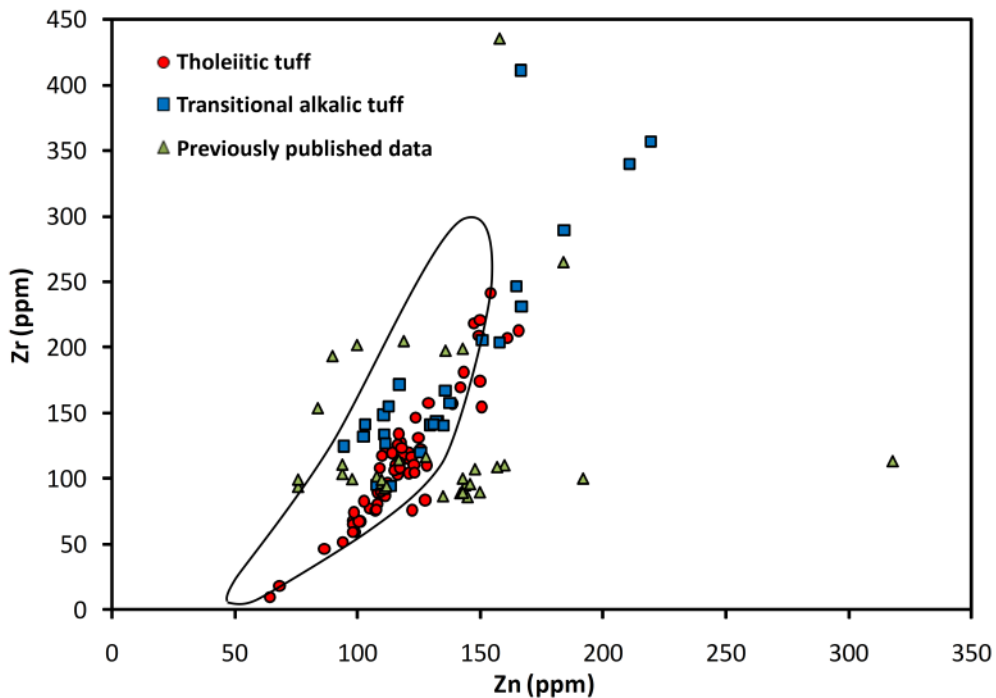


Figure 117. *The relationship between the Zr and Zn contents of the hyaloclastite tuff samples. Outlined area denotes the range of Holocene lavas from the WRZ.*

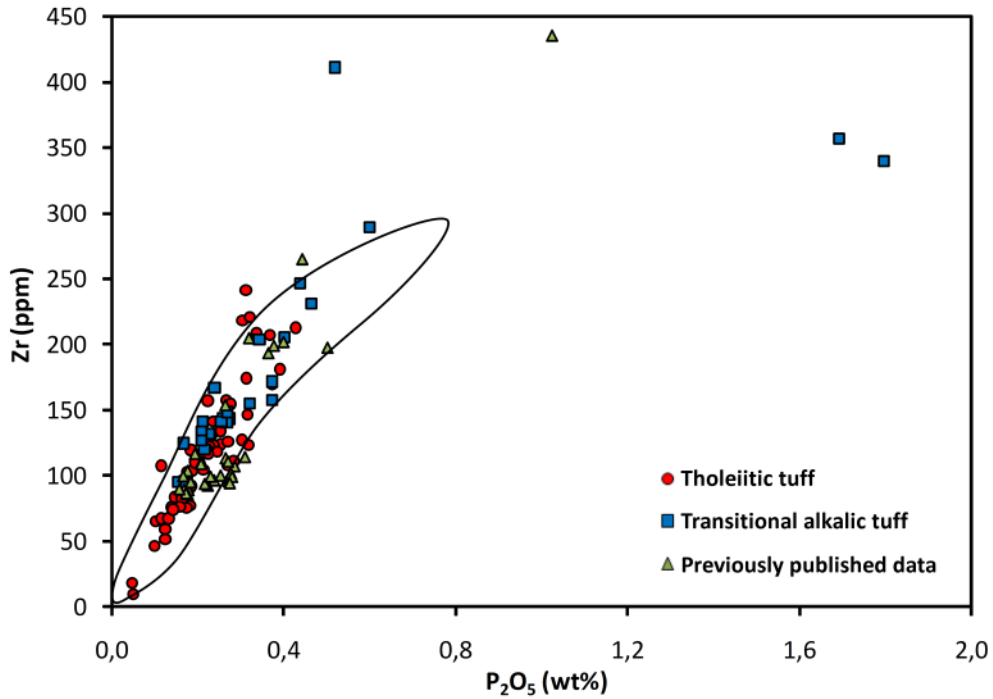


Figure 118. The relationship between the Zr and P_2O_5 contents of the hyaloclastite tuff samples. Outlined area denotes the range of Holocene lavas from the WRZ.

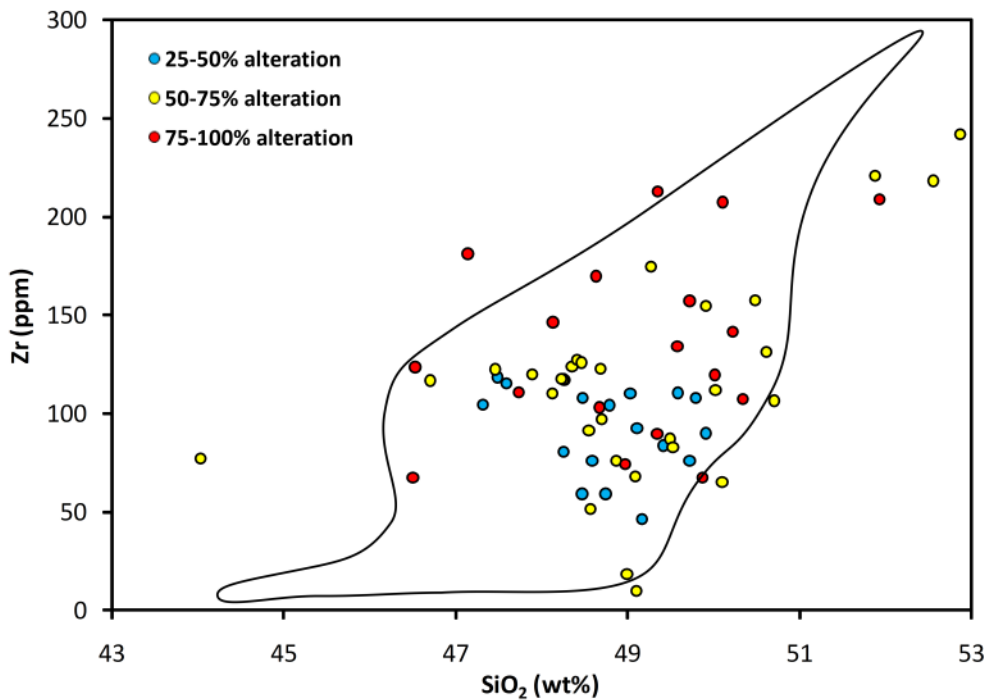


Figure 119. Zr content versus SiO_2 content of the tholeiitic hyaloclastite tuff samples from the WRZ (filled circles) in comparison with samples of fresh Holocene lavas (outlined field).

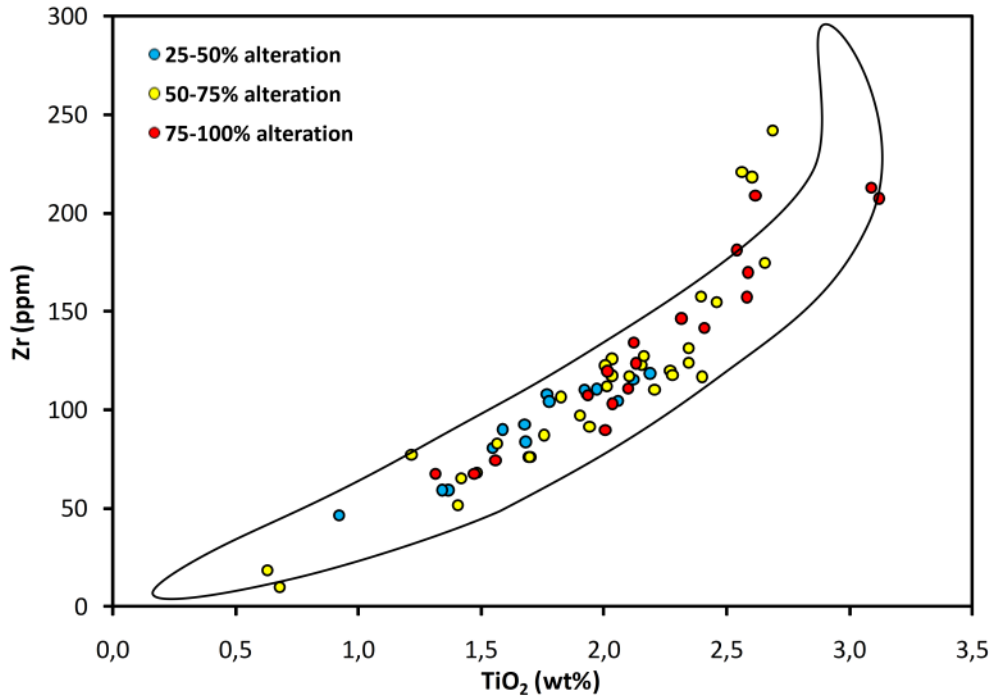


Figure 120. *Zr content versus TiO_2 content of tholeiitic hyaloclastite tuff samples from the WRZ (filled circles) in comparison with samples of fresh Holocene lavas (outlined field).*

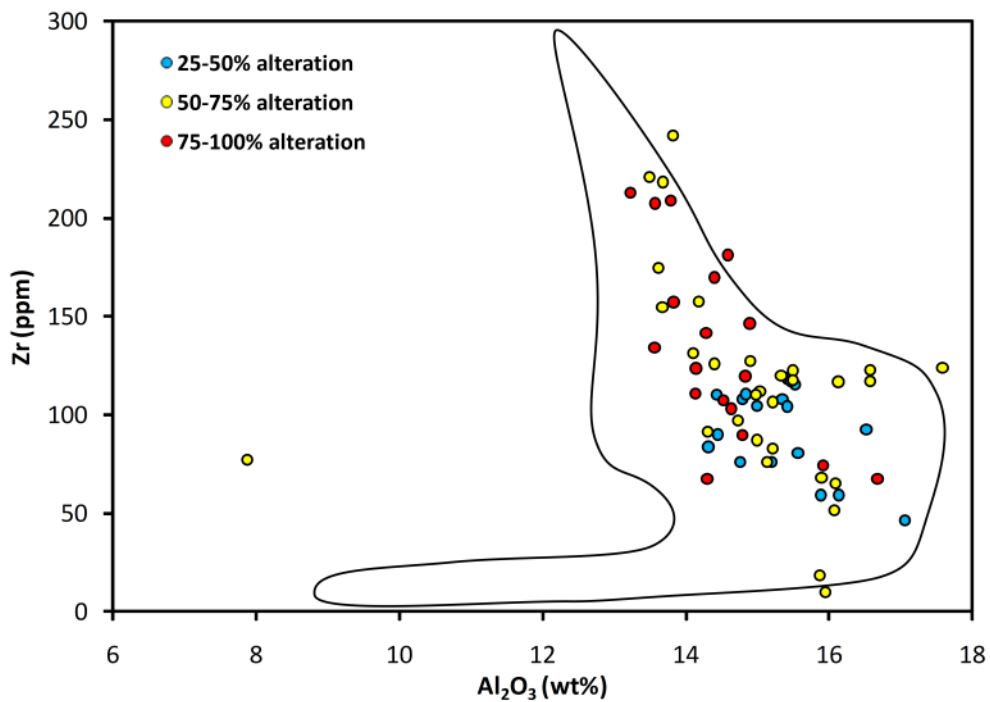


Figure 121. *Zr content versus Al_2O_3 content of tholeiitic hyaloclastite tuff samples from the WRZ (filled circles) in comparison with samples of fresh Holocene lavas (outlined field).*

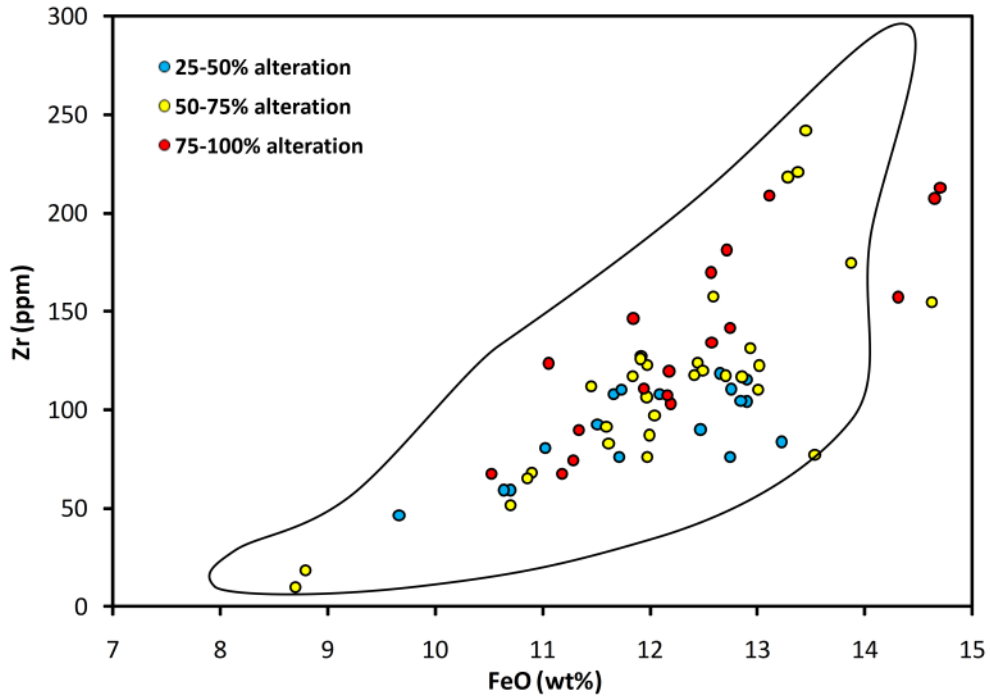


Figure 122. *Zr content versus FeO content of tholeiitic hyaloclastite tuff samples from the WRZ (filled circles) in comparison with samples of fresh Holocene lavas (outlined field).*

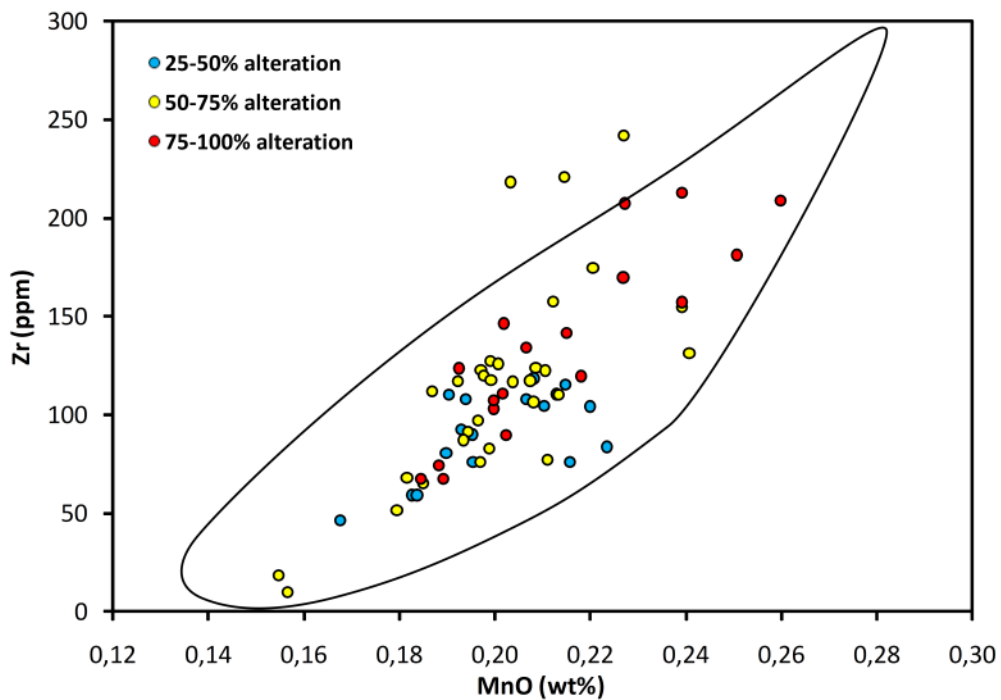


Figure 123. *Zr content versus MnO content of tholeiitic hyaloclastite tuff samples from the WRZ (filled circles) in comparison with samples of fresh Holocene lavas (outlined field).*

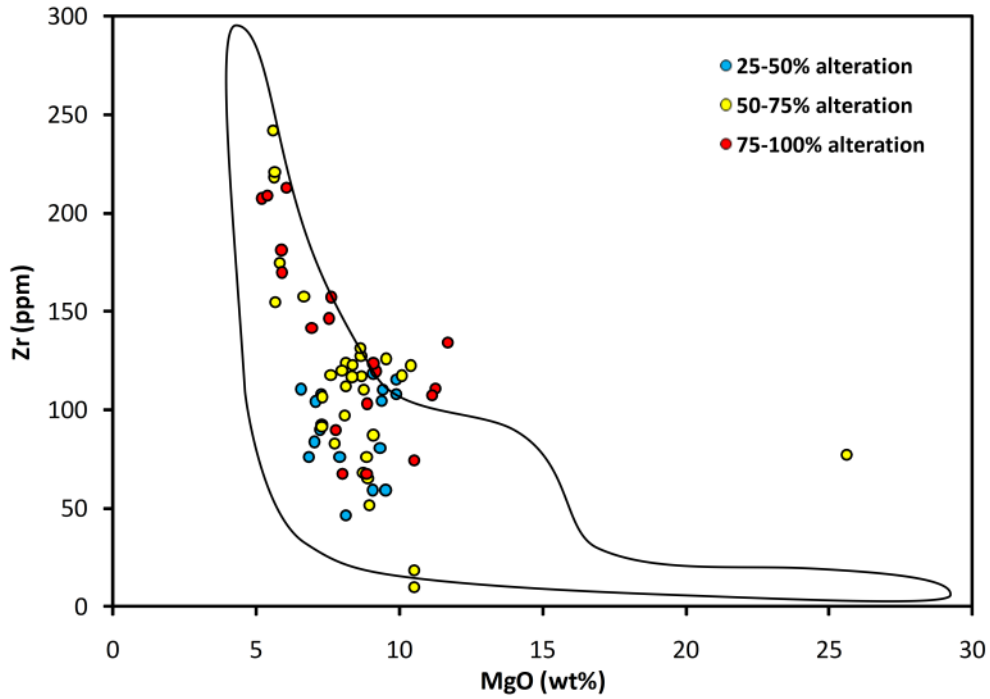


Figure 124. *Zr content versus MgO content of tholeiitic hyaloclastite tuff samples from the WRZ (filled circles) in comparison with samples of fresh Holocene lavas (outlined field).*

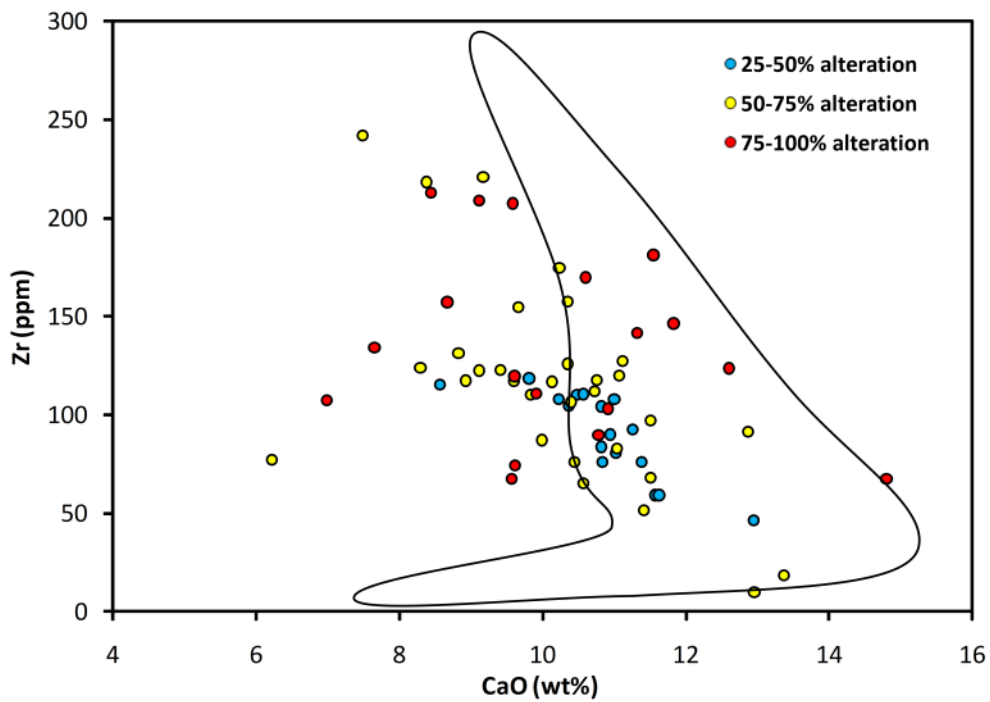


Figure 125. *Zr content versus CaO content of tholeiitic hyaloclastite tuff samples from the WRZ (filled circles) in comparison with samples of fresh Holocene lavas (outlined field).*

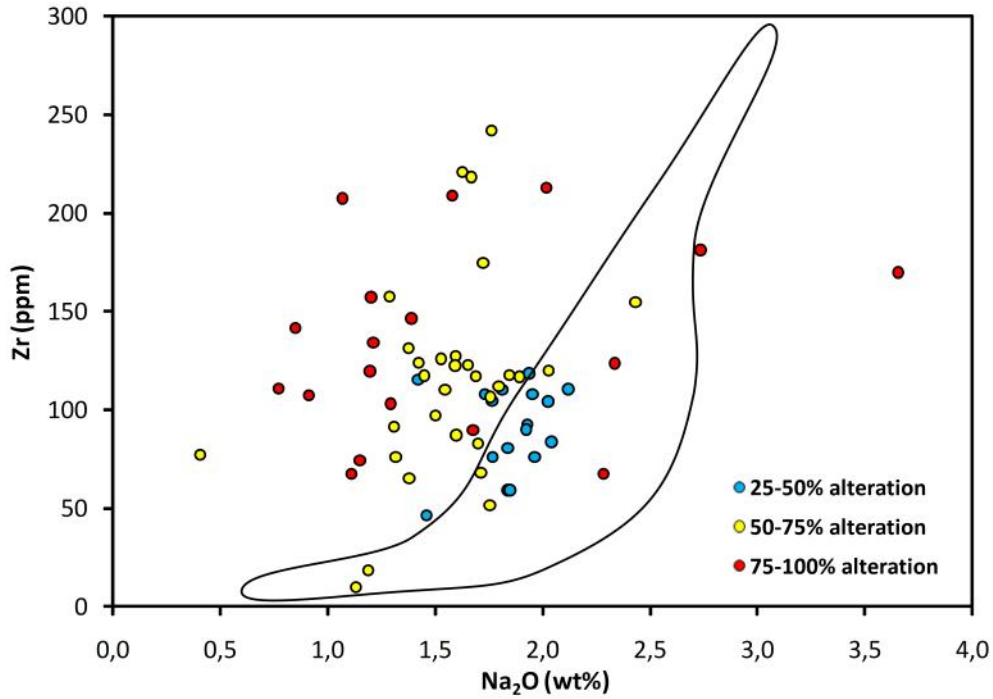


Figure 126. *Zr content versus Na₂O content of tholeiitic hyaloclastite tuff samples from the WRZ (filled circles) in comparison with samples of fresh Holocene lavas (outlined field).*

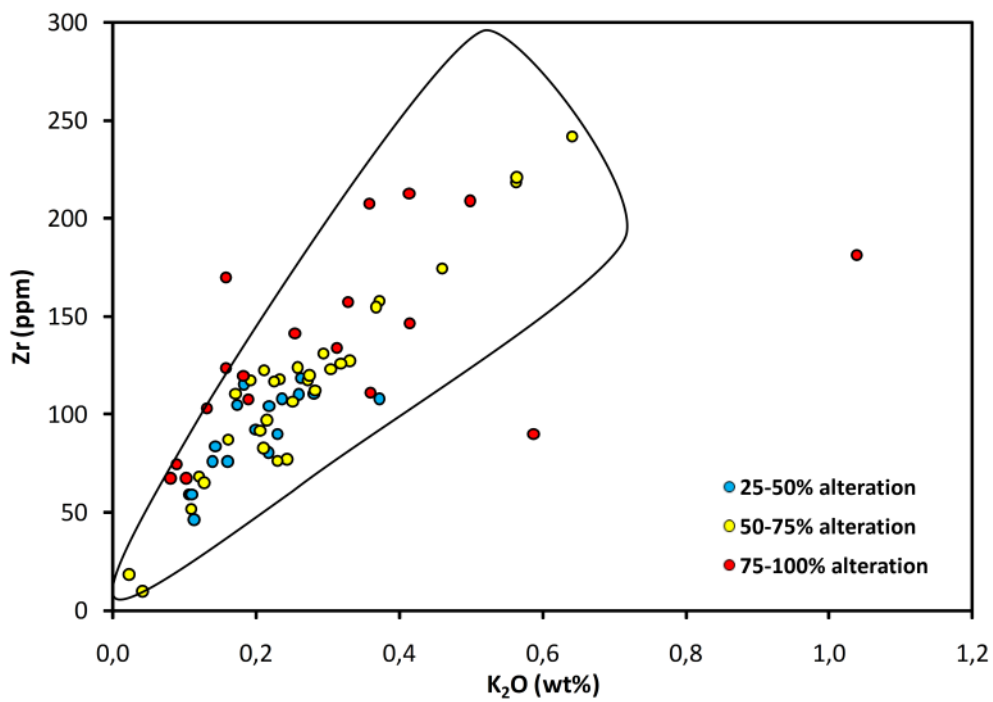


Figure 127. *Zr content versus K₂O content of tholeiitic hyaloclastite tuff samples from the WRZ (filled circles) in comparison with samples of fresh Holocene lavas (outlined field).*

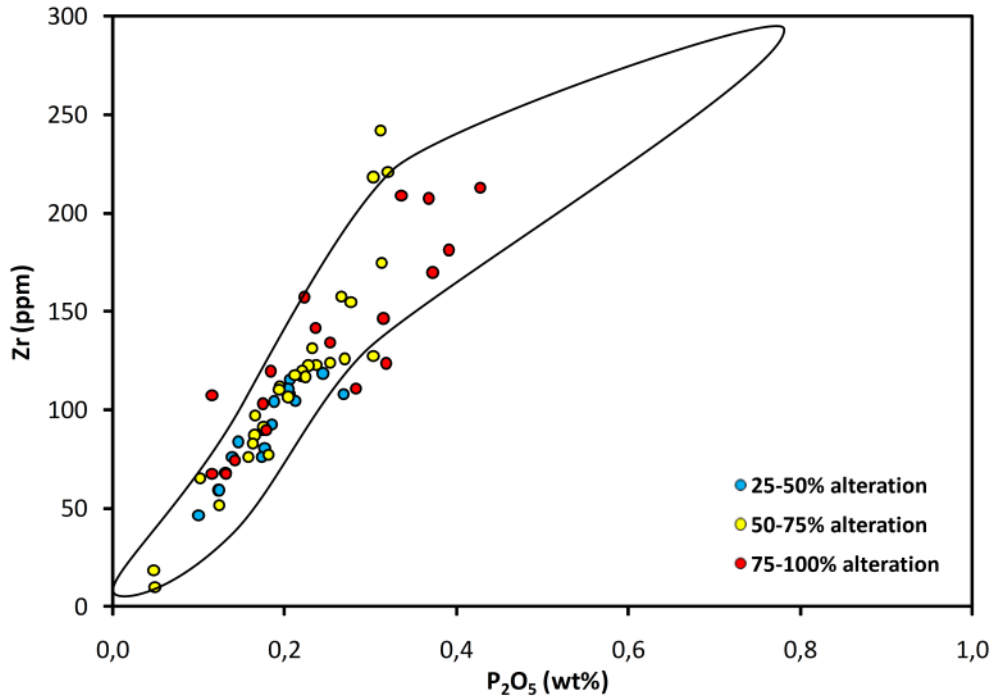


Figure 128. *Zr content versus P_2O_5 content of tholeiitic hyaloclastite tuff samples from the WRZ (filled circles) in comparison with samples of fresh Holocene lavas (outlined field).*

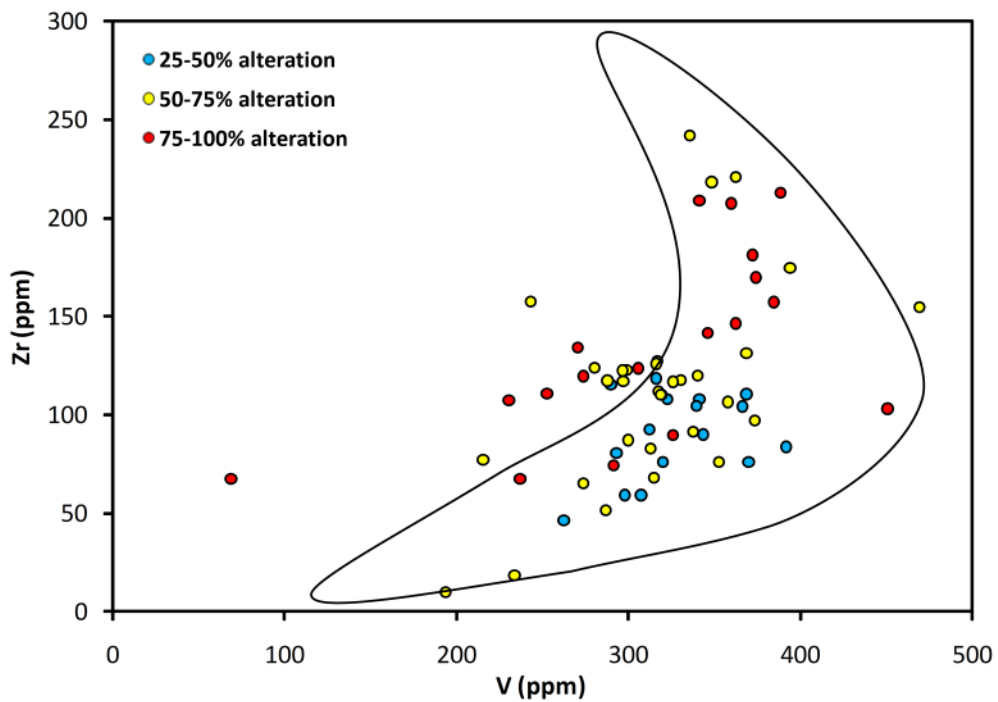


Figure 129. *Zr content versus V content of tholeiitic hyaloclastite tuff samples from the WRZ (filled circles) in comparison with samples of fresh Holocene lavas (outlined field).*

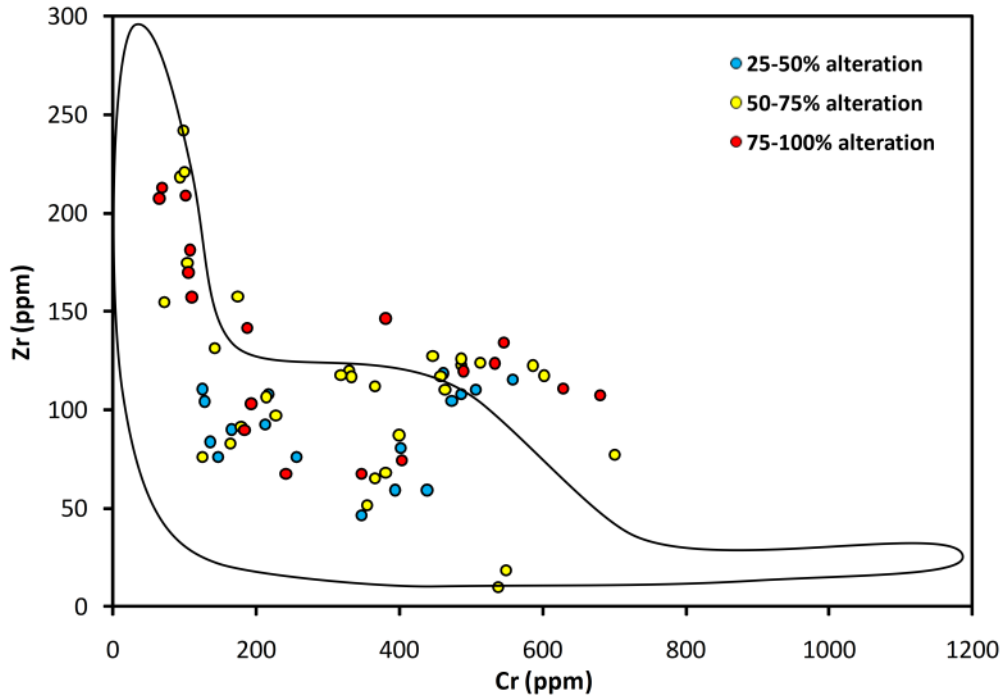


Figure 130. *Zr content versus Cr content of tholeiitic hyaloclastite tuff samples from the WRZ (filled circles) in comparison with samples of fresh Holocene lavas (outlined field).*

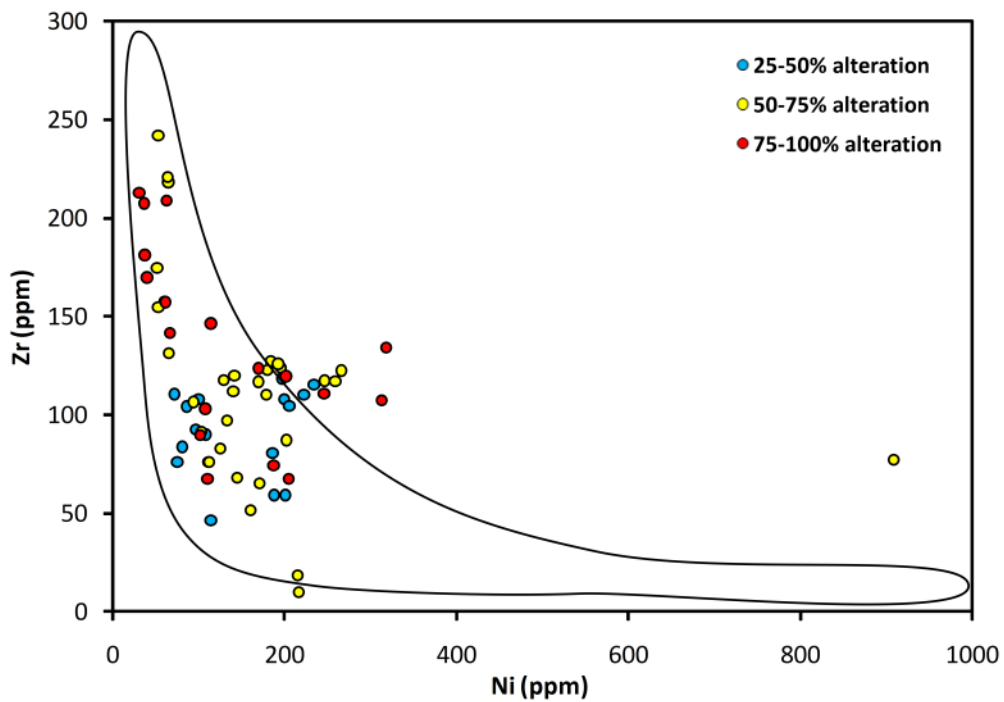


Figure 131. *Zr content versus Ni content of tholeiitic hyaloclastite tuff samples from the WRZ (filled circles) in comparison with samples of fresh Holocene lavas (outlined field).*

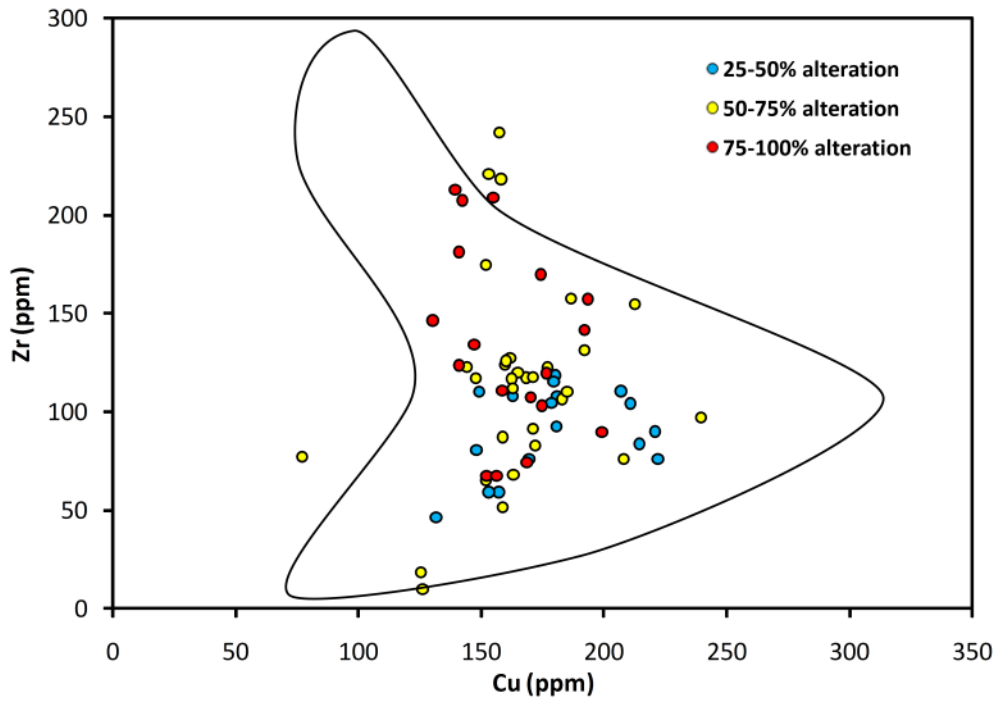


Figure 132. *Zr content versus Cu content of tholeiitic hyaloclastite tuff samples from the WRZ (filled circles) in comparison with samples of fresh Holocene lavas (outlined field).*

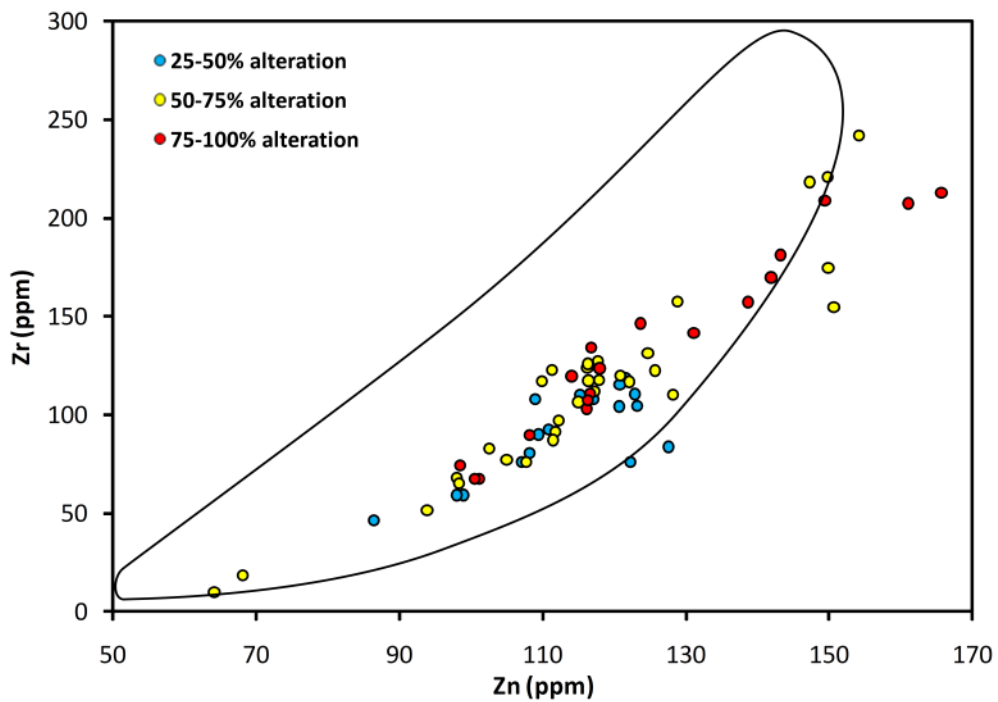


Figure 133. *Zr content versus Zn content of tholeiitic hyaloclastite tuff samples from the WRZ (filled circles) in comparison with samples of fresh Holocene lavas (outlined field).*

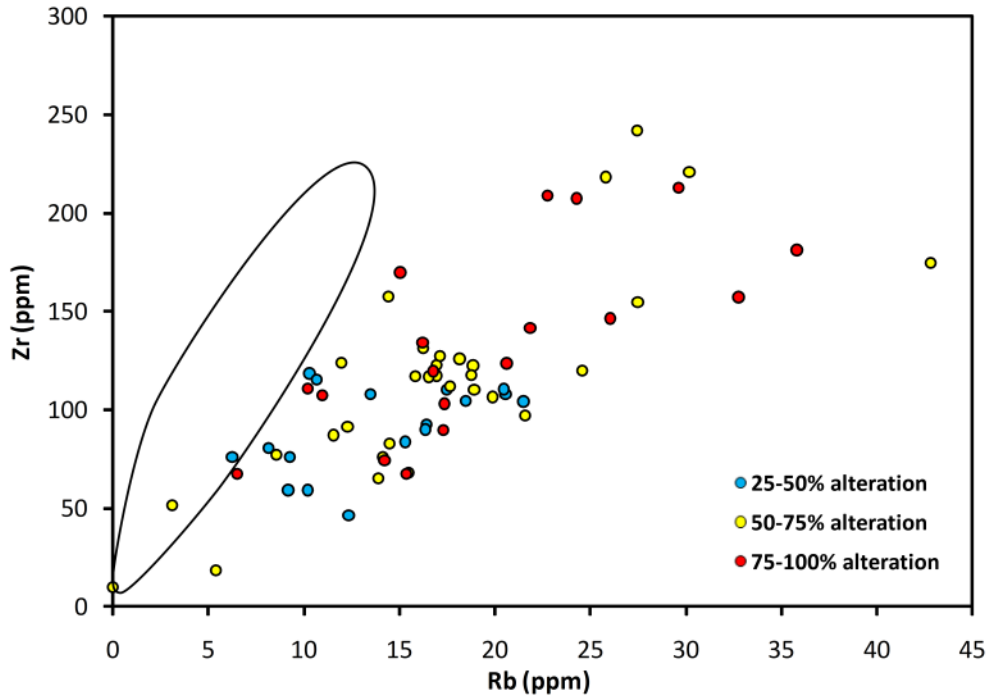


Figure 134. *Zr content versus Rb content of tholeiitic hyaloclastite tuff samples from the WRZ (filled circles) in comparison with samples of fresh Holocene lavas (outlined field).*

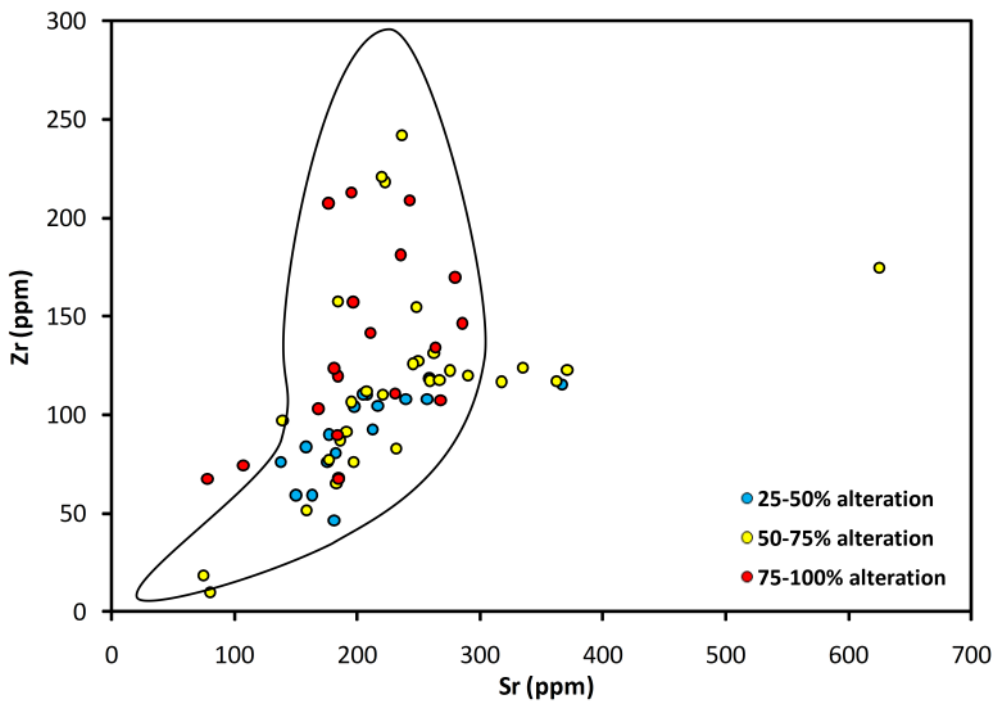


Figure 135. *Zr content versus Sr content of tholeiitic hyaloclastite tuff samples from the WRZ (filled circles) in comparison with samples of fresh Holocene lavas (outlined field).*

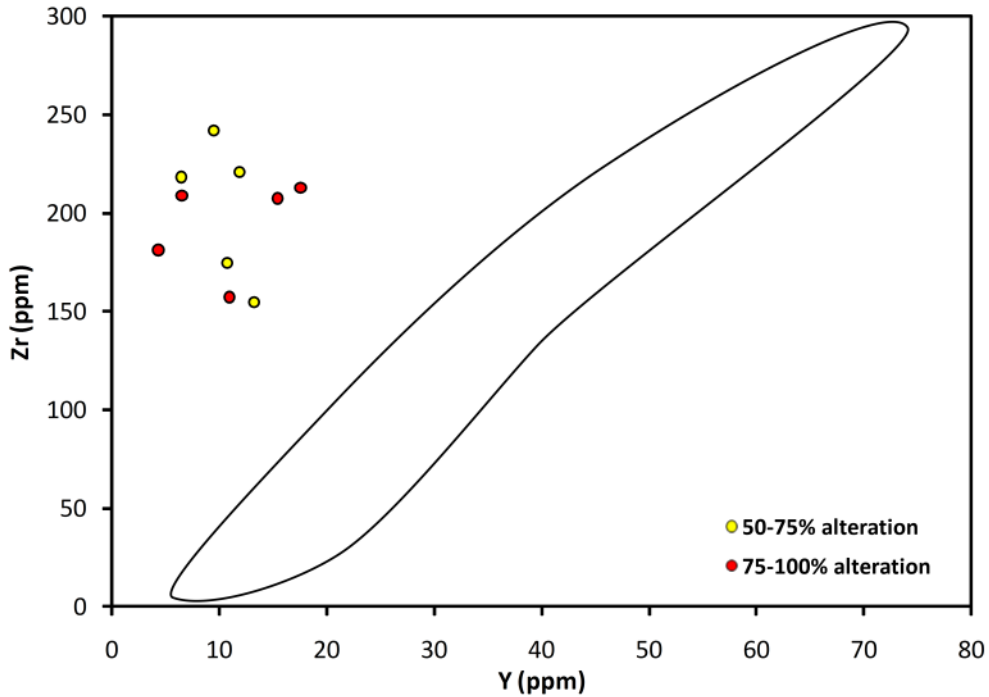


Figure 136. *Zr content versus Y content of tholeiitic hyaloclastite tuff samples from the WRZ (filled circles) in comparison with samples of fresh Holocene lavas (outlined field).*

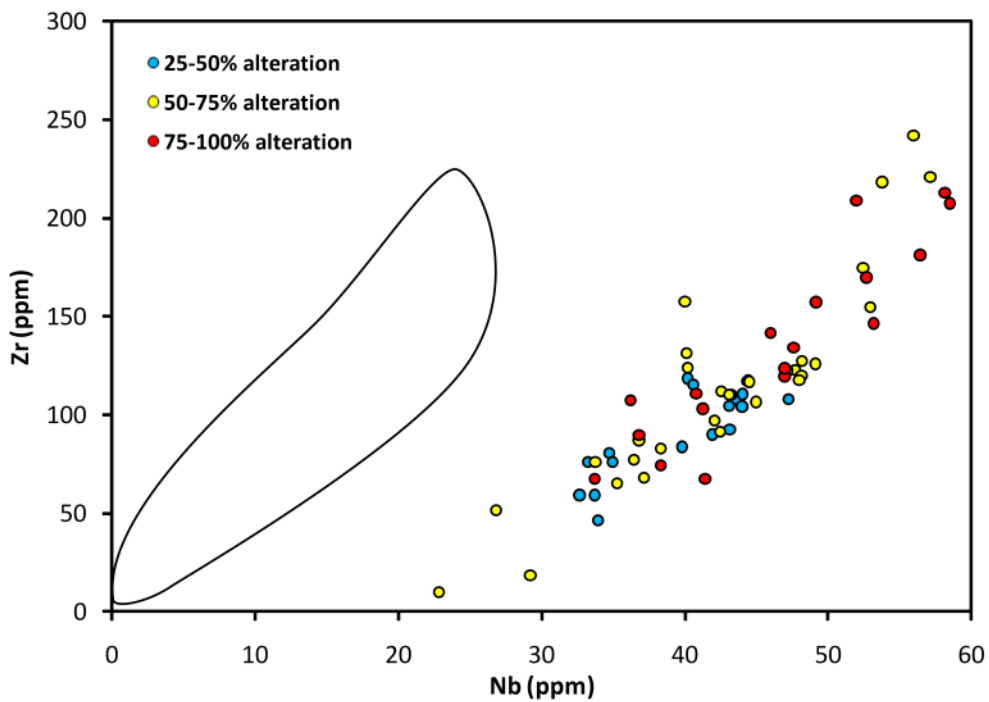


Figure 137. *Zr content versus Nb content of tholeiitic hyaloclastite tuff samples from the WRZ (filled circles) in comparison with samples of fresh Holocene lavas (outlined field). The offset between the tuff samples and the range of the Holocene samples is apparently caused by a systematic error in the Nb analyses of the tuff samples.*

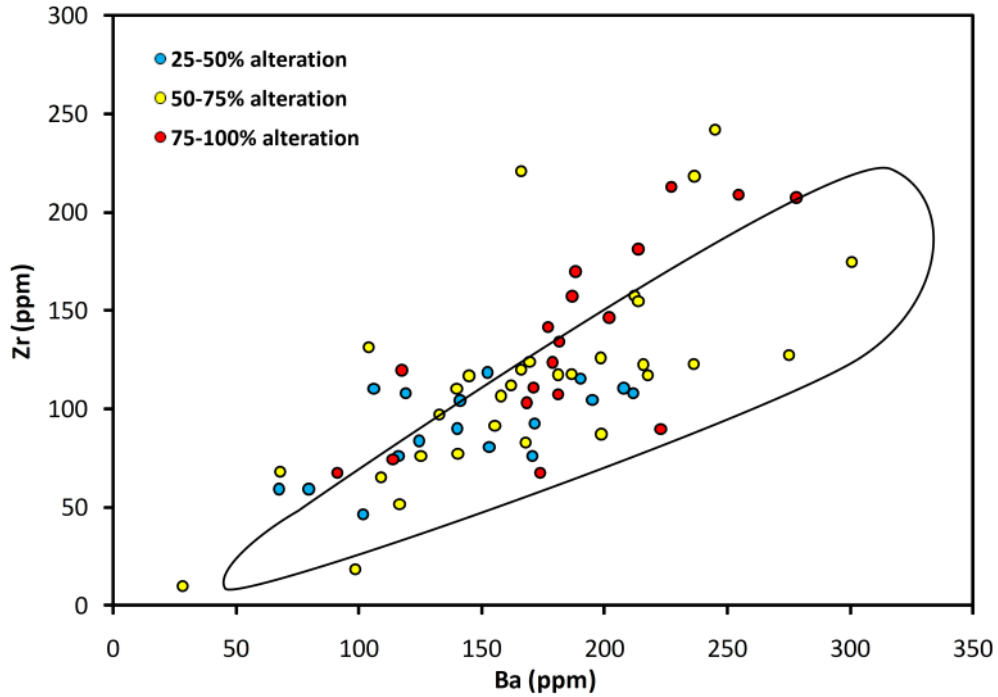


Figure 138. *Zr content versus Ba content of tholeiitic hyaloclastite tuff samples from the WRZ (filled circles) in comparison with samples of fresh Holocene lavas (outlined field).*

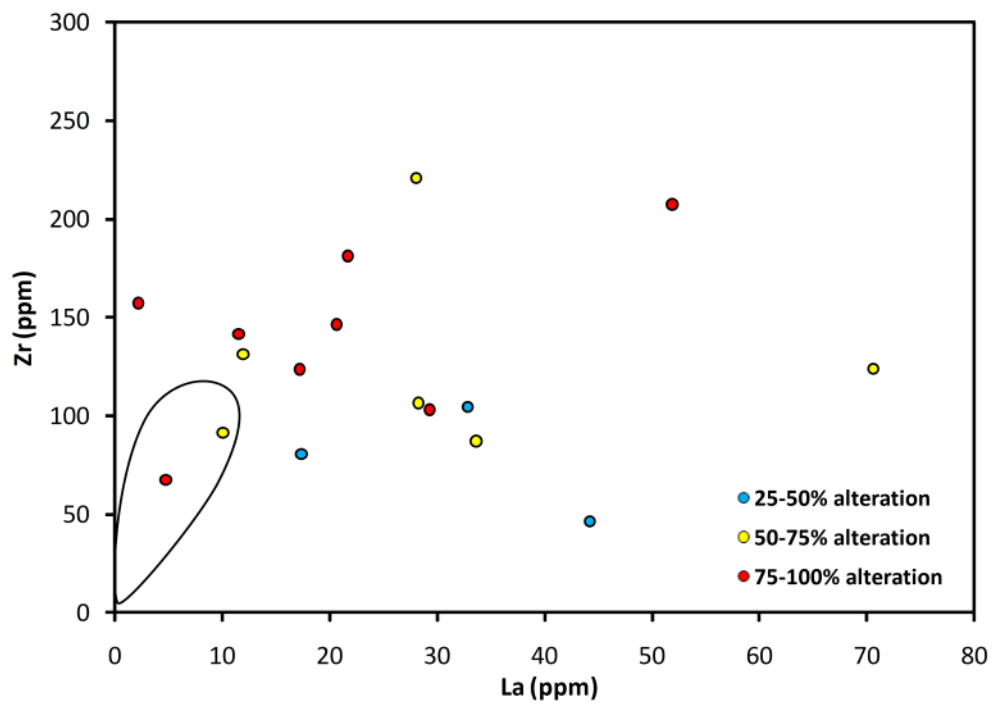


Figure 139. *Zr content versus La content of tholeiitic hyaloclastite tuff samples from the WRZ (filled circles) in comparison with samples of fresh Holocene lavas (outlined field).*